Generalized parton distributions of pseudoscalar mesons in a relativistic Bethe-Salpeter framework

Annelies Van Dyck

Promotor: Prof. Dr. Jan Ryckebusch

Co-promotor: Dr. ir. Tim Van Cauteren

Proefschrift ingediend tot het behalen van de academische graad van
Doctor in de Wetenschappen: Natuurkunde

Universiteit Gent
Faculteit Wetenschappen
Vakgroep Subatomaire en Stralingsfysica
Academiejaar 2007-2008

Cover: "Le Retour" by René Magritte (1898-1967)

Woord van dank

Een doctoraatsproefschift komt niet uit de lucht vallen. Er gaan jaren van onderzoek aan vooraf, met kleine en grote frustraties, grote en kleine momenten van euforie. Zonder mensen om me heen waarmee ik deze momenten kon delen, had ik dit onderzoek nooit kunnen afronden.

Jan, dankjewel voor het vertrouwen dat je in me hebt gesteld. Zonder jou zouden GPD's voor mij onbekend terrein gebleven zijn. Bedankt voor je feedback in het iteratieve proces dat het schrijven van een thesis altijd is.

Tim, ik heb genoten van de samenwerking en van onze discussies met en zonder Skype. Ik heb er echt ontzettend veel van geleerd. Bedankt voor je geduld en je vriendschap: de frustraties en euforie waarover ik hierboven sprak, heb ik altijd kunnen delen met jou. En natuurlijk ook bedankt om zoveel om mijn conditie te geven - de trappen naar het twixschap en de colafrigo hebben me fit gehouden.

Bernard, dankzij jou heb ik de kans gekregen om mijn berekeningen uit te voeren in het Bonnmodel. Ik wil je graag danken voor de vele boeiende en verhelderende discussies, voor je geduldige uitleg en voor je gastvrijheid. Het was telkens weer een plezier om langs te mogen komen in Bonn.

Dank ben ik ook verschuldigd aan de (ex-)collega's van het INW. Dimitri, van harte bedankt voor de interesse en voor de boeiende discussies over de numerieke code en de gebruikte algoritmes. Simon, het was fijn om met jou een bureau te delen. Mandarijntjes en The Beach Boys zullen nooit meer dezelfde zijn. Tamara en Anneleen, onze theepauzes en wandelingetjes waren voor mij een rustpunt in woelige tijden. Rudi, duizendmaal dank voor je omslagontwerp, voor de mooie figuren die je maakte voor deze thesis en mijn poster, en voor de bijstand wanneer ik zelf aan de slag ging met CorelDRAW. Dank, dank, dank, SuperComputerMannen Bart VC en Klaas, voor de hulp bij crashende harde schijven, in rook opgaande programma's en andere computerfrustraties. Pieter, Klaas en Bart VC, bedankt dat jullie zo welwillend mijn cakes op hebben gegeten. Bedankt, Bart VO, Wim, Christophe, Lesley, Olga, Arne, Cris, Natalie, Bartel en alle anderen, voor de leuke sfeer, de gedeelde UZ-vreugde en de

vrijdagmiddagse pizza-en-Couplingmomenten.

Mijn familie en vrienden hebben me de voorbije jaren door dik en dun gesteund. Ik wil hen dan ook danken voor de oprechte interesse, de enthousiaste aanmoedigingsmails, de lieve en opbeurende telefoontjes. Mama en papa, bedankt voor de vele morele én praktische steun tijdens al die jaren in (het verre) Gent. Annelies Ph, bedankt voor je luisterend *oor*. Lutgart, Willy, Wouter VD, Jeroen, Elke VN, Erika, Elke M, Saskia, Michael, Dimitri, Els, Thibaut, Wouter D, Susanne, Veerle, Ben, Catherine en nog zovele, zovele anderen: dankjewel, uit de grond van mijn hart.

Het meeste dank ben ik verschuldigd aan een heel bijzonder iemand. Lieve Jeroen, niemand heeft me de voorbije jaren zó hard gesteund als jij. Bedankt voor het nalezen, het luisteren, het geduld, de peptalk en het bereiden van liters thee. Maar boven alles bedankt voor je rust en voor je gave om met je omhelzing alle zorgen te doen verdwijnen.

Ik draag deze thesis op aan mijn Bomma, die overleed terwijl ik dit proefschrift schreef. Haar moed en sterkte zullen voor mij altijd een voorbeeld blijven.

Annelies Van Dyck,
maart 2008

Contents

1 Introduction

Melkweg

Je kunt in de wei uit een melkweg van wit
één takje fluitenkruid plukken om thuis
in een vaasje te zetten en van dat takje
één twijgje afbreken en daarvan één
steeltje en daarvan één bloempje
en van dat bloempje één pointe
van het godganse pointillisme.
Nee, dat kun je niet.

H. de Coninck

A matter of scale

The idea that everyday matter is composed of discrete building blocks has lived for thousands of years. Centuries before Demokritos adopted the term ἄτομος (indivisible) for the presumed constituents of matter, Indian schools of philosophy were teaching the theory that matter consisted of small units that were attached together. Whereas the concept of atoms was a mere philosophical question before, it was adopted by modern science after Dalton had formulated his atomic theory in the beginning of the 19th century.

Yet, a wooden table doesn't reveal anything of the table's microscopic units when we look at it with our eyes, and one might be tempted to ignore the very existence of these particles. Indeed, when calculating the gravitational force between the table and the earth, the concept of small building blocks with their own mass and size would severely complicate things. The only properties that are relevant in this macroscopic description are the table's mass and the position of its center-of-mass.

On the other hand, when a cell biologist is interested in the tree that yielded the table's wood, he or she might want to have a look at the DNA structure inside the wood's cells, and by doing so, try to find information on the tree species and characteristics. The relevant degrees of freedom to describe the DNA chain are no longer macroscopic. Instead, the researcher will look for sequences of three nucleotides (codons) and for sets of these codons, called genes.

This example illustrates the notion of *scale*, one of the most elementary and important concepts in physics [1]. The scale constrains the degrees of freedom: the smaller the scale, the smaller the building blocks needed to model the problem of interest. Keeping in mind the idea of discrete units, we know that at the maximal resolution, those constituents will be encountered which are considered to be the fundamental building blocks of matter in contemporary physics.

The work presented in this thesis is situated in the field of hadron physics. Hadrons, *e.g.* protons, neutrons and pions, consist of quarks and gluons. Two classes of hadrons can be distinguished: the *baryons*, which are fermionic hadrons with a half-integer spin, and the *mesons*, which are bosonic hadrons with an integer spin. The laws obeyed are those of quantum field theories such as QCD, theories which are combined in the *standard model of particle physics*. However, due to some particular properties of QCD, the description of hadrons in terms of their elementary constituents is far from straightforward.

The standard model

The standard model of particle physics was established in the early 1970s. It is the theory of fundamental particles and their interactions through the electromagnetic, weak and strong force. Gravity, which is the fourth fundamental interaction, is not included in the standard model due to its weakness at the subatomic scale. The fundamental matter particles can be classified in two families of six particles: the *leptons* (the electron, its heavy counterparts muon and tau, and a neutral, almost massless neutrino corresponding to each of these species) and the *quarks* (up, down, strange, charm, bottom and top). Interactions are mediated by the exchange of vector bosons called *gauge bosons*. A particle can couple to the gauge boson of a specific interaction if it carries the corresponding charge:

- all leptons and quarks carry weak charge. Therefore, all matter particles can couple to the mediators of the weak force, the $W^{\pm}$ and Z^0 bosons;

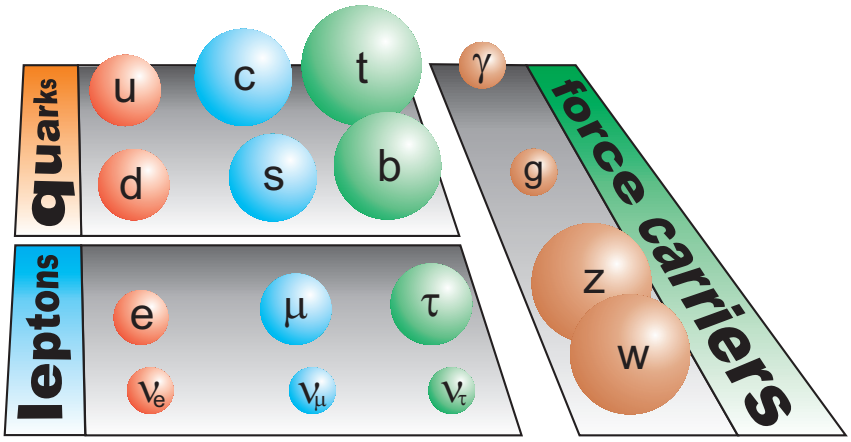

Figure 1.1 Schematic overview of the elementary particles in the standard model of particle physics.

- all quarks and some leptons (electron, muon, tau) carry electrical charge and couple to the gauge boson of electromagnetic interaction, the photon;
- all quarks carry color charge and couple to the gluons, the force-carriers of the strong interaction. None of the leptons carry color charge.

An overview of the fundamental matter particles and gauge bosons is presented in Fig. 1.1.

The electromagnetic and weak interactions are unified in the Glashow-Salam-Weinberg model of electroweak interactions [2]. The unification with the theory of the strong interaction, QCD, is investigated in the grand unified theories or GUTs [3]. Beyond grand unification, researchers are looking for a theory of everything, in an attempt to merge gravity with the three gauge symmetries of the standard model.

This neat picture doesn't imply that the interactions amongst the fundamental constituents of matter are fully understood. After 35 years of research, a lot of open questions remain, many of which are related to the theory of the strong interaction.

Quantum chromodynamics

Quantum chromodynamics or QCD is the quantum field theory which describes the interactions between quarks and gluons. It was established in the 1960s, after Gell-Mann, Ne'eman and Zweig had proposed the existence of quarks [4, 5, 6, 7, 8] in an attempt to bring order in the myriad of strongly interacting particles, hadrons, that were discovered in reactions with cosmic rays and at particle accelerator facilities. However, one hadron caused problems: the wave function of the Δ^{++}, a spin-$3/2$ baryon,

appeared to be symmetrical in flavor, configuration and spin spaces, in violation with the well-known Pauli principle. Nambu and Han resolved this problem by proposing the novel $SU(3)_c$ gauge group, containing color charge as a new quantum number for the quarks [9, 10]. The color charge can take three values, usually called red, blue and green. Accordingly, the antiquarks carry the anticolors antired, antiblue and antigreen. An antisymmetrical wave function of the Δ^{++} would then imply an antisymmetrical color wave function, in which each quark has a different color, leaving the Δ^{++} itself colorless or white. Nowadays, all hadrons are known to be composite particles made of the colored quarks and gluons, but which themselves are color neutral.

Many similarities exist between the strong interaction (QCD) and the electromagnetic interaction (QED). Both take place via the exchange of massless gauge bosons. The fact that colorless hadrons interact strongly with each other to form atomic nuclei, can be understood by an analogy with atomic physics: although atoms are electrically neutral, they bind electromagnetically to form molecules. Similarly, the color neutral protons and neutrons will bind strongly to form an atomic nucleus. However, there is one major difference between the electromagnetic and the strong interaction: whereas photons are electrically neutral, the gluons carry color charge, allowing them to interact with other gluons. This gluon self-interaction should not be marginalized, as it causes the coupling constant of the strong force, α_s, to become larger as quarks are separated [11]. As a result, free quarks and gluons cannot be observed at finite energies. This effect is called *confinement*, and it is still not fully understood, being one of the ten most important unsolved problems in physics formulated at the beginning of the new millennium. The presence of confinement complicates QCD tremendously. Whereas bound states are calculable from first principles in the quantum field theory of the electromagnetic interaction, QED, they are far more challenging objects in QCD. This is due to the large coupling constant which arises in the calculation of bound states of quarks and gluons and prevents the use of perturbation theory.

In contrast, as the distance between the quarks becomes smaller (or, equivalently, at increasing energy scales), the interaction strength becomes weaker. This feature is known as *asymptotic freedom*, and its discovery by Gross, Wilczek and Politzer[1] led to the Nobel Prize in physics in 2004 [13, 14, 15, 16]. Because α_s varies so strongly with the scale, it is often called a *running* coupling constant. Denoting the energy scale as

[1] Asymptotic freedom was discovered independently by 't Hooft, who did not publish his results but showed them in the margin of a conference talk [12].

Q^2, the running coupling constant can be written as follows:

$$\alpha_s(Q^2) = \frac{12\pi}{(33 - 2N_f)\ln\frac{Q^2}{\Lambda^2}}\,, \tag{1.1}$$

where N_f is the number of quark flavors and $\Lambda \sim 200$ MeV is the fundamental QCD scale, *i.e.* the parameter which fixes the coupling: as Q^2 approaches Λ^2, α_s goes to infinity.

As a direct result of the behavior of the coupling constant, Eq. (1.1), different scales are met when dealing with the strong interaction. As mentioned in the outset of this chapter, different scales lead to different degrees of freedom. At high energy scales, a proton, or more generally speaking a non-exotic baryon, can be described as consisting of three valence quarks and a sea of quark-antiquark pairs interacting with gluons. A non-exotic meson such as the pion, then consists of a valence quark-antiquark pair surrounded by gluons and the sea[2]. In the description of hadron properties at lower scales, the relevant degrees of freedom are not unambiguously defined and various complementary approaches exist. Calculating hadron properties from first principles is only possible in lattice QCD, where the QCD equations of motion are discretized on a space-time lattice and solved numerically [17]. At present, some approximations cannot be avoided, though, and calculations are usually performed at high pion masses, making comparison with experiments difficult. Another way of dealing with QCD is chiral perturbation theory [18], an effective field theory that uses hadronic fields as the degrees of freedom. In this thesis, a constituent quark model is adopted [19], in which the degrees of freedom are constituent quarks. These might be regarded as dressed valence quarks having a constituent quark mass which is different from the more fundamental current quark mass that appears in the QCD Lagrangian, the base equation of the strong interaction.

Many processes in nature are a combination of parts with a different energy scale, and thus a different interaction strength α_s. Deeply virtual Compton scattering (DVCS) and hard exclusive meson production (HEMP), through which the generalized parton distributions (GPDs) can be accessed, are examples of such processes. As will be explained in Chapter 2, these reactions typically consist of a hard scattering part where perturbation theory can be used, and a soft part where non-perturbative quantities are defined. In DVCS and HEMP, it is proven that these hard and soft parts are factorizable [20, 21], which allows the use of dynamic models for the soft part.

[2] Hadrons with a different valence quark configuration, the so-called *exotic and hybrid hadrons*, cannot be excluded from theoretical principles. However, these hadrons, such as the much debated pentaquark ($qqqq\bar{q}$), the tetraquarks ($qq\bar{q}\bar{q}$), glueballs (no valence quarks, only gluonic degrees of freedom, e.g. ggg) and hybrids (e.g. $q\bar{q}g$) go beyond the scope of this dissertation.

Outline

In this work, the calculation of generalized parton distributions in a Bethe-Salpeter constituent quark model will be evaluated.

In Chapter 2, the GPDs are defined for both pseudoscalar mesons and spin-$1/2$ baryons. The electromagnetic form factors and parton distribution functions are introduced and their relation with GPDs is discussed. The evolution of model calculations to other kinematical regimes is discussed and an overview is presented of GPD model calculations.

The Bonn constituent quark model is presented in Chapter 3. The Bethe-Salpeter equation and the corresponding Bethe-Salpeter amplitudes are discussed for the meson case. It is shown how the Bethe-Salpeter equation can be turned into a solvable integral equation, the Salpeter equation. The interactions used in this model, namely the confinement interaction and the instanton induced interaction, are discussed.

In Chapter 4, the generalized parton distributions are derived through the "Mandelstam formalism". The numerical implementation of the GPD formula is described. In particular, we focus on the boost properties of the GPDs and the numerical integration routines. It is indicated how the proton GPDs can be derived.

The results of the numerical calculations of the GPDs are presented in Chapter 5. It is shown that the Bonn model might suffer from a support problem. The model is tested for stability against the choice and the number of radial basis functions. The GPD results are put to three stringent model tests. To investigate the support properties of the GPDs, three model variants are introduced.

Chapter 6 states our conclusions and presents a brief outlook for the future. Recommendations are given for future model calculations of generalized parton distributions in a Bethe-Salpeter framework.

The notations and conventions used in this work are presented in detail in Appendix A. Appendix B focuses on details in the derivation of GPDs in the Bonn model, more specifically on the Fourier transformation of the six-point Green's function. A brief introduction into the Bonn model for baryons is given in Appendix C.

2 Generalized parton distributions

QCD nowadays has a split personality.
It embodies "hard" and "soft" physics,
both being hard subjects, and the softer the harder.

Y. Dokshitzer, 1998

2.1 Studying hadron structure

At energy scales of the order of a typical hadron mass (1 GeV), hadrons are complex objects of quarks and gluons whose behavior cannot be described in perturbative QCD. The cross sections for scattering of particles from hadrons are expressed in terms of non-perturbative quantities which reflect the internal structure of the hadron. Depending on the nature of the scattering reaction, the non-perturbative quantities in the cross section are called form factors, parton distribution functions (PDFs), generalized parton distribution functions (GPDs),... At present, it is not feasible to calculate these quantities from first principles, although attempts exist to compute them on the lattice (see Sect. 2.3.3).

The best way to study a complex system is through a known probe. To be able to unambiguously extract the hadron properties from the reaction cross section, one chooses pointlike particles to interact with the hadron. In this work, we will focus on reactions in which the pointlike particle is an electrically charged lepton (usually an electron). The leptonic part of scattering processes between a charged lepton and a hadron is readily described in QED, so that the unknown part of the cross section of this reaction depends solely on the internal, non-perturbative structure of the latter.

Historically, form factors and parton distribution functions have played a key role in unraveling the internal structure of hadrons. During the decades that these quantities have been studied, they have provided us (and still do) with a tremendous amount of information. In the 1990s, a new research tool emerged: the generalized parton dis-

tributions [22, 23, 24, 25, 26, 27, 28], which were proven to be a generalization of both form factors and parton distribution functions and thus constitute a natural unification of these objects. Because of the close relation between GPDs, PDFs and form factors, a clear understanding of the latter two is needed to interpret the first. We therefore start this chapter with a brief introduction to electromagnetic form factors and parton distribution functions.

2.1.1 Electromagnetic form factors

The simplest way to study hadron properties with the electromagnetic interaction is through the *elastic* process

$$l(k) + H(\bar{P}) \to l(k') + H(\bar{P}')\,, \tag{2.1}$$

where l is an electrically charged lepton[1] and H is the studied hadron. The symbols between brackets denote the particle four-momenta. In this type of processes, no hadron constituents are resolved, so that the hadron is studied as one object (with a finite size). The diagram belonging to elastic scattering is shown in Fig. 2.1.

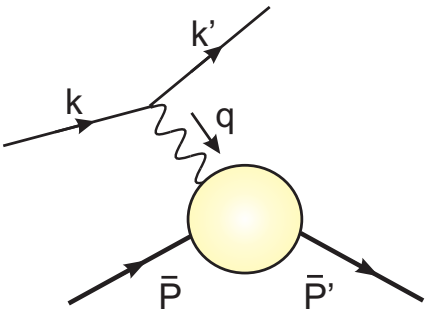

Figure 2.1 The Feynman diagram belonging to the elastic scattering reaction (2.1). The non-perturbative dynamics in the yellow blob give rise to the introduction of form factors.

The leptonic part of the cross section follows from the Feynman rules of quantum electrodynamics. Unfortunately, the calculation of the hadronic part is not as straightforward, because the (essentially non-perturbative) physical processes which take place in the yellow "blob" in Fig. 2.1 are unknown. To overcome this problem, the non-perturbative dynamics are parametrized through *form factors* which depend on the photon virtuality. The hadronic part of the elastic scattering reaction is described by the local current matrix element

$$\langle \bar{P}'|J(x)|\bar{P}\rangle = \langle \bar{P}'|N\{\bar{\psi}(x)\gamma^{\mu}\psi(x)\}|\bar{P}\rangle\,. \tag{2.2}$$

[1] Also elastic scattering processes with the electrically neutral leptons (neutrinos) are the subject of extensive research. These give rise to the *weak* form factors.

The Dirac matrices γ^μ are introduced in App. A. N denotes the normal ordered product of the Heisenberg fermion field operators $\psi(x) = \psi^{(+)}(x) + \psi^{(-)}(x)$, where $\psi^{(+)}(x)$ is the quark annihilation field and $\psi^{(-)}(x)$ the antiquark creation field. The number of form factors needed to parametrize this matrix element depends on the hadron under study [29]. In this work, we will discuss pseudoscalar mesons and spin-$1/2$ baryons. Pseudoscalar mesons, such as the pion and the kaon, have only one electromagnetic form factor:

$$\langle \bar{P}' | N\{\bar{\psi}(x)\gamma^\mu\psi(x)\}|\bar{P}\rangle = 2F(Q^2)\tilde{P}^\mu\,. \tag{2.3}$$

Here, e_m is the total electric charge of the pseudoscalar meson. We have introduced the average hadron four-momentum $\tilde{P}^\mu = \frac{\bar{P}^\mu + \bar{P}'^\mu}{2}$. In view of the upcoming definitions, it is important to remark that in the elastic scattering process defined by Fig. 2.1, the Mandelstam variable $t = \Delta^2 = (\bar{P}' - \bar{P})^2$ and the photon virtuality $Q^2 = -q^2$ only differ by their sign: $t = -Q^2$. The fourmomenta Δ^μ and q^μ are equal: $\Delta^\mu = q^\mu = \bar{P}'^\mu - \bar{P}^\mu$.

Elastic scattering from spin-$1/2$ baryons, such as the nucleon, gives rise to two electromagnetic form factors:

$$\langle \bar{P}', \lambda' | N\{\bar{\psi}(x)\gamma^\mu\psi(x)\}|\bar{P}, \lambda\rangle = \bar{u}_{\lambda'}(\bar{P}')\left[\gamma^\mu F_1(Q^2) + \frac{i\sigma^{\mu\nu}\Delta_\nu}{2M_b}F_2(Q^2)\right]u_\lambda(\bar{P})\,. \tag{2.4}$$

In this equation, u_λ and $\bar{u}_{\lambda'}$ are the spinors describing a baryon with helicities λ and λ', M_b is the baryon mass and e_b the baryon electric charge. One refers to F_1 and F_2 as the Dirac and Pauli form factor, respectively.

In the Breit frame where $\boldsymbol{P} = -\boldsymbol{P}' = -\frac{\boldsymbol{q}}{2} = -\frac{\boldsymbol{\Delta}}{2}$ and $q^0 = \Delta^0 = 0$, the electromagnetic form factors have a special meaning. In the case of a nucleon, for example, one can introduce the Sachs form factors as linear combinations of the Dirac and Pauli form factors:

$$G_E(Q^2) = F_1(Q^2) - \frac{Q^2}{4M_N^2}F_2(Q^2)\,, \tag{2.5}$$

$$G_M(Q^2) = F_1(Q^2) + F_2(Q^2)\,, \tag{2.6}$$

with M_N the nucleon mass. In the Breit frame (and in the non-relativistic limit), the Sachs form factors can be interpreted as the three-dimensional Fourier transforms of (non-relativistic) spatial electric charge and magnetization densities [30]. The expression for the electric charge density in the Breit frame, for example, reads:

$$\rho(\boldsymbol{r}) = \int \frac{\mathrm{d}^3 q}{(2\pi)^3} e^{-i\boldsymbol{q}\cdot\boldsymbol{r}} G_E(\boldsymbol{q}^2)\,. \tag{2.7}$$

A similar expression exists for the magnetization density[2]. This leads to constant form factors for point particles in the non-relativistic limit. In the fully relativistic case, point particles still have constant form factors, up to radiative corrections.

2.1.2 Parton distribution functions

At high photon virtualities, the elastic form factors decrease and inelastic scattering processes become more probable than elastic scattering. As $Q^2 \to \infty$ and the photon energy in the laboratory frame $q^0_{lab} = \nu \to \infty$ (keeping their ratio finite), the process is said to be *deep inelastic*. This kinematical regime is often referred to as the Bjorken limit. The Bjorken regime is reached for $Q^2 > 1$ to 2 GeV^2 and $\nu > 1$ GeV. Whereas in the elastic case the initial hadron remained intact, it falls apart into many hadrons in deep inelastic scattering ("hadronization"):

$$l(k) + H(\bar{P}) \to l(k') + X\,. \tag{2.8}$$

X stands for the (mostly unmeasured) remnants of the reaction. In Fig. 2.2, this reaction is drawn.

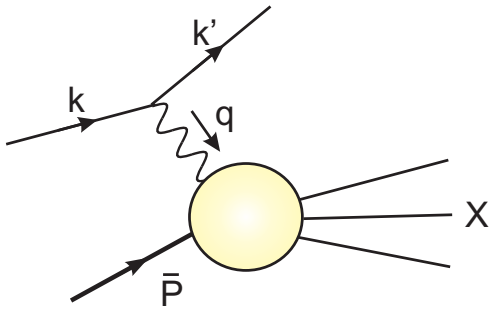

Figure 2.2 Visualisation of the deep inelastic scattering reaction of Eq. (2.8), which is described in terms of the structure functions. These give rise to the introduction of parton distribution functions.

An additional variable is needed in the description of the hadronic part, because the mass of the final state is no longer constrained. As a result, the differential cross section is written in terms of the dimensionless *structure functions* $F(x_B, Q^2)$ (pseudoscalar mesons), $F_1(x_B, Q^2)$ and $F_2(x_B, Q^2)$ (spin-$1/2$ baryons). x_B is called the Bjorken variable and is defined as

$$x_B = \frac{Q^2}{2\bar{P}\cdot q}\,. \tag{2.9}$$

[2] An extensive discussion regarding the Sachs form factors as Fourier transformed densities can be found in Ref. [31].

Experiments at the Stanford Linear Accelerator in the 1960s [32] showed that in the Bjorken limit, the structure functions are independent of the photon virtuality and only depend on x_B. This phenomenon is called Bjorken scaling and it is well described by Feynman's parton model.

The parton model

In accordance with Heisenberg's uncertainty principle, a high photon virtuality Q^2 means that the probed region is small ($\sim 1/\sqrt{Q^2}$). In other words: in deep inelastic scattering, the hadron is no longer seen as one (large) object. In the *parton model*, it is assumed that the lepton scatters *elastically* from the hadron constituents (commonly called "partons"). Moreover, it is postulated that the lepton-hadron interaction can be viewed as the incoherent sum of the interactions between the lepton and the individual partons. This interpretation is valid because the partons themselves do not interact with each other[3] at high Q^2 (asymptotic freedom, see Chapter 1). The observed Q^2-independence implies that the hadron constituents are pointlike.

Choosing the reference frame with care simplifies the interpretation of deep inelastic scattering off hadrons. In the parton model, the reference frame is chosen so that both the hadrons and the partons move infinitely fast, *e.g.* in the three-direction. In such a frame, the hadron light-cone plus-momentum[4] $\bar{P}^+$ is proportional to its three-momentum $\bar{P}^3$, because its transverse momenta and rest mass can be neglected. In this case, the structure of the hadron depends (in first approximation) on the longitudinal momenta of its constituents. In the infinite momentum frame, these longitudinal parton momenta can be written as fractions of the initial hadron momentum $\bar{P}$. It turns out that only those partons are resolved which carry a momentum fraction x_B of the hadron momentum [33, 34]:

$$p^+_{parton} = x_B \bar{P}^+ \,. \tag{2.10}$$

Because deep inelastic lepton-hadron scattering can be described in terms of the elastic scattering of the lepton from the partons, its cross section can be written as the sum of the cross sections of the scattering processes from the partons, weighted by the number density of partons of flavor f that carry a momentum fraction x_B. This is exactly the factorization into a hard and a soft subprocess, as described in Chapter 1: the hard partonic subprocess, *i.e.* the elastic scattering of the lepton from the parton,

[3] To be precise, this statement is only valid up to small, logarithmic corrections, because in an asymptotically free quantum field theory such as QCD, the coupling constant at large, but finite momentum transfers is still nonzero. Violations of Bjorken scaling have been observed and successfully described in QCD (see Sect. 2.3.1).

[4] The light-cone coordinates are introduced in App. A.

is calculable using perturbative QCD and QED, while the soft subprocess is described by the parton number density, or *parton distribution function* $f(x_B)$. It can be proven [34] that the structure functions are proportional to $\sum_f e_f^2 f(x_B)$, where f denotes the probed parton flavor and e_f the charge in units of $|e|$. Therefore, a rigorous description of hadron structure implies the knowledge of the parton distribution functions. The optical theorem provides a prescription on how to calculate these functions.

The optical theorem

The hadronic remnants X in the scattering reaction (2.8) typically consist of a large number of hadrons. In some experiments, one or two final hadrons carrying a large fraction of the transferred energy are detected, and one speaks of a semi-inclusive measurement. If none of the final hadrons are detected, the measurement is called inclusive, as opposed to an exclusive measurement in which all the reaction products are identified.

The hadronic part of the inclusive reaction of Fig. 2.2, which occurs squared in the cross section, is related to the imaginary part of the forward scattering amplitude of Fig. 2.3 (handbag diagram) via the optical theorem [11, 35]:

$$\sum_X |\langle X|J(0)|\bar{P}\rangle|^2 \sim \int \mathrm{d}^4 y \mathfrak{Im} \left(\langle \bar{P}|J(0)J(y)|\bar{P}\rangle\right) . \tag{2.11}$$

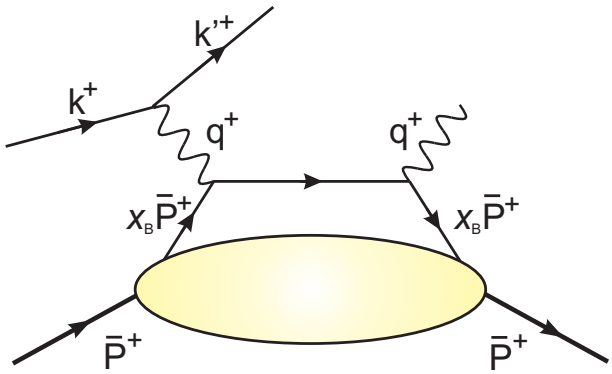

Figure 2.3 The handbag diagram which is related to deep inelastic scattering through the optical theorem. The plus-momenta given refer to the infinite momentum frame. The yellow blob denotes the parton distribution function $f(x_B)$.

The matrix element on the right-hand side of this equation is calculable in QCD, provided that the unknown "blob" in Fig. 2.3 is parametrized. The functions needed in this parametrization are precisely the parton distribution functions $f(x_B)$ [36]. A

calculation yields the following equation which defines the "twist-two" (or leading-order) parton distribution functions:

$$f(x_B) = \frac{1}{2}\int \frac{\mathrm{d}z^-}{2\pi} e^{ix_B \bar{P}^+ z^-} \langle \bar{P}|\bar{\psi}^f(-\frac{z}{2})\gamma^+\psi^f(\frac{z}{2})|\bar{P}\rangle\Big|_{z^+=0,\mathbf{z}_\perp=\mathbf{0}} . \tag{2.12}$$

Notice the occurrence of a *bilocal* current operator, reflecting the interpretation of the blob as a quark-hadron scattering amplitude. Definition (2.12) is Lorentz invariant, so that the parton distribution functions can be calculated in any reference frame. Their interpretation as momentum densities, however, is restricted to the infinite momentum frame.

In the above definition, the PDF $f(x_B)$ was called a twist-two function. Similarly, the operator in the matrix element on the right-hand side of Eq. (2.12) is called a twist-two operator. This "twist" is defined in the operator product expansion (OPE), through which Eq. (2.12) can be rigorously derived. The basic idea of OPE is to expand the hadronic part of the diagram in Fig. 2.3, which contains two vector currents, as a series of *local operators*. As we know, this hadronic part contains the structure functions through the optical theorem (and thus also the parton distribution functions). The twist of a local operator in the expansion is defined as the difference between its mass dimension d and its spin s:

$$\tau = d - s\,, \tag{2.13}$$

where the spin of the operator refers to its transformation properties under Lorentz transformations. It turns out that the leading contribution to the deep inelastic scattering cross section comes from the operators with the lowest twist. For QCD operators other than the unity operator, the smallest possible value for the twist is $\tau = 2$. In short, the twist-two parton distribution function describes the leading part of the structure functions. In the Bjorken limit, only this leading contribution is maintained, since higher-twist (τ') terms are suppressed by a factor $(1/Q^n)$ with $n = \tau' - 2$. More information on twist and the OPE can be found in Refs. [11, 36, 35].

The factorization into a hard and a soft subprocess (or a short- and a long-distance scale) is not restricted to the forward diagram of Fig. 2.3. In fact, it can be generalized to situations where the target receives a finite momentum transfer t. The only requirement for the factorization to remain valid, is that one of the photon virtualities is large [20, 21].

2.2 Generalized parton distributions

The forward scattering process of Fig. 2.3, which prescribes how to calculate the parton distribution functions, was introduced through the optical theorem. Experimentally, however, PDFs are accessed via inclusive deep inelastic scattering reactions of the type (2.8). Nevertheless, Fig. 2.3 shows a process which, albeit difficult, *could* be measured experimentally. In its generalization to the off-forward case, it is important to remark that the off-forward processes can no longer be linked with deep inelastic scattering. Therefore, off-forward processes imply an *exclusive* measurement, requiring high luminosity beams, long run times and sufficient energy resolution. All this makes them extremely challenging quantities to study experimentally.

Regarding the generalized parton distributions, two particular reactions can be studied. The first is called deeply virtual Compton scattering (DVCS). In this process, the final photon is on-shell[5]:

$$l(k) + H(\bar{P}) \to l(k') + H(\bar{P}') + \gamma(q') \,. \tag{2.14}$$

The factorization theorem requires that the virtuality of the incoming photon is large (since $q'^2 = 0$). The momentum transfer to the target $t = (\bar{P}' - \bar{P})^2$ remains finite. The handbag diagram belonging to this process is shown in Fig. 2.4.

In the second case, hard exclusive meson production (HEMP), a light meson is produced:

$$l(k) + H(\bar{P}) \to l(k') + H(\bar{P}') + M(q') \,. \tag{2.15}$$

Because the hadron stays intact during and after the reactions (2.14) and (2.15), these reactions are particularly useful to study parton correlations in the hadron. Both DVCS [37, 38, 39, 40, 41, 42] and HEMP [43, 44, 45, 46] are studied extensively at experimental facilities throughout the world.

The diagram in Fig. 2.4 is the off-forward generalization of the handbag diagram related to deep inelastic scattering. The parametrization of the blob now involves *generalized* parton distributions. In contrast with the PDFs, GPDs cannot be interpreted as probability distributions, as they are no longer related with the squared matrix element of deep inelastic scattering. Instead, GPDs should be seen as the *interference between amplitudes* which describe different hadron states. In the next paragraphs, we will focus on their definition and properties, starting with the GPDs of pseudoscalar mesons, which form the principal research topic in this work.

[5] Notice that the incoming and outgoing hadron are the same. When the outgoing hadron is different, one speaks of transition GPDs. These can be studied in a a straightforward generalization of the theory presented in this thesis.

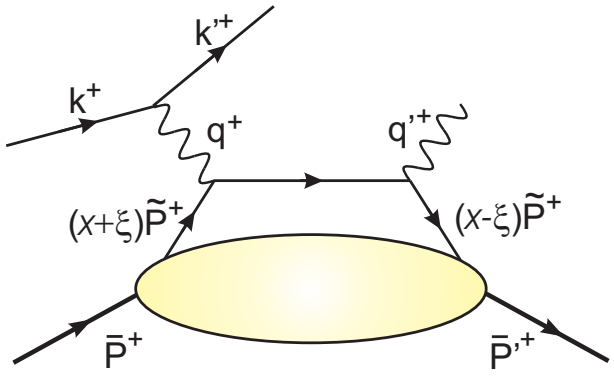

Figure 2.4 The diagram belonging to deeply virtual Compton scattering, Eq. (2.14), which is one of the processes that is described in terms of generalized parton distributions, through the factorization theorem.

2.2.1 Pseudoscalar mesons

Definition

In analogy with the definition of parton distribution functions (2.12), the twist-two generalized parton distribution related to the spin-$1/2$ partons (quarks) in a pseudoscalar meson[6] is defined through a bilocal matrix element of quark operators at a light-like separation [23]:

$$H^f(x,\xi,t) = \frac{1}{2}\int \frac{\mathrm{d}z^-}{2\pi} e^{ix\tilde{P}^+z^-} \left\langle \bar{P}'|\bar{\psi}^f(-\frac{z}{2})\gamma^+\psi^f(\frac{z}{2})|\bar{P}\right\rangle\Big|_{z^+=0,\mathbf{z}_\perp=\mathbf{0}} . \tag{2.16}$$

As before, f refers to the flavor of the probed parton and $\tilde{P}^\mu = \frac{\bar{P}^\mu+\bar{P}'^\mu}{2}$ is the average hadron four-momentum. The skewedness ξ and the average plus-momentum fraction of the struck parton x are defined in Fig. 2.4: x denotes the fraction of the average meson plus-momentum that is reabsorbed by the meson, while ξ is a measure for the plus-momentum that is lost in the process:

$$\xi = \frac{\bar{P}^+ - \bar{P}'^+}{\bar{P}^+ + \bar{P}'^+} . \tag{2.17}$$

These definitions coincide with the symmetrical variables that were introduced by Ji [47]. Their interpretation as plus-momentum fractions holds in the infinite momentum frame. In literature, another set of variables (X,ζ) has been introduced by Radyushkin [24], with $X = \frac{x+\xi}{1+\xi}$ and $\zeta = \frac{2\xi}{1+\xi}$. Although Radyushkin's variables are more closely related to the ones used in forward kinematics, we will use Ji's choice of variables, as they reflect the symmetry between the incoming and outgoing hadron states.

[6] A similar definition exists for the generalized *gluon* distribution. These distributions go beyond the scope of this work, as do the parton helicity changing generalized transversity distributions.

Definition (2.16) is valid in the case where the partons do not transfer helicity. Pseudoscalar mesons only have one such generalized *quark* distribution associated with them, whereas the nucleon has four (see next paragraph). The definition only holds in a coordinate system where $\boldsymbol{q}$ and $\tilde{\boldsymbol{P}}$ are collinear and in the three-direction [23]. From the above definition, it is clear that the GPDs are Lorentz invariant quantities. This means that, although they are defined on the light-cone, the GPDs can be calculated in any convenient reference frame, provided that the average transverse hadron momentum $\tilde{\boldsymbol{P}}_\perp = \boldsymbol{0}$. Whenever a specific choice is needed, we will choose a Breit frame which matches these conditions.

The skewedness ξ is restricted to the interval $[0, \xi_{max}]$ with

$$\xi_{max} = \sqrt{\frac{-t}{4M_m^2 - t}}\,, \tag{2.18}$$

where M_m is the meson mass. This equation is readily proven by using $t = \Delta^2$ and $|\boldsymbol{\Delta}_\perp|^2 \geq 0$, together with definition (2.17). The average plus-momentum fraction of the struck parton x is restricted to the interval $[-1, 1]$ since the partons are on-shell in the parton model (asymptotic freedom). An on-shell parton cannot carry a larger plus-momentum than the parent hadron, as this would require other partons to carry a negative plus-momentum, a condition which cannot be met by on-shell particles.

With these observations, the interpretation of the generalized parton distribution is found to be restricted to three regions, which are presented in Fig. 2.5:

- $x \in [-1, -\xi]$: emission and absorption of an antiquark,
- $x \in [-\xi, \xi]$: emission of both a quark and an antiquark, and
- $x \in [\xi, 1]$: emission and absorption of a quark.

These regions are referred to as the *support* regions of GPDs and will turn out to be of great importance in the remainder of this work. We will come back to them in Sect. 2.3.1.

Properties

In the introduction to this section, the generalized parton distribution was introduced through the analogy with parton distribution functions. It is important to remark that in general, $x \neq x_B$. In fact, applying four-momentum conservation to the process of Fig. 2.4, it is straightforward to prove that in the Bjorken limit,

$$\xi \approx \frac{x_B}{2 - x_B}\,. \tag{2.19}$$

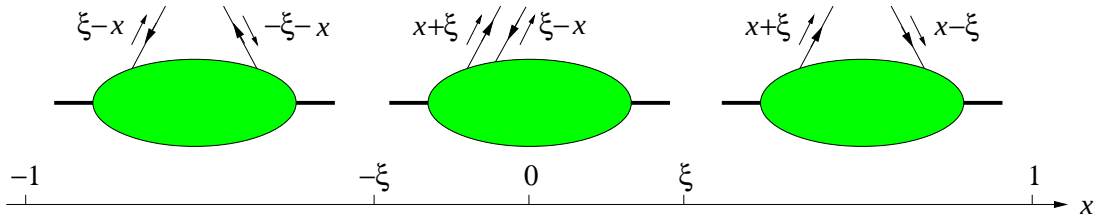

Figure 2.5 Schematic overview of the three distinct regions in the interpretation of generalized parton distributions. Figure taken from Ref. [25].

However, taking the forward limit of the generalized parton distributions, *i.e.* $t = 0$ and $\xi = 0$, the PDFs are retrieved as functions of x:

$$H^f(x, \xi = 0, t = 0) = f(x)\,. \tag{2.20}$$

The comparison of Eqs. (2.3) and (2.16) makes clear that GPDs are related to the electromagnetic form factors, both being defined through an off-diagonal matrix element. Their difference lies in the current operator used: the form factors are defined through a local current, while the GPDs imply the use of a bilocal current. Defining the partial electromagnetic form factors F^f as

$$F = \sum_f e_f F^f\,, \tag{2.21}$$

where e_f is the electric charge of a parton with flavor f, it is possible to write the form factors in terms of the GPDs:

$$\int dx H^f(x, \xi, t) = F^f(t)\,. \tag{2.22}$$

Remark that we have written $F^f(t)$ here instead of $F^f(Q^2)$, to be consistent with notation in DVCS kinematics where $Q^2 \to \infty$ while t remains finite. A simple interpretation of the above equation is that GPDs measure the contribution of quarks of a certain flavor and (average) longitudinal momentum fraction x to the form factor. As a result of Lorentz invariance, the ξ-dependence drops out when the GPD is integrated over x. Notice that neither the form factor nor the parton distribution functions depend on the skewedness. The fact that the GPDs are ξ-dependent shows that, besides providing a unifying framework of PDFs and form factors, DVCS is sensitive to physics which is absent in the "classic" elastic and deep inelastic scattering reactions.

Hence, it can be concluded that the generalized parton distributions present a natural unification of parton distribution functions and form factors. This is visualized in Fig. 2.6. The interpretation given in this picture holds for $\xi = 0$ in the infinite momentum frame (fast moving hadron) [48, 49], where $p^+_{parton} \to \infty$. We know that in this

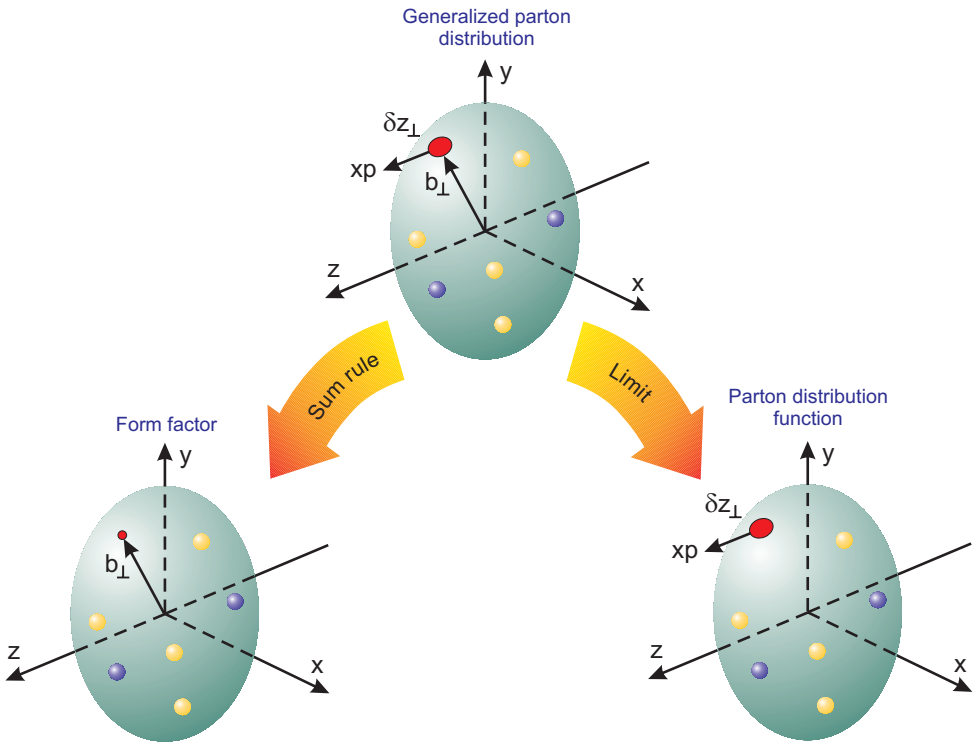

Figure 2.6 Schematic overview of the relation between generalized parton distributions, electromagnectic form factors and parton distribution functions.

frame, the parton distribution functions provide knowledge of the *longitudinal* parton momentum fractions inside the hadron. Moreover, the form factors can be interpreted as functions which encode the *transverse* localization of partons. As a result of the unification of form factors and PDFs in the framework of GPDs, the latter provide a three-dimensional picture of hadrons.

Using the operator product expansion, it can be proven that relation (2.22) is a special case of a more general relation, called the *polynomiality condition*, which states that the nth Mellin moment of the GPD is a polynomial in ξ of order $\leq n$ [23]:

$$\int \mathrm{d}x \; x^{n-1} H^f(x,\xi,t) = P_n^f(\xi,t)\,, \tag{2.23}$$

where the coefficients of the polynomial depend on t.

For pions, isospin invariance and charge conjugation lead to the following relation:

$$H^u_{\pi^+}(x,\xi,t) = -H^d_{\pi^+}(-x,\xi,t)\,. \tag{2.24}$$

Similar expressions exist for the π^- and π^0 GPD. Together with expressions (2.22) and (2.23), this relation will be used as a model check in Chapter 5.

2.2.2 Spin-$1/2$ baryons

Definition

Also for spin-$1/2$ baryons, the leading-twist generalized parton distributions are defined on the light-cone. Now, four functions need to be considered. The baryon GPDs H, E, $\tilde{H}$ and $\tilde{E}$ are defined as

$$\begin{aligned} A_{\lambda'\lambda} &= \frac{1}{2}\int\frac{\mathrm{d}z^-}{2\pi}e^{ix\tilde{P}^+z^-}\,\langle\bar{P}',\lambda'|N\{\bar{\psi}^f(-\frac{z}{2})\gamma^+\psi^f(\frac{z}{2})\}|\bar{P},\lambda\rangle\Big|_{z^+=0,\mathbf{z}_\perp=\mathbf{0}} \\ &= \frac{1}{2\tilde{P}^+}\left[H^f(x,\xi,t)\bar{u}_{\lambda'}(\bar{P}')\gamma^+u_\lambda(\bar{P}) + E^f(x,\xi,t)\bar{u}_{\lambda'}(\bar{P}')\frac{i\sigma^{+\alpha}\Delta_\alpha}{2M_b}u_\lambda(\bar{P})\right], \\ \tilde{A}_{\lambda'\lambda} &= \frac{1}{2}\int\frac{\mathrm{d}z^-}{2\pi}e^{ix\tilde{P}^+z^-}\,\langle\bar{P}',\lambda'|N\{\bar{\psi}^f(-\frac{z}{2})\gamma^+\gamma^5\psi^f(\frac{z}{2})\}|\bar{P},\lambda\rangle\Big|_{z^+=0,\mathbf{z}_\perp=\mathbf{0}} \\ &= \frac{1}{2\tilde{P}^+}\left[\tilde{H}^f(x,\xi,t)\bar{u}_{\lambda'}(\bar{P}')\gamma^+\gamma^5u_\lambda(\bar{P}) + \tilde{E}^f(x,\xi,t)\bar{u}_{\lambda'}(\bar{P}')\frac{i\gamma^5\Delta^+}{2M_b}u_\lambda(\bar{P})\right]. \end{aligned} \tag{2.25}$$

The GPD of pseudoscalar mesons is the analogue of the nucleon GPD H. The analogue of $\tilde{H}$ is zero because of parity invariance. The definition of the kinematical variables x, ξ and t, as well as the coordinate system in the above equations is the same as above.

With the matrix elements A and $\tilde{A}$ of Eq. (2.25), it can be proven that the generalized parton distributions H, E, $\tilde{H}$ and $\tilde{E}$ are found through the system of equations [25]

$$\begin{aligned} A_{++} &= A_{--} = \sqrt{1-\xi^2}\left(H - \frac{\xi^2}{1-\xi^2}E\right), \\ \tilde{A}_{++} &= -\tilde{A}_{--} = \sqrt{1-\xi^2}\left(\tilde{H} - \frac{\xi^2}{1-\xi^2}\tilde{E}\right), \\ A_{+-} &= -A^*_{+-} = e^{i\varphi}\frac{\sqrt{t_0-t}}{2M_b}E, \\ \tilde{A}_{-+} &= \tilde{A}^*_{+-} = e^{i\varphi}\frac{\sqrt{t_0-t}}{2M_b}\xi\tilde{E}. \end{aligned} \tag{2.26}$$

Here, t_0 is defined as

$$t_0 = -\frac{4\xi^2M_b^2}{1-\xi^2}, \tag{2.27}$$

while φ is the azimuthal angle of the vector

$$D = \frac{\bar{P}'}{1-\xi} - \frac{\bar{P}}{1+\xi}, \tag{2.28}$$

so that

$$e^{i\phi} = \frac{D^1 + iD^2}{|\boldsymbol{D}|}. \tag{2.29}$$

Equations (2.26) are helpful in extracting the nucleon generalized parton distributions from model calculations of the bilocal current matrix elements A and $\tilde{A}$.

Properties

Most of the properties for the GPDs of pseudoscalar mesons have their analogue for spin-$1/2$ baryons. The generalization of the form factor sum rule reads

$$\begin{aligned}
\int \mathrm{d}x H^f(x,\xi,t) &= F_1^f(t)\,, \\
\int \mathrm{d}x E^f(x,\xi,t) &= F_2^f(t)\,, \\
\int \mathrm{d}x \tilde{H}^f(x,\xi,t) &= g_A^f(t)\,, \\
\int \mathrm{d}x \tilde{E}^f(x,\xi,t) &= g_P^f(t)\,,
\end{aligned} \tag{2.30}$$

where the axial and pseudoscalar form factors g_A and g_P are the equivalents of the Dirac and Pauli form factors, defined by replacing the vector current by an axial vector current in Eq. (2.4). Also the polynomiality property holds for spin-$1/2$ baryons. We give the expressions for the Mellin moment of order $(n+1)$ where the resulting polynomials have a maximal order of $(n+1)$ for H and E and n for $\tilde{H}$ and $\tilde{E}$:

$$\begin{aligned}
\int \mathrm{d}x\; x^n H^f(x,\xi,t) &= \sum_{\substack{i=0\\ \text{even}}}^{n} (2\xi)^i A_{n+1,i}^f(t) + mod(n,2)(2\xi)^{n+1} C_{n+1}^f(t)\,, \\
\int \mathrm{d}x\; x^n E^f(x,\xi,t) &= \sum_{\substack{i=0\\ \text{even}}}^{n} (2\xi)^i B_{n+1,i}^f(t) - mod(n,2)(2\xi)^{n+1} C_{n+1}^f(t)\,, \\
\int \mathrm{d}x\; x^n \tilde{H}^f(x,\xi,t) &= \sum_{\substack{i=0\\ \text{even}}}^{n} (2\xi)^i \tilde{A}_{n+1,i}^f(t)\,, \\
\int \mathrm{d}x\; x^n \tilde{E}^f(x,\xi,t) &= \sum_{\substack{i=0\\ \text{even}}}^{n} (2\xi)^i \tilde{B}_{n+1,i}^f(t)\,,
\end{aligned} \tag{2.31}$$

with $A_{n+1,i}$, $\tilde{A}_{n+1,i}$, $B_{n+1,i}$, $\tilde{B}_{n+1,i}$ and $C_{n+1,i}$ the t-dependent *generalized form factors*. The forward limits of the GPDs read

$$\begin{aligned}
H^f(x,0,0) &= f(x)\,, \\
\tilde{H}^f(x,0,0) &= \Delta f(x)\,,
\end{aligned} \tag{2.32}$$

for quarks, with analogous relations for antiquarks. The functions Δf are the helicity distributions, defined by the difference between the number densities of quarks with a positive helicity and those with a negative helicity (in a positive helicity baryon). The GPDs E and $\tilde{E}$ do not appear in the theory of deep inelastic scattering, as they

are multiplied with $\Delta = (\bar{P}' - \bar{P})$ in the defining equations (2.25). Indeed, $\Delta = 0$ in the forward process of Fig. 2.3. As a result, the forward limit $t = \xi = 0$ to these functions can only be found via exclusive processes with a finite momentum transfer to the target, giving access to new physics. As an example, we mention the possibility to measure the orbital angular momentum of the quarks, which might well be one of the most intriguing aspects of the spin-$1/2$ GPDs. It can be proven [23, 50] that in the limit $t \to 0$, the angular momentum carried by the quarks is found through the sum rule

$$\langle J_f^3 \rangle = \lim_{t\to 0} \frac{1}{2} \int \mathrm{d}x \, x \left(H^f(x,\xi,t) + E^f(x,\xi,t) \right) , \tag{2.33}$$

where the ξ-dependence drops out according to Eq. (2.31). It was precisely this property that gave rise to the revival of GPD research, as it might offer an outcome of the intriguing *proton spin puzzle* [51]. For pseudoscalar mesons, such a sum rule does not exist, so that the orbital angular momentum of the quarks in the pion cannot be measured via the GPDs [52].

2.3 Models for generalized parton distributions

In the above equations, we have defined the generalized parton distributions and parton distribution functions as Q^2-independent quantities. It seems logical that this can only be an approximation, as Q^2 defines the resolution with which one looks at the hadron. At low energy scales, mainly the valence quarks are resolved, while more and more $q\bar{q}$ pairs and gluons are probed when Q^2 increases. This intuitive picture is proved correct in QCD, where it is found that the PDFs and GPDs are scale-dependent and that radiative corrections should be included. As a consequence, the distribution functions evolve with Q^2. The relation between the functions at different Q^2 is given by the *evolution equations*: once they are known at a certain scale (Q_0^2), they can be calculated at any other scale.

In this section, we comment on the evolution of generalized parton distributions, starting from a prediction at an initial scale Q_0^2. We point out that dynamic models can be used to predict the GPD at low scales, and give an overview of model approaches that are discussed in literature.

2.3.1 Evolution equations

The evolution of PDFs and GPDs to other energy scales is described in a similar, but not entirely equal fashion. The regular parton distribution functions are evolved through

the Dokshitzer-Gribov-Lipatov-Altarelli-Parisi or DGLAP equations [53, 54, 55]. The observation that these equations neatly describe the Q^2-dependence of the proton electromagnetic structure functions was a tremendous success of perturbative QCD. In the case of generalized parton distributions, the situation is slightly different. As we have seen in Sect. 2.2.1, the finite momentum transfer to the hadron allows for three regions to be distinguished (see Fig. 2.5). For $x \in [\xi, 1]$ and $x \in [-1, -\xi]$, a "classic" handbag diagram emerges and the process can be interpreted as the emission and absorption of a parton (either a quark or an antiquark). In these kinematical regimes, the GPDs follow the DGLAP evolution equations. When $x \in [-\xi, \xi]$, both a quark and an antiquark are emitted, and the correlation matrix element describes the amplitude for taking out a $q\bar{q}$ pair with momentum $-\Delta$. In this case, which has no counterpart in forward parton distribution functions due to their ξ-independence, the evolution follows the Efremov-Radyushkin-Brodsky-Lepage or ERBL equations [56, 57].

It is interesting to remark that also Mellin moments of (valence) quark distribution functions can be evolved [34]. It follows from the non-singlet evolution equations that

$$\int \mathrm{d}x\; x^{n-1} f_{valence}(x, Q^2) = \left(\frac{\alpha_s(Q^2)}{\alpha_s(Q_0^2)}\right)^{d_{ns}^{(0),n}} \int \mathrm{d}x\; x^{n-1} f_{valence}(x, Q_0^2) \tag{2.34}$$

where $d_{ns}^{(0),n} \geq 0$ is defined through the "splitting function" which enters the DGLAP equations and depends on the order of the moment. For the GPDs, this relation is only valid when $\xi = 0$.

With the DGLAP and ERBL equations, the distribution functions can be calculated at any scale Q^2, provided that their value at a scale Q_0^2 is known. Unfortunately, parton distributions are soft, non-perturbative QCD quantities whose calculation from first principles is not feasible at present. In the next paragraph, we will see how dynamic models can be used to predict this value.

2.3.2 Linking perturbative and non-perturbative physics

In essence, calculating PDFs and GPDs boils down to the calculation of a bilocal current matrix element (see Eqs. (2.12) and (2.16)). Such matrix elements can be computed in a constituent quark model, as we will discuss extensively in the forthcoming chapters. In 1980, Jaffe [58] proposed the use of a quark model, namely the MIT bag model, to predict the value of the twist-two matrix element, and to use that prediction in the evolution equations to calculate the distribution functions at a higher Q^2 (where the twist-two matrix element is the leading contribution).

In most constituent quark models, a hadron is described in terms of the valence quarks. Because this picture is only valid at a low scale in QCD, the model calculation will yield an estimate of the matrix element at low Q^2. This means that the evolution equations from perturbative QCD need to be extrapolated to this low scale. The justification of this approach lies in the validity of its results [58, 59, 60].

It is important to remark that constituent quark models are not necessarily compatible with the parton model. In many models, the constituent quarks are off-shell in general, even after a boost to the infinite momentum frame. As such, it might happen that the distribution functions do not disappear for $|x| > 1$ [58, 61, 62, 63]. One then speaks of a *support problem* or a *support violation*, since the support of these functions is restricted to the region $|x| < 1$. As yet, it is not clear how the evolution should be performed when this happens, making the comparison with experimental data (which are gathered at high Q^2), and even with other models (which in general have a different intrinsic scale) difficult.

2.3.3 Model approaches

In literature, various ways are described to calculate generalized parton distributions. Lattice simulations of the Mellin moments are available for both the nucleon [64, 65, 66] and pion [67, 68] GPDs. These moments yield important information, e.g. regarding the quark angular momentum in the nucleon. To gain information on the functional form of the GPDs, however, one has to rely on model predictions.

In general, two model based approaches can be distinguished. First, one can search for *parametrizations* of the GPDs. This can be done by expressing the bilocal current matrix elements in terms of the so-called double distributions [22, 69, 70], defined through a Fourier transform of the matrix element in two Lorentz scalars. Other ways to parametrize GPDs start from GPD properties such as its forward limit and form factor sum rule [71], by fitting to data and lattice results [72], etc.

The second approach is to calculate the GPDs directly in a specific *dynamic model*. The first model calculation was performed in the MIT bag model [73]. Later, several other models have been investigated, *a.o.* the chiral quark soliton model [74], the meson-cloud model [75, 76] and various non-relativistic [60, 61], relativized [77, 78] and intrinsically covariant [62, 79, 80, 81, 82, 83, 84, 85, 86, 87] constituent quark models.

In this work we present the first calculations of GPDs within the framework of the Bonn constituent quark model. This Poincaré covariant model is based on the Bethe-Salpeter formalism.

3 The Bonn model

Models are to be used, not believed.

H. Theil

3.1 Constituent quark models

When Gell-Mann, Ne'eman and Zweig proposed the existence of quarks as the fundamental degrees of freedom in hadrons, they revolutionized the field of hadron physics. Before the 1960s, hadrons were considered elementary, even though their abundance in high-energy experiments hinted at the existence of a substructure. With the newly proposed $SU(3)_f$ group[1], the hadron "zoo" could be classified into multiplets of this group. The light quarks u, d and s form the fundamental triplet and, likewise, the antiquarks $\bar{u}$, $\bar{d}$ and $\bar{s}$ form the corresponding antitriplet. The quarks could be identified as the constituents of matter due to the mathematical property of $SU(n)$ groups that all higher-dimensional representations (multiplets) can be built from direct products of the fundamental representation(s). This classification is known as the *Eightfold Way*. Mesons are $q\bar{q}$ bound states in $SU(3)_f$, while baryons are qqq bound states. Precisely this picture forms the basis of the constituent quark model (CQM): the quark-sea and gluon degrees of freedom are effectively described in terms of *constituent quarks* with a phenomenological mass, a concept that was introduced in Chapter 1 of this thesis.

The first CQM which included dynamics and could go beyond the ground states was the one of Isgur and Karl [88, 89]. It is a non-relativistic model, based on the Schrödinger equation with a harmonic-oscillator potential. Although non-relativistic CQMs are conceptually simple, they are able to predict the correct hadron multiplets and even some hadron masses. But when it comes to dynamic properties of hadrons,

[1] $SU(3)_f$ is the *flavor-*$SU(3)$ group and should not be confused with the *color-*$SU(3)_c$ gauge group of QCD.

such as electromagnetic form factors or decay widths, the non-relativistic CQM fails [90]. Inclusion of elements of relativity often improves the description of the data, yielding a so-called relativized CQM. However, by doing so, one introduces additional parameters, thereby lowering the predictive power of the model. An alternative strategy is to abandon the use of the Schrödinger equation and to construct a relativistic model, starting from the Lorentz covariant Bethe-Salpeter equation. In this way, there is no direct need for additional parameters, while the conceptual simplicity of the constituent quark model is maintained. An additional advantage of the formal covariance of the model is the fact that negative energy components of the fields are included. This is important in the calculation of GPDs, as these negative energy components allow us to study the contribution to the ERBL region of the GPDs without any need for model truncation. However, in Chapter 5, it will be pointed out how studying the support regions hints at the limitations of various models.

The Bethe-Salpeter formalism that is adopted in this work was developed at Bonn University. A detailed description of the meson model can be found in Refs. [19, 91, 90, 92]. The baryon model is nicely described in Refs. [93, 94, 95, 96]. In the next sections, the characteristics of the Bonn model will be reviewed. The main subject of this work is the pion GPD in the Bonn model, so the focus will be on the model for mesons. In App. C, the most peculiar features of the Bonn model for baryons are highlighted.

3.2 The Bethe-Salpeter equation for mesons

3.2.1 The four-point Green's function

In relativistic quantum field theory, a system of two interacting fermions is described by the four-point Green's function,

$$G_{\alpha\alpha'\beta\beta'}(x_1', x_2'; x_1, x_2) = -\langle\Theta|T\{\psi^1_\alpha(x_1')\bar{\psi}^2_\beta(x_2')\psi^2_{\beta'}(x_2)\bar{\psi}^1_{\alpha'}(x_1)\}|\Theta\rangle\,, \tag{3.1}$$

where T is the time ordering operator acting on the Heisenberg fermion field operators ψ_α, which were introduced in Eq. (2.2). $|\Theta\rangle$ denotes the physical (Heisenberg) ground state. The indices in Dirac, flavor and color space are combined in the multi-indices $\alpha \equiv (\alpha, f, c)$, which will often be left out to keep the notation concise. In the remainder of this chapter, the quark (antiquark) field will always be given a superscript 1 (2).

In one specific time ordering, the four-point Green's function G gives the probability that a fermion-antifermion bound pair propagates from space-time coordinates (x_1, x_2) to space-time coordinates (x_1', x_2'). Due to the interactions between the con-

stituents and the self-interactions of the constituents, the four-point Green's function G contains an infinite number of diagrams, as depicted in Fig. 3.1.

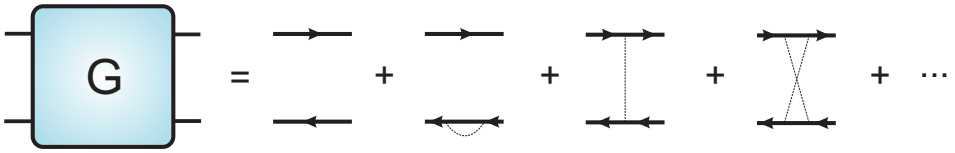

Figure 3.1 The diagrams which contribute to the four-point Green's function of Eq. (3.1).

Introducing the interaction kernel K and the full quark propagator $S_F(x_1', x_1) = \langle\Theta|N\{\psi(x_1')\bar{\psi}(x_1)\}|\Theta\rangle$, the Green's function can be rewritten in a compact form. The quark propagator S_F represents a bare quark which is dressed with self-interactions. The interaction kernel K is depicted in Fig. 3.2. It contains all the *irreducible* interquark interaction diagrams. These diagrams are defined as graphs which cannot be split into two simpler graphs by cutting only two (internal) fermion lines.

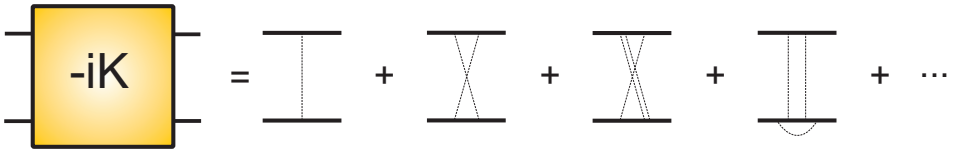

Figure 3.2 Two-particle irreducible Feynman diagrams contributing to the kernel K in Eq. (3.2).

Gell-Mann and Low have provided a rigorous proof for the following inhomogeneous integral equation of the four-point Green's function [97]:

$$\begin{aligned} G_{\alpha\alpha'\beta\beta'}(x_1', x_2'; x_1, x_2) &= S^1_{F\alpha\alpha'}(x_1', x_1) S^2_{F\beta\beta'}(x_2, x_2') \\ &\quad - i \int \mathrm{d}^4 y_1 \int \mathrm{d}^4 y_2 \int \mathrm{d}^4 y_1' \int \mathrm{d}^4 y_2' \; S^1_{F\alpha\gamma}(x_1', y_1') S^2_{F\beta\delta}(y_2', x_2') \\ &\quad \times K_{\gamma\gamma'\delta\delta'}(y_1', y_2'; y_1, y_2) G_{\gamma'\alpha'\delta'\beta'}(y_1, y_2; x_1, x_2)\,. \end{aligned} \tag{3.2}$$

The graphical representation of this equation is given in Fig. 3.3.

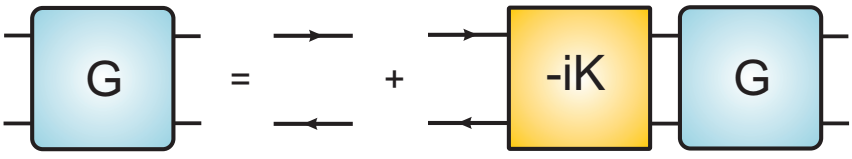

Figure 3.3 Graphical representation of the four-point Green's function as given by the equation of Gell-Mann and Low (3.2).

With the conventions from Appendix A, we can write Eq. (3.2) in a shorthand way as

$$G = G_0 - iG_0KG = G_0 - iGKG_0\,. \tag{3.3}$$

In this equation, the free Green's function G_0 was defined as a direct product of the full quark propagators:

$$G_{0\alpha\alpha'\beta\beta'}(x_1', x_2'; x_1, x_2) = S^1_{F\alpha\alpha'}(x_1', x_1) S^2_{F\beta\beta'}(x_2, x_2') \,. \tag{3.4}$$

With the interaction kernel K and the free Green's function G_0, all diagrams of the four-point Green's function G can be found by iteration, just as Eq. (3.2) states.

In the remainder of this work we will frequently make use of the the Fourier transforms of the above-mentioned quantities. Due to the translational invariance of the Green's function, it is instructive to introduce the Jacobi coordinates[2]:

$$\left\{ \begin{array}{lcl} X &=& \eta_1 x_1 + \eta_2 x_2 \\ \zeta &=& x_1 - x_2 \end{array} \right. \quad \text{and} \quad \left\{ \begin{array}{lcl} P &=& p_1 + p_2 \\ p &=& \eta_2 p_1 - \eta_1 p_2 \end{array} \right. . \tag{3.5}$$

The parameters η_1 and η_2 are only constrained by $\eta_1 + \eta_2 = 1$. In the following, we will choose $\eta_1 = \eta_2 = \frac{1}{2}$. The transformation (3.5) has a Jacobian $|\mathcal{J}| = 1$. With the Jacobi coordinates, the four-point Green's function (3.1) can be rewritten as follows:

$$G(x_1', x_2'; x_1, x_2) \equiv G(X' - X; \zeta', \zeta) \,, \tag{3.6}$$

where the dependence on the difference between X and X' reflects translational invariance. It is clear that a similar expression holds for the free Green's function G_0 and the interaction kernel K. In momentum space, translational invariance is equivalent to the conservation of the total four-momentum, so that the Fourier transform of a general four-point function F can now be defined as

$$F(x_1', x_2'; x_1, x_2) \equiv \int \frac{\mathrm{d}^4 P}{(2\pi)^4} e^{iP\cdot(X'-X)} \int \frac{\mathrm{d}^4 p}{(2\pi)^4} e^{-ip\cdot\zeta} \int \frac{\mathrm{d}^4 p'}{(2\pi)^4} e^{ip'\cdot\zeta'} F_P(p', p) \,. \tag{3.7}$$

The total four-momentum P is written as a subscript to the four-point function in momentum space, because F depends only parametrically on P (*i.e.*, in the Fourier transform of a relation between Green's functions and kernels such as Eq. (3.3), all Green's functions and kernels effectively depend on the same total four-momentum P).

3.2.2 Bound state contributions

To investigate the bound state contributions to the four-point Green's function, consider a bound $q\bar{q}$ system with on-shell four-momentum $\bar{P}^\mu = (\omega_P, \boldsymbol{P})$ and (positive) mass M. The energy of this state can be written as $\omega_P = \sqrt{|\boldsymbol{P}|^2 + M^2}$; its momentum

[2] Note that the Jacobi coordinates X and ζ are not related to Radyushkin's set of GPD variables which were mentioned in Sect. 2.2.1. The former denote space-time coordinates, while the latter refer to plus-momentum fractions.

eigenstate in the $q\bar{q}$ sector of Fock space is denoted by $|\bar{P}\rangle$, with a covariant normalization according to

$$\langle \bar{P}|\bar{P}'\rangle = (2\pi)^3 2\omega_P \delta^{(3)}(\boldsymbol{P}-\boldsymbol{P}')\,. \tag{3.8}$$

This meson is described by the Bethe-Salpeter amplitude

$$\chi_{\bar{P}\alpha\beta}(x_1,x_2) = \langle\Theta|T\{\psi^1_\alpha(x_1)\bar{\psi}^2_\beta(x_2)\}|\bar{P}\rangle\,, \tag{3.9}$$

and the adjoint Bethe-Salpeter amplitude

$$\bar{\chi}_{\bar{P}\beta\alpha}(x_1,x_2) = \langle\bar{P}|T\{\psi^2_\beta(x_2)\bar{\psi}^1_\alpha(x_1)\}|\Theta\rangle\,. \tag{3.10}$$

In momentum space, the Bethe-Salpeter amplitude and its adjoint are defined as follows:

$$\begin{aligned}\chi_{\bar{P}}(x_1,x_2) &= e^{-i\bar{P}\cdot X}\chi_{\bar{P}}(\zeta)\\ &= e^{-i\bar{P}\cdot X}\int\frac{\mathrm{d}^4p}{(2\pi)^4}e^{-ip\cdot\zeta}\chi_{\bar{P}}(p)\,, \qquad (3.11)\\ \bar{\chi}_{\bar{P}}(x_1,x_2) &= e^{i\bar{P}\cdot X}\bar{\chi}_{\bar{P}}(\zeta)\\ &= e^{i\bar{P}\cdot X}\int\frac{\mathrm{d}^4p}{(2\pi)^4}e^{ip\cdot\zeta}\bar{\chi}_{\bar{P}}(p)\,, \qquad (3.12)\end{aligned}$$

In the above equations, the $\bar{P}$-dependent phase on the right-hand side is the result of a translation of the Bethe-Salpeter amplitude.

In quantum field theory, bound states are related to the occurrence of poles in the total energy variable P^0 in the Green's functions. It can be proven that the residue of the four-point Green's function at these bound state poles is proportional to the product of the Bethe-Salpeter amplitude χ and its adjoint $\bar{\chi}$ [92, 98]:

$$G_{\bar{P}}(p',p) \xrightarrow{P^0\to\omega_P} -\frac{i}{(2\pi^4)}\frac{1}{2\omega_P}\frac{\chi_{\bar{P}}(p')\bar{\chi}_{\bar{P}}(p)}{(P^0-\omega_P+i\epsilon)} + \text{terms regular for } P^0\to\omega_P\,. \tag{3.13}$$

From Eqs. (3.2) and (3.13), the Bethe-Salpeter equation can be derived [92, 99]:

$$\chi_{\bar{P}} = -iG_{0\bar{P}}K_{\bar{P}}\chi_{\bar{P}}\,, \tag{3.14}$$

with the normalization equation:

$$\bar{\chi}_{\bar{P}}\left[P^\mu\frac{\partial}{\partial P^\mu}(G^{-1}_{0P}+iK_P)\right]_{P=\bar{P}}\chi_{\bar{P}} = 2iM^2\,. \tag{3.15}$$

Note that eq. (3.15) is written in a frame independent way. The diagrammatic analogue of Eq. (3.14) is presented in Fig. 3.4.

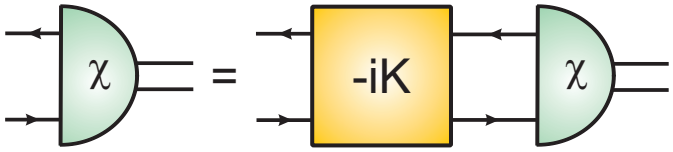

Figure 3.4 Diagrammatic representation of the Bethe-Salpeter equation (3.14).

3.3 Reduction to the Salpeter equation

In principle, the Bethe-Salpeter equation (3.14) and the normalization condition (3.15) would be the ideal starting point for a covariant description of mesons as $q\bar{q}$ bound states. Given the single quark propagators S_F and the interaction kernel K, the full $q\bar{q}$ spectrum can be calculated. Unfortunately, both S_F and K are only formal quantities at this point, defined as infinite sums of (self-)interaction diagrams. To calculate static and dynamic properties of mesons, suitable approximations are required.

Various methods to reduce the Bethe-Salpeter equation have been outlined in literature. To start with, one can assume that the Bethe-Salpeter amplitude depends on the relative four-momentum p only through the single quark propagators S_F, which are multiplied by a constant (with respect to the relative momentum):

$$\chi_{\bar{P}\alpha\beta}(p) = gS^1_{F\alpha\alpha'}(\frac{\bar{P}}{2}+p)\lambda_{\alpha'\beta'}S^2_{F\beta'\beta}(\frac{\bar{P}}{2}-p)\,, \tag{3.16}$$

where g and λ do not depend on the momentum. The assumptions made in the effective chiral quark model of Nambu and Jona-Lasinio, commonly known as the NJL model [100, 101], lead to this form. In this model, g is proportional to the quark-pion coupling constant, $g = -ig_{\pi pp}$, and $\lambda = \boldsymbol{\tau}\gamma_5$ with τ the isospin Pauli matrices [79].

Another option is to perform a three-dimensional reduction of the Bethe-Salpeter equation, a so-called *instantaneous approximation*. In Refs. [81, 82, 83], such a reduction is performed on the light-front in the scalar Wick-Cutkosky model by assuming the potentials to be p^--independent. Refs. [84, 85, 86] also present a light-front reduction, but they follow a slightly different approach and replace the Bethe-Salpeter amplitudes by wave functions obtained in a light-front quark model. In the Bonn model, however, the three-dimensional reduction is performed in the instant frame, because of the functional dependence of the confining potential on the length of the three-vector $\boldsymbol{r} = \boldsymbol{x}_1 - \boldsymbol{x}_2$, following the successful non-relativistic CQMs. This choice was made since a four-dimensional confinement potential does not lead to a discrete spectrum [102]. The same approximation will be adopted for the residual 't Hooft interaction. Both the confinement potential and the 't Hooft interaction will be introduced in Section 3.5.2.

The choice of an interaction kernel which is instantaneous in the instant frame is not without ambiguities when computing a light-front quantity such as the GPD. This approximation *could* give rise to a support problem (see Chapter 5). The mere equations do not help to draw conclusions with regard to the support problem, however. Moreover, the results of the electromagnetic form factor calculations in the Bonn model are very promising [19, 103, 104]. Consequently, an explicit calculation of the GPDs in the model is needed to clarify the issue.

3.3.1 Approximations

To perform the three-dimensional reduction in a consistent manner, two assumptions are made in the Bonn model. The first concerns the interaction kernel, while the second has an impact on the quark propagators. These *Ansätze* are discussed in more detail below.

Interaction kernel

First, the interaction kernel is chosen to be independent of the relative energy variable in the rest frame of the meson. As mentioned above, this approximation will be referred to as the instantaneous approximation, because assuming an independence of the relative energy variables corresponds to adding a δ-function that depends on the relative time variables in configuration space, $\delta(x'^0 - x^0)$.

In the meson rest frame, we can write this assumption as follows:

$$K_{\bar{P}}(p', p)\Big|_{\bar{P}=(M,\mathbf{0})} = V(\boldsymbol{p}', \boldsymbol{p})\,. \tag{3.17}$$

This approximation makes sure that a close connection is maintained with the non-relativistic CQM, which can describe the gross features of the meson spectrum surprisingly well and which uses static two-quark potentials. Nevertheless, the instantaneous approximation does not destroy the formal covariance of the model. Equation (3.17) can be formulated covariantly as follows [105]:

$$K_{\bar{P}}(p', p) \equiv V(p'_{\perp\bar{P}}, p_{\perp\bar{P}}), \tag{3.18}$$

where $p^\mu_{\perp P} \equiv p^\mu - (p\cdot P/P^2)P^\mu$ is the four-vector perpendicular to P with p the relative four-momentum between the constituent quark and the constituent antiquark in the meson. Similarly, a scalar component can be defined which is parallel to P: $p_{\parallel P} \equiv (p\cdot P)/\sqrt{P^2}$. In the rest frame of a meson with $P^\mu = \bar{P}^\mu = (M, \mathbf{0})$, these new variables simplify to $p^\mu_{\perp P} = (0, \boldsymbol{p})$ and $p_{\parallel P} = p^0$. In the remainder of this thesis, equations will

often be defined in the meson rest frame. It is clear that these equations can be written covariantly with the above-mentioned definitions.

Quark propagator

The full or "dressed" quark propagator consists of an infinite sum of terms and can be written as follows [11]:

$$S_F(p) = \frac{i}{\not{p} - m_0 - \Sigma(\not{p}) + i\epsilon}\,. \tag{3.19}$$

The second approximation in the Bonn model states that the momentum-dependent self-energy Σ can be replaced by a constant. In other words, the full quark propagators $S_F^j(p)$ are replaced by free fermion propagators with an effective constituent quark mass m_j:

$$S_F^j(p) \equiv \frac{i}{\not{p} - m_j + i\epsilon} \qquad \text{with } j = 1, 2\,. \tag{3.20}$$

The constituent quark masses m_j are model parameters. Because isospin symmetry is assumed exact in the Bonn model, the calculation of the low-lying meson spectrum requires only two mass parameters: the non-strange quark mass $m_u = m_d = m_n$ and the strange quark mass m_s.

3.3.2 Salpeter equation

With the instantaneous approximation of Eq. (3.18), the Bethe-Salpeter equation can be reduced to a form which is easier to solve. In particular, the specific structure of the quark propagators, Eq. (3.20), allows for an analytical integration over the relative energy components in Eq. (3.14) by making use of the residue theorem [98].

Defining the Salpeter amplitude $\Phi(\boldsymbol{p})$ in the rest frame of the bound state as

$$\Phi(\boldsymbol{p}) = \int \frac{\mathrm{d}p^0}{2\pi} \chi_{\bar{P}}(p^0, \boldsymbol{p})\Big|_{\bar{P}=(M,\boldsymbol{0})}\,, \tag{3.21}$$

the Salpeter equation can be written [106]:

$$\begin{aligned}\Phi(\boldsymbol{p}) = &\int \frac{\mathrm{d}^3p'}{(2\pi)^3} \frac{\Lambda_1^-(\boldsymbol{p})\gamma^0[V(\boldsymbol{p},\boldsymbol{p'})\Phi(\boldsymbol{p'})]\gamma^0\Lambda_2^+(-\boldsymbol{p})}{M + \omega_1 + \omega_2} \\ &- \int \frac{\mathrm{d}^3p'}{(2\pi)^3} \frac{\Lambda_1^+(\boldsymbol{p})\gamma^0[V(\boldsymbol{p},\boldsymbol{p'})\Phi(\boldsymbol{p'})]\gamma^0\Lambda_2^-(-\boldsymbol{p})}{M - \omega_1 - \omega_2}\,,\end{aligned} \tag{3.22}$$

with the energy projection operators $\Lambda_j^\pm = (\omega_j \pm H_j)/(2\omega_j)$, the Dirac Hamiltonian $H_j(\boldsymbol{p}) = \gamma^0(\boldsymbol{\gamma}\cdot\boldsymbol{p} + m_j)$ and the energy $\omega_j = \sqrt{m_j^2 + |\boldsymbol{p}|^2}$ for the jth constituent quark.

Also the normalization condition (3.15) can be rewritten in terms of the Salpeter amplitudes [92]. In the meson rest frame, it reads:

$$\int \frac{\mathrm{d}^3 p}{(2\pi)^3} Tr[\Phi_1^\dagger(\boldsymbol{p})\Lambda_1^+(\boldsymbol{p})\Phi_2(\boldsymbol{p})\Lambda_2^-(-\boldsymbol{p}) - \Phi_1^\dagger(\boldsymbol{p})\Lambda_1^-(\boldsymbol{p})\Phi(\boldsymbol{p})\Lambda_2^+(-\boldsymbol{p})] = 2M\,. \tag{3.23}$$

The Salpeter amplitudes Φ are calculated by solving Eq. (3.22). Imposing normalization condition (3.23) yields the mass spectrum [91].

Despite the above-mentioned assumptions, the interaction potential in Eqs. (3.22) and (3.23) still consists of a sum over an infinite number of interaction diagrams. In practice, the interaction kernel needs to be approximated by reducing it to a well-chosen, finite amount of interaction terms. Due to the complexity of the second-order terms and their corresponding limited applicability, the Bonn model adopts a lowest-order approximation (Born approximation, see Ref. [93] for a detailed discussion in the framework of the baryon model).

3.4 Reconstruction of the Bethe-Salpeter amplitudes

The Bonn model allows for a simultaneous calculation of both the $q\bar{q}$ meson mass spectrum and the Salpeter amplitudes of the meson bound states. For the calculation of generalized parton distributions in the Bonn model, it is important to reconstruct the Bethe-Salpeter amplitudes from the Salpeter amplitudes. We therefore define the vertex function as the *amputated* Bethe-Salpeter amplitude, describing the meson vertex without the quark propagators:

$$\Gamma_{\bar{P}}(p) = \left[S_F^1\right]^{-1}(p_1)\chi_{\bar{P}}(p)\left[S_F^2\right]^{-1}(-p_2)\,. \tag{3.24}$$

Inserting the vertex function into the Bethe-Salpeter equation (3.14) and making use of Eq. (3.21), we find:

$$\begin{aligned}\Gamma_{\bar{P}}(p)|_{\bar{P}=(M,\mathbf{0})} &= -i\int \frac{\mathrm{d}^3 p'}{(2\pi)^3} V(\boldsymbol{p},\boldsymbol{p}')\Phi(\boldsymbol{p}') \\ &= \Gamma_M(\boldsymbol{p})\,.\end{aligned} \tag{3.25}$$

Knowing the Salpeter amplitudes $\Phi(\boldsymbol{p})$, the vertex functions $\Gamma_M(\boldsymbol{p})$ can be found with Eq. (3.25). The Bethe-Salpeter amplitude $\chi_{\bar{P}}(p)$ can then be reconstructed by means of Eq. (3.24).

3.5 Interactions

In the preceding sections, we have only briefly mentioned the specific structure of the four-point instantaneous interaction kernel V. Two interactions are adopted: the confinement interaction, acting on all meson states, and the instanton induced interaction, which acts on scalar and pseudoscalar mesons and accounts for the strong binding of the pion.

3.5.1 Confinement

In Section 1, the running coupling constant of QCD was introduced with its two main features: asymptotic freedom and confinement. The latter is the key property in the description of hadrons as colorless bound states of colored quarks and gluons. Despite the existing experimental evidence, a rigorous theoretical proof of confinement is still lacking. Therefore, it is included in the Bonn model via a suitable phenomenological two-body potential.

In a confining potential, the potential energy between the quark and antiquark should become larger as the $q\bar{q}$ separation length $\boldsymbol{r} = (\boldsymbol{x}_1 - \boldsymbol{x}_2)$ becomes larger. The confinement potential in the Bonn model rises linearly with the interquark distance $r = |\boldsymbol{r}|$. In the meson rest frame, this potential takes the form

$$\mathcal{V}(r) = a_c + b_c r \,. \tag{3.26}$$

The confinement offset a_c and the slope b_c are both treated as free parameters in the Bonn model. This linear behavior is inspired by a remarkable experimental outcome, namely the linear dependence between the angular momentum J and the squared mass M^2 of meson (and baryon) bound states, called Regge trajectories. It is possible to show in a simple model how a linear, string-like potential gives rise to this behavior [107]. In addition, lattice QCD calculations have shown that such a string picture of the confinement force is justified in the static limit of heavy quarks [108, 109].

The confining potential should contain an appropriate Dirac structure to optimize the observed spin-orbit splittings in the meson spectrum. As the Dirac structure of confinement is not clear from first principles, a justified choice should be made. The calculations in this work have been performed with the following Dirac structure, which was also adopted in Model $\mathcal{B}$ of Ref. [110]:

$$\Gamma \otimes \Gamma = \frac{1}{2}(\mathbb{1} \otimes \mathbb{1} - \gamma^5 \otimes \gamma^5 - \gamma_\mu \otimes \gamma^\mu) \,. \tag{3.27}$$

Model $\mathcal{B}$ was preferred over Model $\mathcal{A}$ (in which the Dirac structure $\Gamma \otimes \Gamma = \frac{1}{2}(\mathbb{1} \otimes \mathbb{1} - \gamma_0 \otimes \gamma^0)$ was adopted) of the same reference because of its superior performance in the calculation of the meson spectrum and electromagnetic form factors [110]. Summarizing, the following confinement potential is used in the framework of the Bonn model:

$$\begin{aligned} V_c(r) &= \mathcal{V}(r)(\Gamma \otimes \Gamma)\,, \\ &= \frac{1}{2}(a_c + b_c r)(\mathbb{1} \otimes \mathbb{1} - \gamma^5 \otimes \gamma^5 - \gamma_\mu \otimes \gamma^\mu)\,. \end{aligned} \tag{3.28}$$

The confinement interaction V_c acts on all $q\bar{q}$ meson states in the spectrum. In fact, the confinement potential alone, with appropriate values for the parameters a_c and b_c and a well-chosen Dirac structure $\Gamma \otimes \Gamma$ as described in the previous section, accounts for the Regge trajectories of the mesons with total angular momentum $J \neq 0$ and provides an excellent description of the corresponding meson mass spectrum. To also include the $J = 0$ states in the calculated Regge trajectories, the 't Hooft instanton induced interaction is implemented.

3.5.2 't Hooft instanton induced interaction

A study of the meson spectrum shows that, besides the confining interaction, an additional flavor dependent interaction is necessary in the study of the $J = 0$ meson sector: the large mass difference between the η (547.75 ± 0.12 MeV [111]) and the pion (134.9766 ± 0.0006 MeV for the π^0 [111]) as well as the experimentally observed $\eta\eta'$ mixing cannot be described by a confining force alone. The instanton induced interaction has all the necessary ingredients to tackle these issues: it is flavor dependent and acts only in the (pseudo-)scalar $J = 0$ sector [112]. This interaction was proposed by 't Hooft and others [113] and will therefore be referred to as the 't Hooft (instanton induced) interaction.

Instantons are special solutions of the classical Yang-Mills equations of motion in Euclidean space-time. Since they cannot be deformed continuously into classical solutions involving gluon fields, they lead to a non-perturbative effective interaction which is substantially different from a one-gluon exchange potential [92, 114].

In momentum space, the 't Hooft interaction can be written as

$$\begin{aligned} &\int \frac{\mathrm{d}^3 p'}{(2\pi)^3} V_{III}(\boldsymbol{p}, \boldsymbol{p}')\Phi(\boldsymbol{p}') \\ &\quad = 4G(g, g') \int \frac{\mathrm{d}^3 p'}{(2\pi)^3} \mathcal{R}_\Lambda(\boldsymbol{p}, \boldsymbol{p}')(\mathbb{1} Tr[\Phi(\boldsymbol{p}')] + \gamma^5 Tr[\gamma^5 \Phi(\boldsymbol{p}')])\,. \end{aligned} \tag{3.29}$$

The matrix $G(g, g')$ includes the flavor dependent couplings g and g'. These are free parameters in the Bonn model, as is the range of the interaction Λ. $\mathcal{R}_\Lambda$ is a regulating function describing the three-dimensional extension of the interaction:

$$\mathcal{R}_\Lambda(\boldsymbol{p}, \boldsymbol{p}') = \int \mathrm{d}^3 r \frac{1}{(\Lambda\sqrt{\pi})^3} e^{i(\boldsymbol{p}-\boldsymbol{p}')\cdot\boldsymbol{r}} e^{-\frac{|\boldsymbol{r}|^2}{\Lambda^2}}, \tag{3.30}$$

with $\boldsymbol{r} = \boldsymbol{x}_1 - \boldsymbol{x}_2$. It is clear that when Λ approaches 0, $\mathcal{R}_\Lambda(\boldsymbol{p}, \boldsymbol{p}') \to 1$ and $\mathcal{R}_\Lambda(\boldsymbol{r}) \to \delta(\boldsymbol{r})$.

3.5.3 Fixing the parameters

It follows from the above introduction to the Bonn model that the model contains seven parameters: two constituent quark masses (m_n and m_s), two parameters of the confinement interaction (a_c and b_c) and three parameters coming from the 't Hooft instanton induced interaction (g, g' and Λ). In Chapter 5, we will come back to these parameters and discuss how altering them can learn us more on generalized parton distributions of pseudoscalar mesons in the framework of the Bonn model.

4 Generalized parton distributions in the Bonn model

All exact science is dominated
by the idea of approximation.

B. Russell

4.1 GPDs of pseudoscalar mesons

The Bethe-Salpeter formalism, introduced in the preceding chapter, allows for the calculation of both static and dynamic properties of mesons. In fact, the covariance of the model is of high value in the calculation of dynamic observables such as electromagnetic form factors [19]. Despite the analogy with form factors, the calculation of generalized parton distributions needs to be performed with great care due to subtle differences, *e.g.* between a bilocal and a local current.

The definition of the generalized parton distribution of pseudoscalar mesons was given in Eq. (2.16). To derive an expression for the GPD in the Bethe-Salpeter approach, we will start with the bilocal current matrix element, which reads

$$\langle \bar{P}' | N\{\bar{\psi}(y')\gamma^{\mu}\psi(y)\} | \bar{P} \rangle \,, \tag{4.1}$$

in the Heisenberg picture. We will use the Mandelstam formalism [115], starting from the six-point Green's function. It will be proven that by calculating this Green's function in two different ways, a prescription for the related time-ordered matrix element,

$$\langle \bar{P}' | T\{\bar{\psi}(y')\gamma^{\mu}\psi(y)\} | \bar{P} \rangle \,, \tag{4.2}$$

can be found. Through Wick's theorem, the normal-ordered matrix element can finally be extracted.

4.1.1 The six-point Green's function

Writing the time-ordered bilocal quark current in a general way as $T\{\bar{\psi}(y')\gamma^\mu\psi(y)\} = O^\mu(y,y')$, we define the following six-point Green's function:

$$G^\mu_{\alpha\alpha'\beta\beta'}(x_1', x_2'; y', y; x_1, x_2) = \langle\Theta|T\{\psi^1_\alpha(x_1')\bar{\psi}^2_\beta(x_2')O^\mu(y,y')\psi^2_{\beta'}(x_2)\bar{\psi}^1_{\alpha'}(x_1)\}|\Theta\rangle\,. \tag{4.3}$$

Since the aim is to describe the coupling of a current to a meson which is initially and finally unperturbed, special attention will be paid to that part of the Green's function where the time-ordering is $(x_1'^0, x_2'^0) \gg (y^0, y'^0) \gg (x_1^0, x_2^0)$. Isolating this part of the Green's function and inserting two sets of on-shell bound meson states yields

$$\begin{aligned} G^\mu_{\alpha\alpha'\beta\beta'}(x_1', x_2'; y', y; x_1, x_2) = &\int \frac{\mathrm{d}^3P}{(2\pi)^3\,2\omega_P}\int \frac{\mathrm{d}^3P'}{(2\pi)^3\,2\omega_{P'}}\langle\Theta|T\{\psi^1_\alpha(x_1')\bar{\psi}^2_\beta(x_2')\}|\bar{P}'\rangle \\ &\times\ \langle\bar{P}'|O^\mu(y,y')|\bar{P}\rangle\langle\bar{P}|T\{\psi^2_{\beta'}(x_2)\bar{\psi}^1_{\alpha'}(x_1)\}|\Theta\rangle \\ &\times\ \theta\left(\min(x_1'^0, x_2'^0) - \max(y^0, y'^0)\right) \\ &\times\ \theta\left(\min(y^0, y'^0) - \max(x_1^0, x_2^0)\right) \\ &+\ \text{terms arising from other time-orderings} \\ &+\ \text{terms arising from other intermediate states}\,. \end{aligned} \tag{4.4}$$

For a general Green's function (and thus without at this point specifying the interactions acting between the quark states), the on-shell bound states do not form a complete set on their own. Inserting a complete set of states implies the inclusion of other intermediate states (asymptotic, non-bound states) . It is clear that in the description of bound $q\bar{q}$ states and using a linear, confining interaction, we do not need to consider these latter terms in detail. In the following, we will refer to the terms arising from other time-orderings or from other intermediate states with the abbreviation $O.T.$ (other terms).

Equation (4.4) can be rewritten by making use of the definitions of the meson Bethe-Salpeter amplitude (3.9) and adjoint amplitude (3.10):

$$\begin{aligned} G^\mu_{\alpha\alpha'\beta\beta'}(x_1', x_2'; y', y; x_1, x_2) = &\int \frac{\mathrm{d}^3P}{(2\pi)^3\,2\omega_P}\int \frac{\mathrm{d}^3P'}{(2\pi)^3\,2\omega_{P'}}\chi_{\bar{P}'\alpha\beta}(x_1', x_2')\langle\bar{P}'|O^\mu(y,y')|\bar{P}\rangle \\ &\times\ \bar{\chi}_{\bar{P}\beta'\alpha'}(x_1, x_2)\,\theta\left(\min(x_1'^0, x_2'^0) - \max(y^0, y'^0)\right) \\ &\times\ \theta\left(\min(y^0, y'^0) - \max(x_1^0, x_2^0)\right) +\ O.T. \end{aligned} \tag{4.5}$$

With the transformation of variables $z = y - y'$ and $Z = (y + y')/2$ (with Jacobian

$|\mathcal{J}| = 1$), and the translational invariance of the six-point Green's function we find:

$$\begin{aligned} G^{\mu}_{\alpha\alpha'\beta\beta'}(x_1', x_2'; y', y; x_1, x_2) &\equiv \tilde{G}^{\mu}_{\alpha\alpha'\beta\beta'}(x_1', x_2'; Z, z; x_1, x_2) \\ &= \int \frac{\mathrm{d}^3 P}{(2\pi)^3\, 2\omega_P} \int \frac{\mathrm{d}^3 P'}{(2\pi)^3\, 2\omega_{P'}} \chi_{\bar{P}'\alpha\beta}(x_1' - Z, x_2' - Z) \\ &\times\ \langle \bar{P}' | O^{\mu}(-\frac{z}{2}, \frac{z}{2}) | \bar{P} \rangle\ \bar{\chi}_{\bar{P}\beta'\alpha'}(x_1 - Z, x_2 - Z) \\ &\times\ \theta\left(\min(x_1'^0 - Z^0, x_2'^0 - Z^0) - \max(-\frac{z^0}{2}, \frac{z^0}{2}) \right) \\ &\times\ \theta\left(\min(-\frac{z^0}{2}, \frac{z^0}{2}) - \max(x_1^0 - Z^0, x_2^0 - Z^0) \right) \\ &+\ O.T.\,, \end{aligned} \tag{4.6}$$

or

$$\begin{aligned} \tilde{G}^{\mu}_{\alpha\alpha'\beta\beta'}(x_1', x_2'; Z, z; x_1, x_2) &= \int \frac{\mathrm{d}^3 P}{(2\pi)^3\, 2\omega_P} \int \frac{\mathrm{d}^3 P'}{(2\pi)^3\, 2\omega_{P'}}\, e^{-i(\bar{P} - \bar{P}')Z} \chi_{\bar{P}'\alpha\beta}(x_1', x_2') \\ &\times\ \langle \bar{P}' | O^{\mu}(-\frac{z}{2}, \frac{z}{2}) | \bar{P} \rangle \bar{\chi}_{\bar{P}\beta'\alpha'}(x_1, x_2) \\ &\times\ \theta\left(\min(x_1'^0, x_2'^0) - Z^0 - \frac{1}{2}|z^0| \right) \\ &\times\ \theta\left(-\frac{1}{2}|z^0| - \max(x_1^0, x_2^0) + Z^0 \right) \\ &+\ O.T. \end{aligned} \tag{4.7}$$

In deriving Eq. (4.7) we have used the following relation (reflecting translational symmetry)

$$\chi_{\bar{P}'\alpha\beta}(x_1' - Z, x_2' - Z) = e^{i\bar{P}'Z} \chi_{\bar{P}'\alpha\beta}(x_1', x_2') \tag{4.8}$$

In App. B, it is shown that in momentum space, Eq. (4.7) becomes

$$\begin{aligned} G^{\mu}_{P;P'}(p'; k', k; p) \xrightarrow{P^{(\prime)0} \to \omega_P^{(\prime)}} &- \frac{(2\pi)^4}{4\omega_P \omega_{P'}} \frac{\chi_{\bar{P}'}(p') \langle \bar{P}' | O^{\mu}(\frac{k - k'}{2}) | \bar{P} \rangle \bar{\chi}_{\bar{P}}(p)}{((P'^0 - \omega_{P'}) + i\epsilon)((P^0 - \omega_P) + i\epsilon)} \\ &\times\ \delta^{(4)}(P' - P + k + k') \\ &+\ \text{regular terms for } P^0 \to \omega_P \text{ and } P'^0 \to \omega_{P'}\,. \end{aligned} \tag{4.9}$$

The above equation states that the six-point Green's function G^{μ} has poles when the four-momenta P and P' are on-shell, and that the residue at these poles is proportional to the bilocal current matrix element. To extract a prescription for the calculation of this matrix element, we need an independent way to calculate the residue of the six-point Green's function. The Mandelstam formalism provides such an independent calculation.

4.1.2 The Mandelstam formalism

Following a procedure introduced by Mandelstam [115], we express the six-point Green's function G^μ in terms of the four-point Green's function G (which was defined in Eq. (3.1)) and an irreducible kernel K^μ:

$$\begin{aligned} G^\mu_{\alpha\alpha'\beta\beta'}(x_1', x_2'; y', y; x_1, x_2) = \sum_{\delta\delta'} \sum_{\epsilon\epsilon'} \int \mathrm{d}^4x_1'' \mathrm{d}^4x_2'' \mathrm{d}^4x_1''' \mathrm{d}^4x_2''' G_{\alpha\delta\beta\epsilon}(x_1', x_2'; x_1'', x_2'') \\ \times\ K^\mu_{\delta\delta'\epsilon\epsilon'}(x_1'', x_2''; y', y; x_1''', x_2''')\ G_{\delta'\alpha'\epsilon'\beta'}(x_1''', x_2'''; x_1, x_2)\,. \end{aligned} \tag{4.10}$$

This expression is depicted in Fig. 4.1. Equation (4.10) and Fig. 4.1 define the bilocal current kernel K^μ, so that it describes the coupling of a bilocal current to a propagating $q\bar{q}$ system. Similar to the interaction kernel K, K^μ consists of irreducible diagrams. In fact, each diagram in the interaction kernel K (Fig. 3.2) has a counterpart that contributes to the current kernel K^μ.

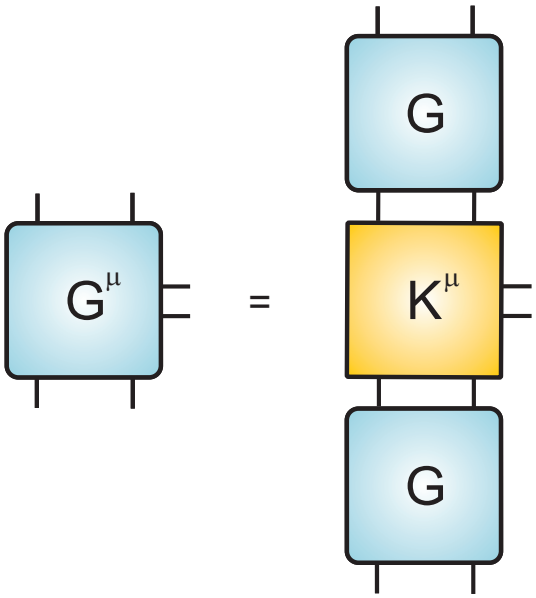

Figure 4.1 According to the Mandelstam formalism, the six-point Green's function G^μ can be expressed in terms of the four-point Green's function G and the irreducible kernel K^μ. This graph is the pictorial analogon of Eq. (4.10).

Introducing two complete sets of intermediate states and the appropriate time-

ordering yields

$$
\begin{aligned}
G^{\mu}_{\alpha\alpha'\beta\beta'}(x_1', x_2'; y', y; x_1, x_2) = &\sum_{\delta\delta'}\sum_{\epsilon\epsilon'}\int \mathrm{d}^4x_1''\mathrm{d}^4x_2''\mathrm{d}^4x_1'''\mathrm{d}^4x_2''' \int \frac{\mathrm{d}^3P}{(2\pi)^3\,2\omega_P}\frac{\mathrm{d}^3P'}{(2\pi)^3\,2\omega_{P'}} \\
&\times\ \chi_{\bar{P}'\alpha\beta}(x_1', x_2')\bar{\chi}_{\bar{P}'\epsilon\delta}(x_1'', x_2'')K^{\mu}_{\delta\delta'\epsilon\epsilon'}(x_1'', x_2''; y', y; x_1''', x_2''') \\
&\times\ \chi_{\bar{P}\delta'\epsilon'}(x_1''', x_2''')\bar{\chi}_{\bar{P}\beta'\alpha'}(x_1, x_2) \\
&\times\ \theta\left(\min(x_1'^0, x_2'^0) - \max(x_1''^0, x_2''^0)\right) \\
&\times\ \theta\left(\min(x_1'''^0, x_2'''^0) - \max(x_1^0, x_2^0)\right) + \ O.T.
\end{aligned}
\tag{4.11}
$$

We make use of the translational invariance of the six-point Green's function once more to obtain

$$
\begin{aligned}
\tilde{G}^{\mu}_{\alpha\alpha'\beta\beta'}(x_1', x_2'; Z, z; x_1, x_2) = &\sum_{\delta\delta'}\sum_{\epsilon\epsilon'}\int \mathrm{d}^4x_1''\mathrm{d}^4x_2''\mathrm{d}^4x_1'''\mathrm{d}^4x_2''' \int \frac{\mathrm{d}^3P}{(2\pi)^3\,2\omega_P}\frac{\mathrm{d}^3P'}{(2\pi)^3\,2\omega_{P'}} \\
&\times\ e^{-i(\bar{P}-\bar{P}')\cdot Z}\chi_{\bar{P}'\alpha\beta}(x_1', x_2')\bar{\chi}_{\bar{P}'\epsilon\delta}(x_1'', x_2'') \\
&\times\ K^{\mu}_{\delta\delta'\epsilon\epsilon'}(x_1'', x_2''; -\frac{z}{2}, \frac{z}{2}; x_1''', x_2''')\chi_{\bar{P}\delta'\epsilon'}(x_1''', x_2''')\bar{\chi}_{\bar{P}\beta'\alpha'}(x_1, x_2) \\
&\times\ \theta\left(\min(x_1'^0, x_2'^0) - Z^0 - \max({x_1}''^0, {x_2}''^0)\right) \\
&\times\ \theta\left(\min({x_1}'''^0, {x_2}'''^0) - \max(x_1^0, x_2^0) + Z^0\right) + \ O.T.
\end{aligned}
\tag{4.12}
$$

Fourier transforming the above equation and making use of the definition of the δ-function yields (see App. B):

$$
\begin{aligned}
G^{\mu}_{P;P'}(p'; k', k; p) \xrightarrow{P^{(\prime)0}\to\omega_P^{(\prime)}} &-(2\pi)^4\int \frac{\mathrm{d}^4p''}{(2\pi)^4}\frac{\mathrm{d}^4p'''}{(2\pi)^4}\frac{1}{2\omega_P}\frac{1}{2\omega_{P'}}\chi_{\bar{P}'}(p')\bar{\chi}_{\bar{P}'}(p'') \\
&\times\ K^{\mu}_{\bar{P};\bar{P}'}(p''; \frac{k-k'}{2}; p''')\ \chi_{\bar{P}}(p''')\bar{\chi}_{\bar{P}}(p) \\
&\times\ \frac{1}{((P'^0 - \omega_{P'}) + i\epsilon)((P^0 - \omega_P) + i\epsilon)} \\
&\times\ \delta^{(4)}(P' - P + k + k') + \text{ regular terms.}
\end{aligned}
\tag{4.13}
$$

Comparison of equations (4.9) and (4.13) gives the expression for the matrix element in momentum space:

$$
\langle\bar{P}'|O^{\mu}(\frac{k-k'}{2})|\bar{P}\rangle = \int \frac{\mathrm{d}^4p''}{(2\pi)^4}\frac{\mathrm{d}^4p'''}{(2\pi)^4}\bar{\chi}_{\bar{P}'}(p'')K^{\mu}_{\bar{P};\bar{P}'}(p''; \frac{k-k'}{2}; p''')\chi_{\bar{P}}(p''')\,, \tag{4.14}
$$

and Fourier transformed in configuration space:

$$
\begin{aligned}
\langle\bar{P}'|T\{\bar{\psi}(-\frac{z}{2})\gamma^{\mu}\psi(\frac{z}{2})\}|\bar{P}\rangle = &\int \mathrm{d}^4x_1''\mathrm{d}^4x_2''\mathrm{d}^4x_1'''\mathrm{d}^4x_2'''\ \bar{\chi}_{\bar{P}'}(x_1'', x_2'') \\
&\times\ K^{\mu}(x_1'', x_2''; -\frac{z}{2}, \frac{z}{2}; x_1''', x_2''')\chi_{\bar{P}}(x_1''', x_2''')\,.
\end{aligned}
\tag{4.15}
$$

With Eq. (4.14) the bilocal current matrix element that appears in the definition (2.16) of the GPD can be calculated, provided that an expression for the bilocal current kernel K^μ can be determined. This will be the subject of the next paragraph.

4.1.3 The bilocal current kernel in lowest order

It was already mentioned in the previous section that K^μ consists of an infinite sum of interaction terms, with each irreducible diagram in the expansion of K^μ corresponding to a diagram in K. A truncation scheme is therefore necessary. To be consistent with the approximations performed in Chapter 3, the expression for the bilocal current kernel will be restricted to *lowest order*. This means that the scattering matrix $U_I(+\infty,-\infty) = T\{e^{-i\int_{-\infty}^{+\infty} H_{int,I}(t)\mathrm{d}t}\}$ equals one, so that there is no difference between interaction picture and Heisenberg picture expressions [116]. As a result, Wick's theorem,

$$T\{\psi(x_1)\psi(x_2)...\psi(x_m)\} = N\{\psi(x_1)\psi(x_2)...\psi(x_m) + \text{all possible pairs of contractions}\}\,, \tag{4.16}$$

can be applied formally to the six-point Green's function that was defined in Eq. (4.3). This leads to (the dots denote the contractions):

$$\begin{aligned} G^{\mu(0)}_{\alpha\alpha'\beta\beta'}(x_1', x_2'; y', y; x_1, x_2) = \\ \sum_{\kappa\kappa'} \big[&\langle\Theta|N\{\psi^{1\cdot}_\alpha(x_1')\bar\psi^{2\cdot\cdot}_\beta(x_2')\bar\psi^{\cdot}_\kappa(y')\gamma^\mu_{\kappa\kappa'}\psi^{\cdot\cdot\cdot}_{\kappa'}(y)\psi^{2\cdot\cdot}_{\beta'}(x_2)\bar\psi^{1\cdot\cdot\cdot}_{\alpha'}(x_1)\}|\Theta\rangle \\ &+ \langle\Theta|N\{\psi^{1\cdot}_\alpha(x_1')\bar\psi^{2\cdot\cdot}_\beta(x_2')\bar\psi^{\cdot\cdot\cdot}_\kappa(y')\gamma^\mu_{\kappa\kappa'}\psi^{\cdot\cdot}_{\kappa'}(y)\psi^{2\cdot\cdot\cdot}_{\beta'}(x_2)\bar\psi^{1\cdot}_{\alpha'}(x_1)\}|\Theta\rangle \\ &+ \langle\Theta|N\{\psi^{1\cdot\cdot\cdot}_\alpha(x_1')\bar\psi^{2\cdot\cdot}_\beta(x_2')\bar\psi^{\cdot}_\kappa(y')\gamma^\mu_{\kappa\kappa'}\psi^{\cdot}_{\kappa'}(y)\psi^{2\cdot\cdot}_{\beta'}(x_2)\bar\psi^{1\cdot\cdot\cdot}_{\alpha'}(x_1)\}|\Theta\rangle\big]\,. \end{aligned} \tag{4.17}$$

The three terms in this expression are represented graphically in Figure 4.2.

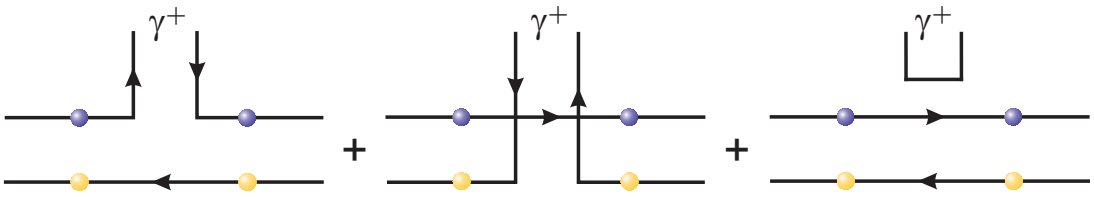

Figure 4.2 Graphical interpretation of the three terms of the zeroth-order Green's function $G^{\mu(0)}_{\alpha\alpha'\beta\beta'}(x_1, x_2; y', y; x_1', x_2')$, Eq. (4.17).

The first term in Eq. (4.17) denotes the coupling of the bilocal current to the constituent quark, the second that to the constituent antiquark. The last term in Eq. (4.17) denotes the coupling of the bilocal current to itself. Intuitively, it is clear that this last term shouldn't contribute to the generalized parton distribution. However, the linked-cluster theorem from quantum field theory is not applicable here. To understand why

it will eventually cancel, we have to look at the origin of the term. Its occurrence is directly related to the fact that the Green's function is a *time*-ordered matrix element. It can be shown that this term equals the contraction term in the relation between the normal- and the time-ordered bilocal current matrix element,

$$\langle \bar{P}'|T\{\bar{\psi}(y')\gamma^\mu\psi(y)\}|\bar{P}\rangle = \langle \bar{P}'|N\{\bar{\psi}(y')\gamma^\mu\psi(y)\}|\bar{P}\rangle + \langle \bar{P}'|\bar{P}\rangle\langle\Theta|\bar{\psi}^{\cdot}(y')\gamma^\mu\psi^{\cdot}(y)|\Theta\rangle\,, \quad (4.18)$$

so that it vanishes in the calculation of the GPD. The straightforward but tedious proof is based on the Mandelstam formalism, by expressing the matrix element $\langle \bar{P}'|\bar{P}\rangle$ in terms of the Bethe-Salpeter amplitudes. To keep the equations readable, only the first term (coupling to the quark) in Eq. (4.17) will be written explicitly in the remainder of this section. This part of the Green's function can be rephrased as

$$\begin{aligned} G^{\mu(0)}_{\alpha\alpha'\beta\beta'}(x_1', x_2'; y', y; x_1, x_2) = -\sum_{\kappa\kappa'}&\langle\Theta|T\{\psi^1_\alpha(x_1')\bar{\psi}_\kappa(y')\}|\Theta\rangle\gamma^\mu_{\kappa\kappa'}\langle\Theta|T\{\psi_{\kappa'}(y)\bar{\psi}^1_{\alpha'}(x_1)\}|\Theta\rangle \\ &\times\ \langle\Theta|T\{\psi^2_{\beta'}(x_2)\bar{\psi}^2_\beta(x_2')\}|\Theta\rangle \\ &+\ \text{coupling to the antiquark} \\ &+\ \text{bilocal current contraction term}\,. \end{aligned} \quad (4.19)$$

The minus sign is a result of interchanging the fermion fields. In order to find an expression similar to the decomposition of Eq. (4.10), we insert δ-functions and Kronecker δ's in Eq. (4.19):

$$\begin{aligned} &G^{\mu(0)}_{\alpha\alpha'\beta\beta'}(x_1', x_2'; y', y; x_1, x_2) = \\ &\quad -\sum_{\kappa\kappa'}\sum_{\epsilon\epsilon'\epsilon'''}\sum_{\lambda}\int \mathrm{d}^4x_1''\mathrm{d}^4x_2''\mathrm{d}^4x_1'''\mathrm{d}^4x_2'''\ \langle\Theta|T\{\psi^1_\alpha(x_1')\bar{\psi}_\epsilon(x_1'')\}|\Theta\rangle \\ &\quad\times\ \delta^{(4)}(x_1''-y')\delta_{\epsilon\kappa}\gamma^\mu_{\kappa\kappa'}\delta^{(4)}(y-x_1''')\delta_{\kappa'\epsilon'}\langle\Theta|T\{\psi_{\epsilon'}(x_1''')\bar{\psi}^1_{\alpha'}(x_1)\}|\Theta\rangle \\ &\quad\times\ \langle\Theta|T\{\psi^2_{\beta'}(x_2)\bar{\psi}^2_{\epsilon'''}(x_2''')\}|\Theta\rangle\ \delta^{(4)}(x_2'''-x_2'')\delta_{\epsilon'''\lambda}\delta^{(4)}(x_2''-x_2')\delta_{\lambda\beta} \\ &\quad+\ \text{coupling to the antiquark} \\ &\quad+\ \text{bilocal current contraction term}\,. \end{aligned} \quad (4.20)$$

The two-point Green's functions are defined through the inhomogeneous equation

$$\sum_\beta (i\ \partial\!\!\!/_x - m)_{\alpha\beta}\langle\Theta|T\{\psi_\beta(x)\bar{\psi}_{\alpha'}(x')\}|\Theta\rangle = i\delta^{(4)}(x-x')\delta_{\alpha\alpha'}\,, \quad (4.21)$$

so that we can rephrase Eq. (4.20) as

$$\begin{aligned} G^{\mu(0)}_{\alpha\alpha'\beta\beta'}(x_1', x_2'; y', y; x_1, x_2) = & \sum_{\epsilon\epsilon'\epsilon''\epsilon'''} \sum_{\kappa\kappa'} \sum_{\lambda} \int \mathrm{d}^4x_1'' \mathrm{d}^4x_2'' \mathrm{d}^4x_1''' \mathrm{d}^4x_2''' \\ & i\langle\Theta|T\{\psi^1_\alpha(x_1')\bar\psi^1_\epsilon(x_1'')\}|\Theta\rangle \delta^{(4)}(x_1''-y')\delta_{\epsilon\kappa}\gamma^\mu_{\kappa\kappa'}\delta^{(4)}(y-x_1''')\delta_{\kappa'\epsilon'} \\ & \times \langle\Theta|T\{\psi_{\epsilon'}(x_1''')\bar\psi_{\alpha'}(x_1)\}|\Theta\rangle\langle\Theta|T\{\psi^2_{\beta'}(x_2)\bar\psi^2_{\epsilon'''}(x_2''')\}|\Theta\rangle\delta^{(4)}(x_2'''-x_2'')\delta_{\epsilon'''\lambda} \\ & \times (i\,\partial\!\!\!/_{x_2''} - m_2)_{\lambda\epsilon''}\langle\Theta|T\{\psi^2_{\epsilon''}(x_2'')\bar\psi^2_\beta(x_2')\}|\Theta\rangle \\ & + \text{coupling to the antiquark} \\ & + \text{bilocal current contraction term}\,, \end{aligned} \tag{4.22}$$

with m_2 the constituent mass of the antiquark. In the antiquark term, the constituent mass of the quark m_1 arises.

To find an expression of the bilocal current kernel K^μ, Eq. (4.10) is also written in lowest order:

$$\begin{aligned} & G^{\mu(0)}_{\alpha\alpha'\beta\beta'}(x_1', x_2'; y', y; x_1, x_2) = \\ & \quad \sum_{\epsilon\epsilon'\epsilon''\epsilon'''} \int \mathrm{d}^4x_1'' \mathrm{d}^4x_2'' \mathrm{d}^4x_1''' \mathrm{d}^4x_2'''\; S^1_{F\alpha\epsilon}(x_1', x_1'') S^2_{F\epsilon''\beta}(x_2'', x_2') \\ & \quad \times\; K^{\mu(0)}_{\epsilon\epsilon'\epsilon''\epsilon'''}(x_1'', x_2''; y', y; x_1''', x_2''') S^1_{F\epsilon'\alpha'}(x_1''', x_1) S^2_{F\beta'\epsilon'''}(x_2, x_2''')\,, \end{aligned} \tag{4.23}$$

Comparison of Eqs. (4.22) and (4.23) yields the expression for the bilocal current kernel in zeroth order:

$$\begin{aligned} K^{\mu(0)}_{\epsilon\epsilon'\epsilon''\epsilon'''}(x_1'', x_2''; y', y; x_1''', x_2''') = & \sum_{\kappa\kappa'} \sum_{\lambda} i\,\delta^{(4)}(x_1''-y')\delta_{\epsilon\kappa}\gamma^\mu_{\kappa\kappa'}\delta^{(4)}(y-x_1''')\delta_{\kappa'\epsilon'} \\ & \times\; \delta^{(4)}(x_2'''-x_2'')\delta_{\epsilon'''\lambda}(i\,\partial\!\!\!/_{x_2''} - m_2)_{\lambda\epsilon''} \\ & + \text{coupling to the antiquark} \\ & + \text{bilocal current contraction term}\,. \end{aligned} \tag{4.24}$$

This expression states that in lowest order, the four-momentum and spin need to be conserved when the bilocal current is coupled to the quark. The antiquark propagates without interacting with the bilocal current. However, the Bethe-Salpeter amplitudes which occur in Eq. (4.14) each implicitly contain an antiquark propagator, in contrast with the vertex functions which are amputated Bethe-Salpeter amplitudes (see Eq. (3.24)). Equation (4.24) shows that the appropiate inverse propagator is included in the bilocal current kernel, so that the redundant propagator is cancelled.

With expression (4.24) for the kernel, all ingredients necessary for the calculation of the bilocal current matrix element, and thus for the computation of the GPD, are found. In the next paragraphs, we will derive the corresponding expressions.

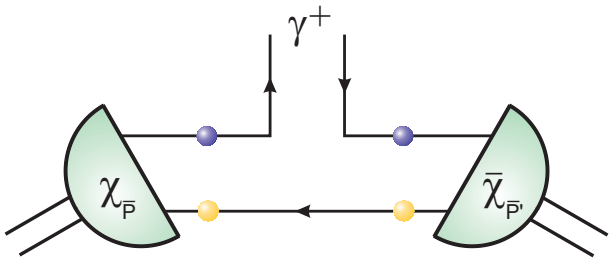

Figure 4.3 Schematic representation of the expression of the bilocal current matrix element (coupling to the quark) in lowest order in terms of Bethe-Salpeter amplitudes, Eq. (4.25).

4.1.4 The bilocal current matrix element

The time-ordered matrix element (4.2) is found by inserting Eq. (4.24) into Eq. (4.15). The normal-ordered matrix element, needed for the calculation of the generalized parton distribution, differs from the time-ordered matrix element through a contraction term only. As mentioned above, this contraction term cancels the peculiar bilocal current self-coupling term.

Adding the antiquark coupling term again, we can now extract the zeroth-order normal-ordered bilocal current matrix element in the Bethe-Salpeter formalism:

$$\begin{aligned}\langle \bar{P}'|N\{\bar{\psi}(-\frac{z}{2})\gamma^\mu\psi(\frac{z}{2})\}|\bar{P}\rangle = &\int \mathrm{d}^4x'\; i\mathrm{Tr}\left\{\left((i\;\partial\!\!\!/_{x'} - m_2)\bar{\chi}_{\bar{P}'}(-\frac{z}{2},x')\right)\gamma^\mu\chi_{\bar{P}}(\frac{z}{2},x')\right\}\\ &+\int \mathrm{d}^4x'\; i\mathrm{Tr}\left\{\bar{\chi}_{\bar{P}'}(x',\frac{z}{2})\left((i\;\partial\!\!\!/_{x'} - m_1)\chi_{\bar{P}}(x',-\frac{z}{2})\right)\gamma^\mu\right\}.\end{aligned} \tag{4.25}$$

The quark term is visualised in Fig. 4.3.

4.1.5 Expressions for the GPDs

The quark and the antiquark GPDs can be derived with equation (2.16):

$$H^q(x,\xi,t) = \frac{1}{2}\int\frac{\mathrm{d}z^-}{2\pi}e^{ix\tilde{P}^+z^-}\;\langle\bar{P}'|N\{\bar{\psi}^1(-\frac{z}{2})\gamma^+\psi^1(\frac{z}{2})\}|\bar{P}\rangle\Big|_{z^+=0,\mathbf{z}_\perp=\mathbf{0}}, \tag{4.26}$$

$$H^{\bar{q}}(x,\xi,t) = \frac{1}{2}\int\frac{\mathrm{d}z^-}{2\pi}e^{ix\tilde{P}^+z^-}\;\langle\bar{P}'|N\{\bar{\psi}^2(-\frac{z}{2})\gamma^+\psi^2(\frac{z}{2})\}|\bar{P}\rangle\Big|_{z^+=0,\mathbf{z}_\perp=\mathbf{0}}. \tag{4.27}$$

Equation (4.26) refers to that part of the GPD where the current couples to the constituent quark, while Eq. (4.27) denotes the coupling of the current to the constituent antiquark. By inserting the appropriate term from the matrix element (4.25) and Fourier

transforming to momentum space, we find that the quark GPD equals

$$H^q(x,\xi,t) = \frac{i}{2}\int \frac{\mathrm{d}^4p}{(2\pi)^4}\delta\left(x\tilde{P}^+ - \frac{\bar{P}'^+}{2} - p^+\right)\mathrm{Tr}\left\{\left(-\frac{\bar{\not{P}}}{2} + \not{p} - m_2\right)\bar{\chi}_{\bar{P}'}(p+\frac{\bar{P}'}{2}-\frac{\bar{P}}{2})\gamma^+\chi_{\bar{P}}(p)\right\}, \tag{4.28}$$

while the antiquark GPD can be written as

$$H^{\bar{q}}(x,\xi,t) = \frac{i}{2}\int \frac{\mathrm{d}^4p}{(2\pi)^4}\delta\left(x\tilde{P}^+ + \frac{\bar{P}'^+}{2} - p^+\right)\mathrm{Tr}\left\{\bar{\chi}_{\bar{P}'}(p+\frac{\bar{P}}{2}-\frac{\bar{P}'}{2})\left(\frac{\bar{\not{P}}}{2} + \not{p} - m_1\right)\chi_{\bar{P}}(p)\gamma^+\right\}. \tag{4.29}$$

In these expressions, the inverse quark and antiquark propagators can be recognized (see also Eq. (4.21)):

$$\begin{aligned}\left[S_F^1(p)\right]^{-1} &= -i(\not{p} - m_1) \quad \text{and}\\ \left[S_F^2(p)\right]^{-1} &= -i(\not{p} - m_2)\,.\end{aligned} \tag{4.30}$$

With the definitions of x, ξ and Δ from Chapter 2 we can reformulate the quark GPD in terms of the vertex functions (3.24):

$$\begin{aligned}H^q(x,\xi,t) = -\frac{1}{2}\int \frac{\mathrm{d}^4p}{(2\pi)^4}\delta\left(\frac{2x+\xi-1}{2(1+\xi)}\bar{P}^+ - p^+\right)\\ \times\ \mathrm{Tr}\left\{\bar{\Gamma}_{\bar{P}'}(p+\frac{\Delta}{2})S_F^1(\frac{\bar{P}'}{2}+p+\frac{\Delta}{2})\gamma^+S_F^1(\frac{\bar{P}}{2}+p)\Gamma_{\bar{P}}(p)S_F^2(-\frac{\bar{P}}{2}+p)\right\}.\end{aligned} \tag{4.31}$$

The expression for the antiquark GPD can be found in a similar way.

Equation (4.31) is the starting point for the numerical calculation of the GPD. However, a clear understanding of its subtleties is necessary. Therefore, we will address some questions related to the implementation of this equation in great detail in the next section. In particular, we will study the calculation and Lorentz boosting of the vertex functions, and the four-dimensional integration.

4.2 Numerical treatment of the GPD

4.2.1 Calculation of the vertex functions

Equation (4.31) is written in terms of the vertex functions. In the Bonn model, these are calculated in the rest frame of the corresponding particle (incoming or outgoing meson). More specifically, they are calculated through an expansion in radial and angular

basis functions [92]:

$$\Gamma_{J^\pi M_J}(\boldsymbol{p}) = \sum_{k=1}^{8} \sum_{n} a_{kn}^{(\Gamma)} R_{nl_k}(|\boldsymbol{p}|) \gamma_5^{a_k} \gamma_0^{g_k} \left[Y_{l_k}(\hat{p}) \times \gamma^{[s_k]} \right]_{JM_J} , \tag{4.32}$$

where the superscripts a_k, g_k and $s_k \in \{0, 1\}$ should be interpreted as *e.g.* $\gamma_5^0 = \mathbb{1}_4$ and $\gamma_5^1 = \gamma_5$, leading to two sets of eight tensors which form a basis of definite spin and parity $\pi = (-1)^{a_k + l_k + s_k}$. The tensor product is defined as

$$\left[Y_l(\hat{p}) \times \gamma^{[s]} \right]_{JM_J} \equiv \sum_{m_l, m_s} C^{JM_J}_{lm_l sm_s} Y_{lm_l}(\hat{p}) \gamma^{[s]}_{m_s} , \tag{4.33}$$

with $C^{JM_J}_{lm_l sm_s}$ the Clebsch-Gordan coefficient and $\gamma^{[s]}_{m_s}$ the spherical tensors

$$\gamma^{[1]}_{m_s} = \begin{pmatrix} 0 & \sigma_{m_s} \\ -\sigma_{m_s} & 0 \end{pmatrix} , \tag{4.34}$$

for $s = 1$, $m_s = 0, \pm 1$ and $\gamma^{[0]} = \mathbb{1}_4$. The matrices σ_{m_s} are the well-known 2×2 Pauli spin matrices. More details about this expansion can be found in Ref. [92]. As can be seen from these equations, the angular basis functions are the well-known spherical harmonics. There is a large amount of freedom in the choice of the radial basis in which the radial part of the vertex functions are expanded. In the Bonn model for mesons, three sets of radial basis functions are implemented: the Jacobi and Laguerre polynomials, which are explained in detail in Ref. [117], and the harmonic oscillator radial basis functions.

It was pointed out in Chapter 2 that the definition of the GPD, Eq. (2.16), holds only in a coordinate system where $\tilde{\boldsymbol{P}}_\perp$ is zero. Our calculations are performed in the Breit frame, where both the incoming and outgoing meson are moving and $\Delta^0 = \bar{P}'^0 - \bar{P}^0$ vanishes. Taking into consideration that the vertex functions are actually calculated in the rest frame, it is clear that the vertex functions of both incoming and outgoing meson need to be Lorentz boosted. Summarizing, we use the following expressions for $\bar{P}$, $\bar{P}'$, $\tilde{P}$ and Δ:

$$\bar{P} = (\bar{M}, -\frac{|\boldsymbol{\Delta}_\perp|}{2}, 0, \xi\bar{M}) , \tag{4.35}$$

$$\bar{P}' = (\bar{M}, \frac{|\boldsymbol{\Delta}_\perp|}{2}, 0, -\xi\bar{M}) , \tag{4.36}$$

$$\tilde{P} = (\bar{M}, 0, 0, 0) , \tag{4.37}$$

$$\Delta = (0, |\boldsymbol{\Delta}_\perp|, 0, -2\xi\bar{M}) , \tag{4.38}$$

where the 1-axis was chosen parallel with $\boldsymbol{\Delta}_\perp$, fixing the remaining freedom in the choice of the reference system. $\bar{M}$ is defined through

$$\bar{M}^2 = M^2 - \frac{t}{4} . \tag{4.39}$$

Writing the (inverse) Lorentz boost as a boost in the 1-direction followed by a boost in the 3-direction, we find the following relations for the boosted vertex functions:

$$\Gamma_{\bar{P}}(p) = S_{\Lambda_{\bar{P}_{(1)}}} S_{\Lambda_{\bar{P}_{(3)}}} \Gamma_M \left(\Lambda^{-1}_{\bar{P}_{(3)}} \left(\Lambda^{-1}_{\bar{P}_{(1)}} (p) \right) \right) S^{-1}_{\Lambda_{\bar{P}_{(3)}}} S^{-1}_{\Lambda_{\bar{P}_{(1)}}} , \tag{4.40}$$

$$\begin{aligned} \bar{\Gamma}_{\bar{P}'}(p') &= S_{\Lambda_{\bar{P}'_{(1)}}} S_{\Lambda_{\bar{P}'_{(3)}}} \bar{\Gamma}_{M'} \left(\Lambda^{-1}_{\bar{P}'_{(3)}} \left(\Lambda^{-1}_{\bar{P}'_{(1)}} (p') \right) \right) S^{-1}_{\Lambda_{\bar{P}'_{(3)}}} S^{-1}_{\Lambda_{\bar{P}'_{(1)}}} , \\ &= -S_{\Lambda_{\bar{P}'_{(1)}}} S_{\Lambda_{\bar{P}'_{(3)}}} \gamma^0 \Gamma^\dagger_{M'} \left(\Lambda^{-1}_{\bar{P}'_{(3)}} \left(\Lambda^{-1}_{\bar{P}'_{(1)}} (p') \right) \right) \gamma^0 S^{-1}_{\Lambda_{\bar{P}'_{(3)}}} S^{-1}_{\Lambda_{\bar{P}'_{(1)}}} . \end{aligned} \tag{4.41}$$

These equations are readily proven (see App. A in Ref. [92] for helpful relations). The Lorentz boosts considered here are *active*, which means that the meson is boosted, not the reference frame. The Lorentz boosts are chosen so that

$$\Lambda^{-1}_{\bar{P}_{(3)}} \left(\Lambda^{-1}_{\bar{P}_{(1)}} (\bar{P}) \right) = \Lambda^{-1}_{\bar{P}'_{(3)}} \left(\Lambda^{-1}_{\bar{P}'_{(1)}} (\bar{P}') \right) = (M, \mathbf{0}) . \tag{4.42}$$

Using the kinematics of the Breit frame and writing the Lorentz boosts explicitly, we arrive at the following expression for the quark GPD:

$$\begin{aligned} H^q(x,\xi,t) = & \frac{1}{2} \int \frac{\mathrm{d}^4 p}{(2\pi)^4} \delta \left((2x + \xi - 1) \frac{\bar{M}}{2\sqrt{2}} - p^+ \right) \mathrm{Tr} \left\{ S_{\Lambda_{\bar{P}'_{(1)}}} S_{\Lambda_{\bar{P}'_{(3)}}} \gamma^0 \right. \\ & \times \Gamma^\dagger_{M'} \left(\Lambda^{-1}_{\bar{P}'_{(3)}} \left(\Lambda^{-1}_{\bar{P}'_{(1)}} (p + \frac{\Delta}{2}) \right) \right) \gamma^0 S^{-1}_{\Lambda_{\bar{P}'_{(3)}}} S^{-1}_{\Lambda_{\bar{P}'_{(1)}}} S^1_F (\frac{\bar{P}'}{2} + p + \frac{\Delta}{2}) \gamma^+ S^1_F (\frac{\bar{P}}{2} + p) \\ & \left. \times S_{\Lambda_{\bar{P}_{(1)}}} S_{\Lambda_{\bar{P}_{(3)}}} \Gamma_M \left(\Lambda^{-1}_{\bar{P}_{(3)}} \left(\Lambda^{-1}_{\bar{P}_{(1)}} (p) \right) \right) S^{-1}_{\Lambda_{\bar{P}_{(3)}}} S^{-1}_{\Lambda_{\bar{P}_{(1)}}} S^2_F (-\frac{\bar{P}}{2} + p) \right\} . \end{aligned} \tag{4.43}$$

The four Lorentz boosts are characterized by their respective rapidities $\varphi = tgh^{-1}\beta$, where the β are given by the following expressions:

- $\beta_{(3)} = \frac{\xi \bar{M}}{\sqrt{M^2 + \xi^2 \bar{M}^2}}$ and $\gamma_{(3)} = \frac{1}{\sqrt{1-\beta^2_{(3)}}} = \frac{\sqrt{M^2 + \xi^2 \bar{M}^2}}{M}$ for the boost of the incoming meson in the positive 3-direction,
- $\beta_{(1)} = -\frac{\sqrt{\bar{M}^2(1-\xi^2) - M^2}}{\bar{M}}$ and $\gamma_{(1)} = \frac{\bar{M}}{\sqrt{M^2 + \xi^2 \bar{M}^2}}$ for the boost of the incoming meson in the negative 1-direction,
- $\beta'_{(3)} = -\beta_{(3)}$ and $\gamma'_{(3)} = \gamma_{(3)}$ for the boost of the outgoing meson in the negative 3-direction,
- $\beta'_{(1)} = -\beta_{(1)}$ and $\gamma'_{(1)} = \gamma_{(1)}$ for the boost of the outgoing meson in the positive 1-direction.

The spinor representations of these Lorentz transformations are given by *e.g.*

$$S_{\Lambda_{\bar{P}_{(3)}}} = \cosh\frac{\phi_{(3)}}{2}\mathbb{1} + \sinh\frac{\phi_{(3)}}{2}\gamma^0\gamma^3 = \sqrt{\frac{\gamma_{(3)}+1}{2}}\mathbb{1} + \sqrt{\frac{\gamma_{(3)}-1}{2}}\gamma^0\gamma^3\,, \tag{4.44}$$

for a boost in the positive 3-direction.

4.2.2 The integration

Apart from the calculation of the (boosted) vertex functions, Eq. (4.31) requires performing a four-dimensional integral. The expression for the GPD is written in light-cone coordinates. The δ-function suggests the use of these coordinates in the integration, *i.e.* $\mathrm{d}^4p = 2\mathrm{d}p^+\mathrm{d}p^-\mathrm{d}\boldsymbol{p}_\perp$, where the integration over p^+ is trivial. However, the Bonn model is an instant-form model in which the vertex functions are calculated through the expansion (4.32). Because of the strict separation between the energy and three-momentum components in the Bonn model, the infinitesimal four-volume d^4p is written in instant-form instead of light-cone coordinates: $\mathrm{d}^4p = \mathrm{d}p^0\mathrm{d}^3\boldsymbol{p}$, making the numerical integration more straightforward.

The δ-function in Eq. (4.31) can be rewritten in the Breit frame as

$$\delta\left(\frac{2x+\xi-1}{2(1+\xi)}\bar{P}^+ - p^+\right) = \sqrt{2}\,\delta\left((2x+\xi-1)\frac{\bar{M}}{2} - (p^0+p^3)\right)\,, \tag{4.45}$$

so that the p^0-integration is trivial. The integrand which remains after integrating out p^0, is a function of the momentum vector components p^1, p^2 and p^3. The propagators in Eq. (4.31) give rise to a denominator which consists of three factors:

$$\left((\frac{\bar{P}}{2}+p+\Delta)^2-m_1^2+i\epsilon\right) \quad , \quad \left((\frac{\bar{P}}{2}+p)^2-m_1^2+i\epsilon\right) \quad \text{and} \quad \left((-\frac{\bar{P}}{2}+p)^2-m_2^2+i\epsilon\right). \tag{4.46}$$

For most kinematical situations, these factors each form a singular pole in the complex p^3-plane. As will be discussed in more detail in the next chapter, the propagator poles are not the only poles in this plane: the vertex functions also have poles. Depending on the radial basis functions used, these poles are either complex conjugated, multiple poles with a finite imaginary part (Jacobi basis), or poles at $\mathfrak{Re}(p^3) \pm i\infty$. A strategy for the calculation of the integration over p^3 could be to choose the Jacobi basis for the radial part, and to determine the residue of the integrand of Eq. (4.31) by contour integration around the multiple poles, as well as calculating the residue in the (singular) propagator poles in one of the half-planes (Cauchy's theorem). This simple but neat concept was developed for the calculation of electromagnetic form factors in the Bonn model in Ref. [118]. However, it is not useful for the calculation of GPDs in the model.

Due to the separation of radial and angular basis functions, Eq. (4.32), there are cuts in the complex p^3-plane. To prove this, we write the argument of the vertex function in the last line of Eq. (4.43) as $p_{in} = \Lambda^{-1}_{\bar{P}_{(3)}}\left(\Lambda^{-1}_{\bar{P}_{(1)}}(p)\right)$. The momentum p_{in} is the relative momentum between the quark and the antiquark in the rest frame of the incoming meson. We know that in this frame, the radial part of the vertex function only depends on $|\boldsymbol{p_{in}}|$ (see Eqs. (3.25) and (4.32)), which can be written as

$$|\boldsymbol{p}_{in}| = \sqrt{(p^1_{in})^2 + (p^2_{in})^2 + (p^3_{in})^2}\,. \tag{4.47}$$

Bearing in mind that the p^i_{in} are found via two subsequent Lorentz transformations and a δ-function, we find that both p^1_{in} and p^3_{in} are functions of p^3, so that this equation will give rise to a cut in the complex p^3-plane. It turns out that the poles of the Jacobi basis functions are the end points of some of these cuts (see Ref. [118] for an explicit expression of the Jacobi basis functions). A contour integral around such a pole will therefore always cross a cut. As a result, the integration over p^3 cannot be calculated this way, and another strategy must be used for the calculation of the p^3-integral.

At this point, it should be noted that the GPD, calculated from Eq. (4.31), is a complex number, and the hermiticity of the bilocal current matrix element is violated in our model. In the calculation of the electromagnetic form factors, this problem was also encountered. By comparing Bonn model results with results in the Wick-Cutkosky model, it was proven that the (unphysical) imaginary part is caused by the instantaneous approximation [92, 119]. Because the form factors are nothing else but integrated generalized parton distributions (Eq. (2.22)), it is clear that also in the case of generalized parton distributions, it is the instantaneous approximation which violates the hermiticity. However, it was found that the real part of the electromagnetic form factors calculated in the Bonn model nicely agrees with the experimental form factor data [19]. In the form factor calculations, the imaginary part of the form factor could therefore be ignored without losing model agreement with the data and predictive power. Because of the relation between GPDs and form factors, we decide to only keep the real part of the generalized parton distribution, which after integration over x gives rise to that part of the form factor which agrees smoothly with the experimental data.

Considering only the real part, the integration over p^3 can be performed analytically using a result from the principal value technique: for an isolated singularity, the real part of the integration over p^3 equals

$$\mathfrak{Re}\left\{ i \int_{p^3_k - a}^{p^3_k + a} \mathrm{d}p^3 \frac{f(p^3)}{p^3 - p^3_k \pm i\epsilon} \right\} = \pm \pi f(p^3_k)\,. \tag{4.48}$$

For a double pole, the real part becomes

$$\mathfrak{Re}\left\{ i\int_{p_k^3-a}^{p_k^3+a} \mathrm{d}p^3 \frac{f(p^3)}{(p^3-p_k^3\pm i\epsilon)^2}\right\} = \pm\pi f'(p_k^3)\,. \tag{4.49}$$

The remaining integrations over p^1 and p^2 are performed numerically using a variable step size routine based on Gaussian integration. Convergence is checked by comparing the difference between two successive integration steps with a pre-defined integration precision.

4.3 Generalized parton distributions of spin-$1/2$ baryons

In this dissertation the main focus is on computing the GPDs of pseudoscalar mesons in the Bonn model. For future research it is interesting to show how the GPDs of the nucleon could be determined. At this moment, much experimental effort is devoted to the measurement of proton GPDs, and model estimates of H, E, $\tilde{H}$ and $\tilde{E}$ are needed to explain the data. In Appendix C we outline the major differences between computing meson and baryon properties in the Bonn constituent quark model.

From Eqs. (2.25), it is clear that the calculation of the four parton helicity conserving nucleon GPDs starts from matrix elements of the type

$$\langle \bar{P}'|N\{\bar{\psi}(-\frac{z}{2})\Omega^\mu\psi(\frac{z}{2})\}|\bar{P}\rangle\,, \tag{4.50}$$

i.e. bilocal current matrix elements with some specific combination of Dirac matrices Ω^μ. The calculation of these matrix elements in a Bethe-Salpeter framework is very similar to the meson case, explained in Sect. 4.1. Instead of the six-point Green's function, however, we now start from the eight-point Green's function (with $T\{\bar{\psi}(y')\Omega^\mu\psi(y)\} = O^\mu(y,y')$):

$$\begin{aligned} G^\mu_{\alpha\alpha'\alpha''\beta\beta'\beta''}(x_1',x_2',x_3';y',y;x_1,x_2,x_3) = \\ \langle\Theta|T\{\psi^1_\alpha(x_1')\psi^2_{\alpha'}(x_2')\psi^3_{\alpha''}(x_3')O^\mu(y,y')\bar{\psi}^1_\beta(x_1)\bar{\psi}^2_{\beta'}(x_2)\bar{\psi}^3_{\beta''}(x_3)\}|\Theta\rangle\,. \end{aligned} \tag{4.51}$$

The imposed time-ordering now reads: $(x_1'^0,x_2'^0,x_3'^0) \gg (y^0,y'^0) \gg (x_1^0,x_2^0,x_3^0)$. The derivation of the matrix element through the Mandelstam formalism is completely analogous to the derivation in the beginning of this chapter. The only difference is that one now has to consider three intermediate quark lines instead of two. After applying

Wick's theorem, the following kernel is found:

$$\begin{aligned} K^{\mu(0)}_{\delta\delta'\delta''\epsilon\epsilon'\epsilon''}(x_1'', x_2'', x_3''; y', y; x_1''', x_2''', x_3''') = &\sum_{\kappa\kappa'}\sum_{\lambda\lambda'} \delta^{(4)}(x_1'' - y')\delta_{\delta\kappa}\Omega^{\mu}_{\kappa\kappa'}\delta^{(4)}(y - x_1''')\delta_{\kappa'\epsilon} \\ &\times\ \delta^{(4)}(x_2''' - x_2'')\delta_{\delta'\lambda}(i\ \partial\!\!\!/_{x_2''} - m_2)_{\lambda\epsilon'} \\ &\times\ \delta^{(4)}(x_3''' - x_3'')\delta_{\delta''\lambda'}(i\ \partial\!\!\!/_{x_3''} - m_3)_{\lambda'\epsilon''} \\ &+ \text{coupling to particles 2 and 3} \\ &+ \text{self-coupling of the bilocal current.} \end{aligned} \tag{4.52}$$

With this relation and Eqs. (2.26), the nucleon GPDs can be calculated.

5 GPDs of pseudoscalar mesons

It matters not what goal you seek
Its secret here reposes:
You've got to dig from week to week
To get Results or Roses.

E. Guest

5.1 Introduction

In the previous chapter, we have shown how generalized parton distributions of pseudoscalar mesons can be calculated within the framework of the Bonn model. This chapter focuses on the results.

In the Bonn model, isospin symmetry is exact with identical masses for the up and down quarks. As a result, the pion triplet will be degenerate in the mass spectrum. However, the three triplet partners do differ in their isospin projection quantum number and their valence quark flavor content. Also their electromagnetic form factors are different. Similar observations hold for the kaon members of the pseudoscalar octet. Because an interpretation of the GPD results in terms of the flavor content, as well as the comparison with the form factors through the sum rule (2.22) requires a specific choice, we limit the discussion in this chapter to the π^+ ($u\bar{d}$) and K^+ ($u\bar{s}$) octet partners.

Section 5.2 was published in a slightly adapted form in Ref. [63]. A small selection of the GPD calculations in Sect. 5.4 has been published in Ref. [87]. An extensive article containing all the results is in preparation [120].

This chapter is organized as follows. We start with an analytical view on the support properties of GPDs in Bethe-Salpeter models. Next, we test whether the numerical code behaves as required. We end the chapter with a detailed discussion of the results obtained in our model.

5.2 Remarks on the support of the GPDs

The prescription on how to calculate the generalized parton distribution of pseudoscalar mesons was given in Eq. (4.31). A superficial glimpse of this equation does not reveal much about its properties, *e.g.* its dependence on the kinematical variable x. However, a closer look into the analytical structure of Eq. (4.31) shows that this neat formula exhibits some peculiar and unwelcome properties.

Let us first *assume* that the vertex functions in Eq. (4.31) do not depend on p^3. The denominator then immediately suggests the correct support region for the GPDs, which was defined in Sect. 2.2.1. Making use of the δ-function to integrate over p^0, it is possible to write the propagator denominators (4.46) as follows:

$$\begin{aligned}
\big((\frac{\bar{P}}{2}+p+\Delta)^2-m_1^2+i\epsilon\big) &= \mathcal{A}-2\bar{M}(x-\xi)p^3+i\epsilon\,,\\
\big((\frac{\bar{P}}{2}+p)^2-m_1^2+i\epsilon\big) &= \mathcal{B}-2\bar{M}(x+\xi)p^3+i\epsilon\,,\\
\big((-\frac{\bar{P}}{2}+p)^2-m_2^2+i\epsilon\big) &= \mathcal{C}-2\bar{M}(x-1)p^3+i\epsilon\,,
\end{aligned} \tag{5.1}$$

where $\mathcal{A}$, $\mathcal{B}$ and $\mathcal{C}$ do not depend on p^3. From these expressions, it is clear that the propagators have poles in the complex p^3-plane. The position of these poles with respect to the real p^3-axis (upper or lower half-plane) depends on the kinematics, more specifically on the sign of $(x-\xi)$, $(x+\xi)$ and $(x-1)$. For $x\notin[-\xi,1]$, the propagator poles lie on the same side of the real axis. Furthermore, the propagators are analytic in all other points of the complex plane. Assuming that the vertex function Γ does not contain poles in the complex p^3-plane, and making use of Cauchy's theorem, one can conclude that the momentum dependence of the propagators ensures the correct support for the GPDs.

The above considerations are clearly valid when the vertex function Γ and its adjoint do not depend on p^3. This makes Γ free from poles when analytically continued into the complex p^3-plane. The equations (5.1) can be transformed to light-cone coordinates $(p^+,p^-,\boldsymbol{p}_\perp)$. Along similar lines, one can prove that the correct support for the GPDs is guaranteed in these coordinates, when Γ does not depend on p^-. The calculation of the pion GPD with constant vertex functions has been performed by S. Noguera *et al.* in the NJL-model with a Pauli-Villars regularization procedure [79]. The calculation of GPDs with p^--independent vertex functions was performed by H.-M. Choi *et al.* [85, 86], as well as by B.C. Tiburzi and G.A. Miller [81, 82, 83]. These authors made use of a reduction of Bethe-Salpeter amplitudes to light-cone wave functions by projecting on the light-cone. In Refs. [81, 82, 83], the scalar Wick-Cutkosky model was adopted

and successfully applied to the calculation of scalar meson GPDs. In Refs. [85, 86], the light-front Bethe-Salpeter vertex functions were replaced by wave functions obtained in a light-front constituent quark model. All of these calculations yielded the correct support, in agreement with the present analysis.

In the Bonn model, however, the vertex functions depend on p^3 (or, in light-cone coordinates, p^-), which makes them have a more intricate pole structure. In this case, the correct support can no longer be guaranteed. To prove this, we start with Liouville's theorem, which states that *the only bounded entire functions are the constant functions*. As a result, a vertex function which depends on the momentum variable p^3 will not be bounded for all points in the complex p^3-plane. Moreover, the radial part of a vertex function for a ground-state particle is a real-valued function on the real p^3-axis, up to a constant phase factor. This is an important constraint. Indeed, for a holomorphic function f whose restriction to the real numbers is real-valued, it can be proven that $f(p^{3*}) = f^*(p^3)$. Here, * stands for complex conjugation. In other words: if f has a singularity in the upper half-plane, it also has one in the lower half-plane, and vice versa. Combining these two statements, we find that a dynamic, momentum dependent vertex function with no poles on the real axis will either have complex conjugated poles, or a singularity on both complex half-circles at $\mathfrak{Re}(p^3) \pm i\infty$. In the latter case, Cauchy's theorem is no longer applicable, while in the former case, there will always be at least one pole in each half-plane. Consequently, it is not a priori clear whether the quark (antiquark) GPD will vanish outside the interval $x \in [-\xi, 1]$ ($x \in [-1, \xi]$). This means that there is a chance that the correct support is violated in Bethe-Salpeter models for mesons containing momentum-dependent quark dynamics[1].

This does not necessarily point to a support problem for Bethe-Salpeter constituent quark models in which the approximations of Sect. 3.3.1 are adopted - it merely shows that a support problem can *no longer be excluded*. The above considerations indicate that guaranteeing the correct support puts non-trivial constraints on the analytic properties of the Bethe-Salpeter vertex functions. Whether these are fulfilled in particular models has to be checked for each individual case. In the next sections, it will be shown that the Bonn model is prone to a support problem.

To investigate the severeness of the support problem, a support parameter (ϕ) is introduced. For the pion, the generalized quark and antiquark distributions are related via the isospin symmetry relation (2.24), so that the knowledge of one of them implies

[1] Similar arguments apply to relativistic quark-diquark models of the nucleon with pointlike constituents. For qqq-Bethe-Salpeter models, such as the Bonn model for baryons, the propagator poles do not explicitly hint at the correct support region, so that a similar analysis to the one here presented could not be established.

the knowledge of the other. The support parameter is therefore defined through the quark GPD:

$$\phi = \frac{\int_{-\xi}^{1} |H^u_{\pi^+}(x,\xi,t)| \mathrm{d}x}{\int_{-\infty}^{\infty} |H^u_{\pi^+}(x,\xi,t)| \mathrm{d}x} \,. \tag{5.2}$$

ϕ is a measure for the relative support violation: when the correct kinematical regions are resolved, $\phi = 1$. The smaller the ϕ, the worse the support.

For the kaon, however, the isospin symmetry relation (2.24) is not valid and different support parameters are introduced for the quark and antiquark GPDs:

$$\phi^q = \frac{\int_{-\xi}^{1} |H^u_{K^+}(x,\xi,t)| \mathrm{d}x}{\int_{-\infty}^{\infty} |H^u_{K^+}(x,\xi,t)| \mathrm{d}x} \quad \text{and} \quad \phi^{\bar{q}} = \frac{\int_{-1}^{\xi} |H^s_{K^+}(x,\xi,t)| \mathrm{d}x}{\int_{-\infty}^{\infty} |H^s_{K^+}(x,\xi,t)| \mathrm{d}x} \,. \tag{5.3}$$

In Sect. 5.4, we will investigate the flavor dependence of the support problem through the difference between ϕ^q and $\phi^{\bar{q}}$.

Before turning to the numerical evaluation of the GPDs, some critical checks can be performed which put the numerical code to a stringent test. These will be the subject of the next section.

5.3 Numerical tests

In Sect. 4.2.1, it was explained that the Bonn model requires a set of radial and angular basis functions to calculate the vertex functions in the Bonn model. It was mentioned that three sets of radial basis functions were implemented in the Bonn code: the Jacobi and Laguerre polynomials and the harmonic oscillator basis. Theoretically, an infinite amount of these functions is needed to calculate the radial part of the vertex functions. However, a reasonable convergence is expected at a finite basis size N_{max}. In order for the GPD code to be physically acceptable, it is important that:

1. the choice of the radial basis functions has no significant impact on the GPD output, and that

2. N_{max} is chosen such that a satisfactory degree of convergence is achieved.

In former calculations of form factors and mass states in the Bonn model, it was shown that a convergence was reached within a basis with $N_{max} = 10$. Also in the calculations of GPDs, we expect this number to be high enough. In this section, we will show that this is indeed true.

5.3.1 Influence of the radial basis on the GPD

Due to the finite size of the radial basis, the specific choice of basis functions can influence the results. However, when N_{max} is large enough, the impact on the calculations should remain small. In Fig. 5.1, $H^u_{\pi^+}(x, \xi = 0, t = -1.0\ \text{GeV}^2)$ is shown for the three sets of basis functions. The data points were calculated in the full model (see Sect. 5.4.1) with $N_{max} = 10$. In these calculations, the pion masses were $M_\pi = 140.879$ MeV (Jacobi basis), $M_\pi = 140.990$ MeV (Laguerre basis) and $M_\pi = 146.823$ MeV (harmonic oscillator basis).

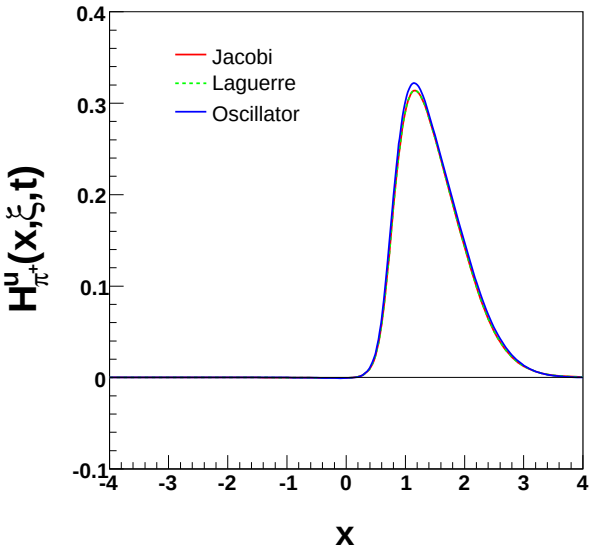

Figure 5.1 The GPD $H^u_{\pi^+}(x, \xi = 0, t = -1.0\ \text{GeV}^2)$, calculated with three different radial bases: the Jacobi functions (red), the Laguerre functions (green) and the harmonic oscillator functions (blue).

From Fig. 5.1, it is obvious that all the different choices for the model states produce a similar x-dependence. Some deviation between the oscillator and Jacobi/Laguerre results is observed. This difference amounts to less than 3% in the peak height and is completely similar to the discrepancy between the pion masses in the three cases. Therefore, we can safely conclude that the choice of the basis indeed does not alter the GPD significantly, and one specific basis can be chosen. The calculations shown in the remainder of this chapter are performed with the Laguerre radial basis functions.

In the light of the above discussion on the support, it is important to remark that the GPD $H^u_{\pi^+}(x, \xi = 0, t = -1.0\ \text{GeV}^2)$ of Fig. 5.1 exhibits a support problem: outside the interval $x \in [0, 1]$, the GPD does not vanish. The size of the support problem

will become clear in Sect. 5.4, where we present our results and investigate which parameters affect the support.

5.3.2 Finite basis size N_{max}

As outlined in the introduction to this section, the numerical calculations require a truncation in the amount of basis states. In earlier Bonn model calculations, convergence was achieved for $N_{max} = 10$. To prove that this number is sufficient for the calculation of generalized parton distributions, too, we show in Fig. 5.2 the convergence of the pion mass and of the GPD in three representative kinematical conditions with respect to the number of basis functions. It is clear that for $N_{max} = 10$, the predictions for both the mass and the GPDs have converged.

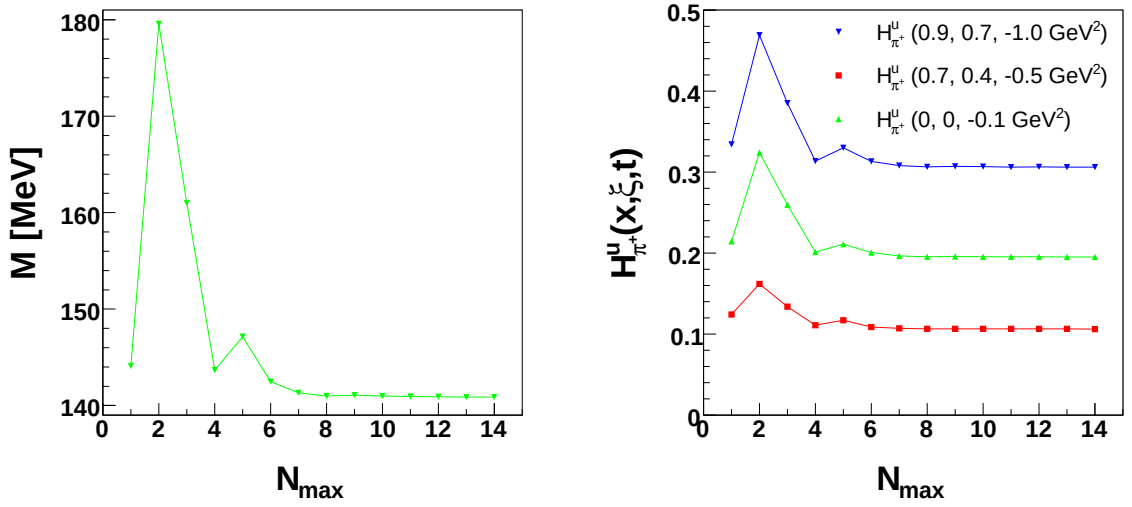

Figure 5.2 The mass (left) and the GPD $H^u_{\pi^+}(x,\xi,t)$ (right) in terms of the number of Laguerre radial basis functions in a full model calculation.

After guaranteeing that the numerical code is under control, we are ready to calculate the generalized parton distributions.

5.4 Results and discussion

In Sect. 5.2, it was argued that the Bonn model might suffer from a support problem. The GPD $H^u_{\pi^+}(x,\xi,t)$ shown in Fig. 5.1 already indicated that the correct support is indeed violated. In this section, we will quantify the severeness of the problem with the aforementioned support parameters ϕ, ϕ^q and $\phi^{\bar{q}}$ and check which physical parameters influence the support. Questions which are addressed in this section, include: is

Parameter	Full model	Reduced model	IQM model
m_n [MeV]	380	380	800
m_s [MeV]	550	550	-
a_c [MeV]	-1135	-1135	-1135
b_c [MeV/fm]	1300	1300	1300
g [GeV^{-2}]	1.62	0.0	1.62
g' [GeV^{-2}]	1.35	0.0	1.35
Λ [fm]	0.42	-	0.42

Table 5.1 Overview of the parameters of the three models that were used in this work: the constituent quark masses, the confinement offset and slope, the 't Hooft interaction range and the 't Hooft interaction strengths. A dash (-) means that the parameter in question had no influence on the presented results.

the deep binding of the pion responsible for (a part of) the support violation? What happens when the kinematical variables ξ and t are altered? How do the constituent quark masses influence the support? What is the role of the constituent quark flavor? And is it possible to build a model, based on the approximations of the Bonn model, which gives rise to the correct support regions? To find an answer to these questions, we have calculated the GPDs of the pion and the kaon. Thereby, we have varied the model parameters. We start this section by introducing the model variants.

5.4.1 Model parameters

To investigate the questions that were addressed above, we will show results for the GPDs of pseudoscalar mesons in three different models: the full model, the reduced model and the increased quark mass (IQM) model. The parameters of these models are tabulated in Table 5.1. Notice that the parameters of the confinement interaction remain the same for all models.

Full model

The full model is the one referred to as Model $\mathcal{B}$ in Ref. [110]. It provides an accurate description of the pion and other meson properties such as its mass, electromagnetic form factor, electroweak decay widths, etc. In the full model, the pion is deeply bound, with a mass of $M_\pi^{full} = 141$ MeV and a mass defect of $\Delta_{M_\pi}^{full} = (2m_n - M_\pi^{full}) = 619$ MeV. The kaon is moderately bound in this model, with a mass of $M_K^{full} = 506$ MeV and a mass defect of $\Delta_{M_K}^{full} = (m_n + m_s - M_K^{full}) = 424$ MeV. In the particle physics book-

Meson	Model	M (MeV)	Δ_M (MeV)	Δ_M/M
Pion	Full model	141	619	4.39
	Reduced model	572	188	0.33
	IQM model	1095	505	0.46
Kaon	Full model	506	424	0.84
	Reduced model	728	202	0.28

Table 5.2 A summary of the masses M, binding energies Δ_M and relative binding energies Δ_M/M of the pion and the kaon in the different models.

let by the Particle Data Group, the mass of the pion is listed as $M_{\pi^\pm} = 139.57018 \pm 0.00035$ MeV and $M_{\pi^0} = 134.9766 \pm 0.0006$ MeV. For the kaon, the experimentally verified masses are $M_{K^\pm} = 493.667 \pm 0.016$ MeV and $M_{K^0} = 497.648 \pm 0.022$ MeV [111].

Reduced model

In the reduced model, the 't Hooft instanton induced interaction is omitted. As we have described in Chapter 3, the instanton interaction accounts for the deep binding of the pion (and to a lesser degree also of the kaon). Neglecting the 't Hooft interaction will therefore give an idea of the importance of deep binding effects in the presented GPD results. As a matter of fact, the calculated pion mass increases to $M_\pi^{red} = 572$ MeV in this approach ($\Delta_{M_\pi}^{red} = 188$ MeV). The kaon mass increases to $M_K^{red} = 728$ MeV ($\Delta_{M_K}^{red} = 202$ MeV).

Increased quark mass (IQM) model

Not only the 't Hooft instanton induced interaction has an effect on the pion binding energy. Also the non-strange constituent quark mass affects the pion mass and mass defect. To investigate the influence of the binding energy on the support of the generalized parton distributions, both mechanisms must be studied.

In the IQM model, we will only show results for the pion GPD. After combining the IQM model results with the kaon results from the full model, one can determine the influence of the heavy quarks. Increasing the non-strange quark mass to $m_n = 800$ MeV yields a pion mass of $M_\pi^{IQM} = 1095$ MeV. The mass defect in this model is $\Delta_{M_\pi}^{IQM} = 505$ MeV.

Model summary

The masses, binding energies and relative binding energies (defined as the binding energy devided by the mass) calculated in the different models are summarized in

Table 5.2. The deep binding of the pion in the full model is reflected in the high relative binding energy. The kaon is relatively much less bound in the full model, although still relatively deeper than in the reduced model, and also than the pion in both the reduced and the IQM model. In the next section, we will come back to these (relative) binding energies.

5.4.2 Results

The π^+ up-quark GPD results in the three different models are shown in Figs. 5.3 - 5.8, the K^+ GPDs in Figs. 5.9 - 5.12. A three-dimensional picture of the (full model) π^+ up-quark GPD as a function of x and t, with skewedness $\xi = 0$, is presented in Fig. 5.15. For all cases, the results are shown in their respective support regions as well as in an extended x-region, for a representative selection of t and ξ values. Remark that ξ has an upper limit $\xi_{max} = \sqrt{\frac{-t}{4M^2-t}}$, as was stated in Eq. (2.18).

To understand the support problem better, we will examine the structure of the GPD curves shortly. First, we will check if the model constraints that were addressed in Chapter 2 are met. These constraints are the isospin symmetry relation (2.24), the relation with the electromagnetic form factor (2.22) and the polynomiality condition (2.23).

Isospin symmetry

The pion up and down quark GPDs should fulfill the isospin symmetry relation of Eq. (2.24):

$$H^u_{\pi^+}(x,\xi,t) = -H^d_{\pi^+}(-x,\xi,t)\,. \tag{5.4}$$

The equality is exact in our calculations. For this reason, only the quark GPDs are presented in Figs. 5.3 - 5.8.

The strange quark content of the kaon prevents an isospin symmetry relation of the type (5.4) to be written. The results indeed show a small difference between the quark and antiquark GPDs at opposite x (*e.g.* in the full model, $H^u_{K^+}(0.5, 0, -0.5\ \text{GeV}^2) = 0.764$ versus $H^s_{K^+}(-0.5, 0, -0.5\ \text{GeV}^2) = -0.784$). Therefore, both quark and antiquark results are presented in Figs. 5.9 - 5.12. We will quantify these differences in the discussion of the support parameters at the end of this chapter.

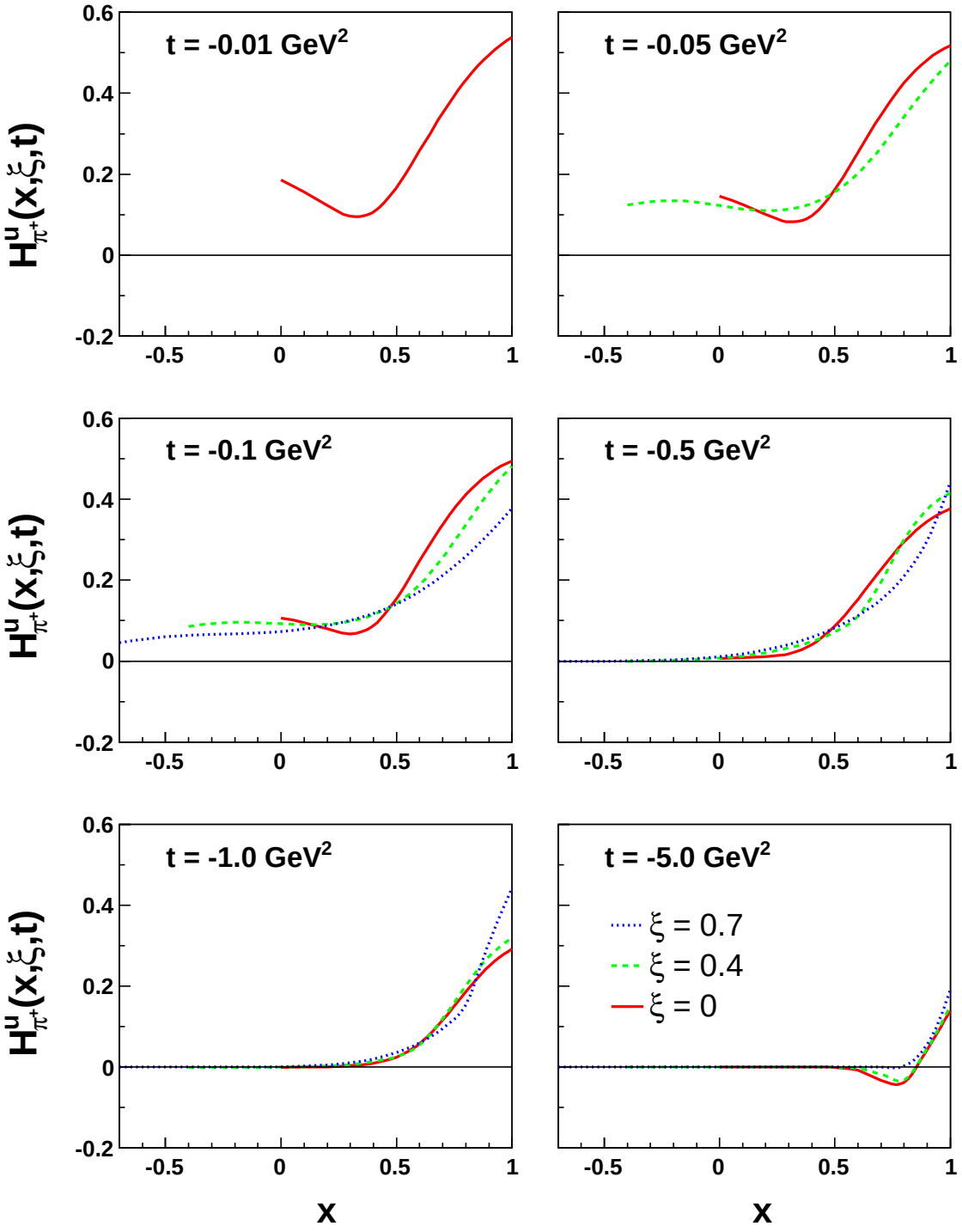

Figure 5.3 The pion GPD $H^u_{\pi^+}$ in the full model. Results are shown for the supported ERBL and DGLAP regions at different values of t. Values for ξ shown are $\xi = 0$ (red, solid line), $\xi = 0.4$ (green, dashed line) and $\xi = 0.7$ (blue, dotted line).

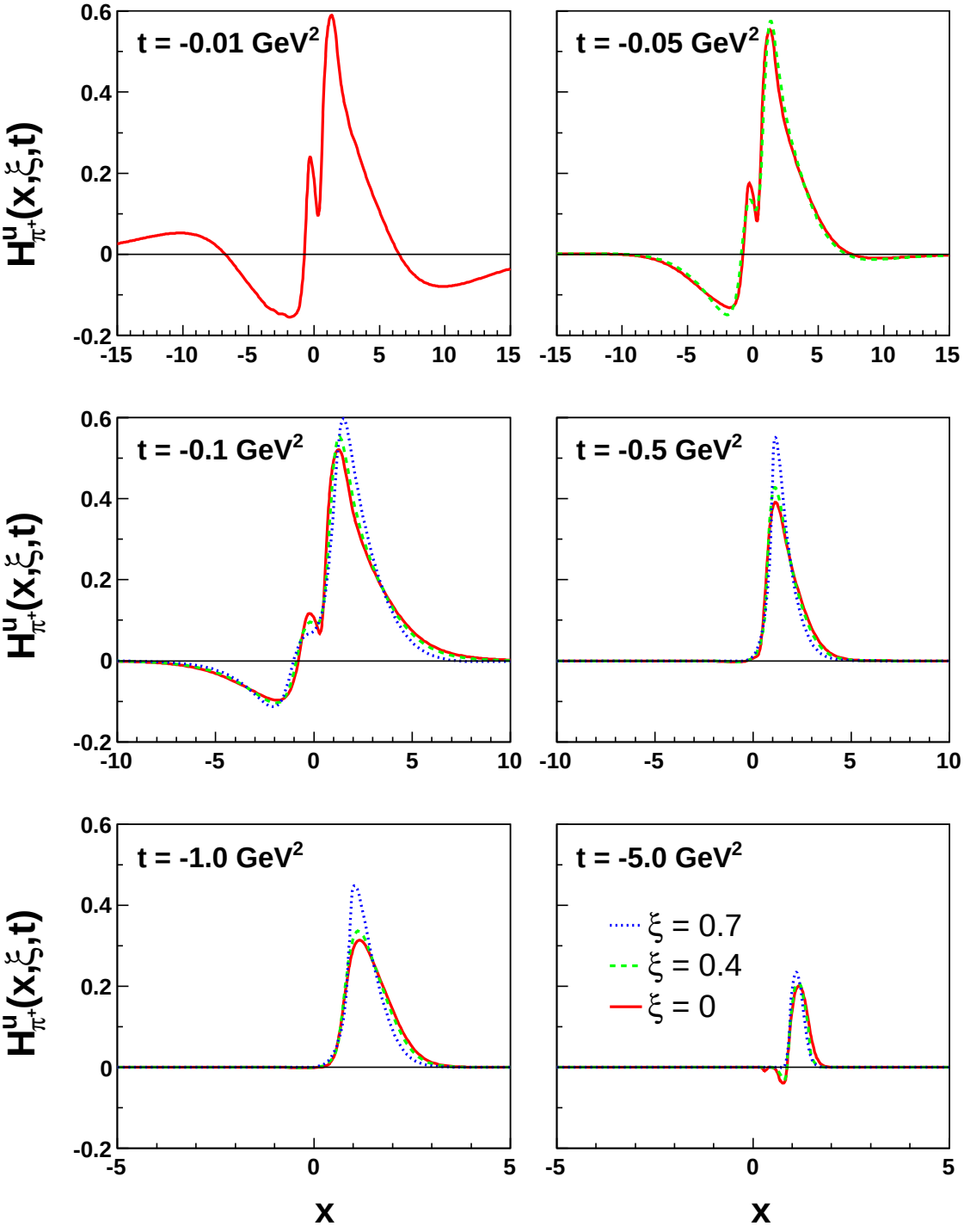

Figure 5.4 Same plots as in Fig. 5.3, but for a broader region in x.

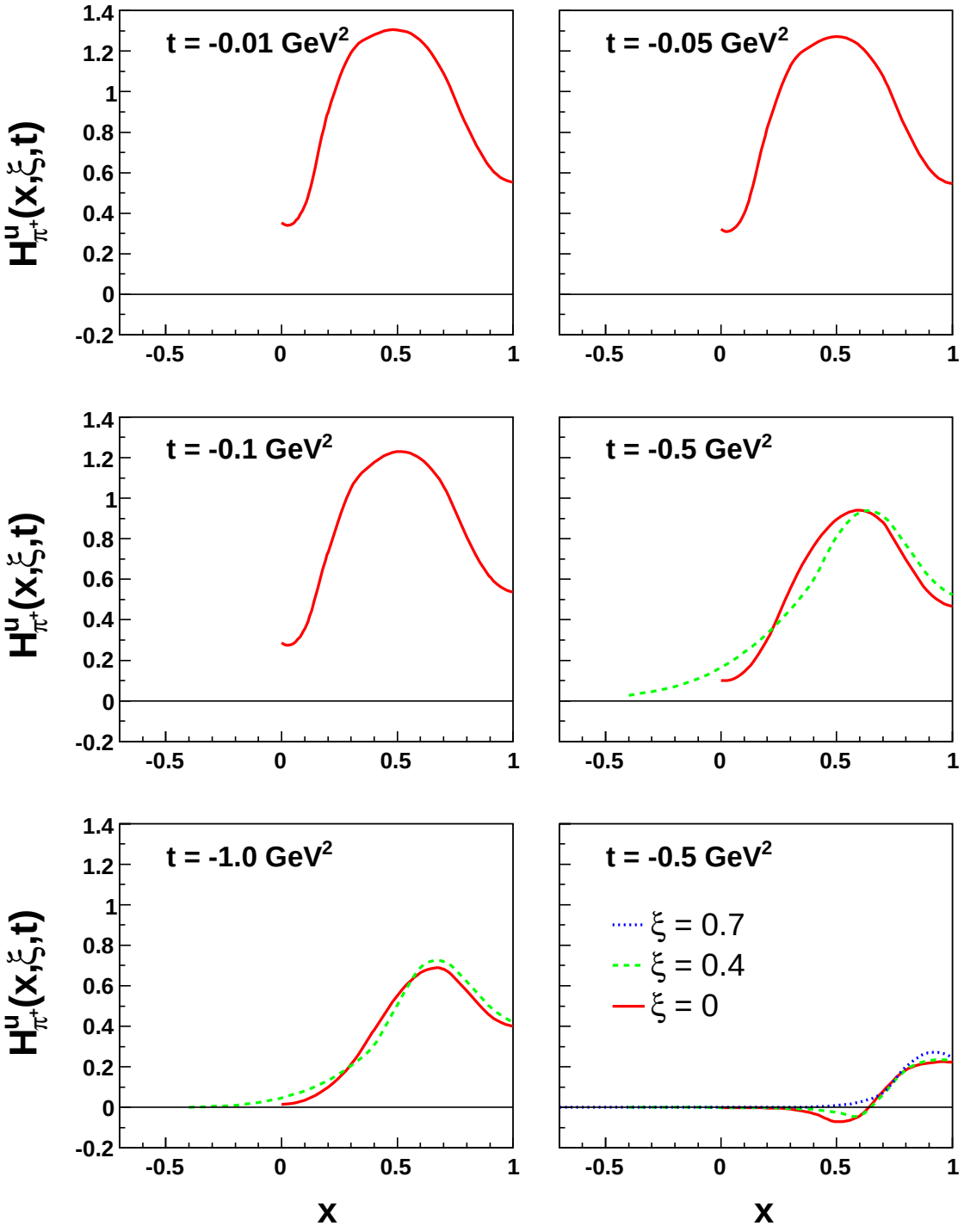

Figure 5.5 The pion GPD $H^u_{\pi^+}$ in the reduced model. Results are shown for the supported ERBL and DGLAP regions at different values of t. Values for ξ shown are $\xi = 0$ (red, solid line), $\xi = 0.4$ (green, dashed line) and $\xi = 0.7$ (blue, dotted line).

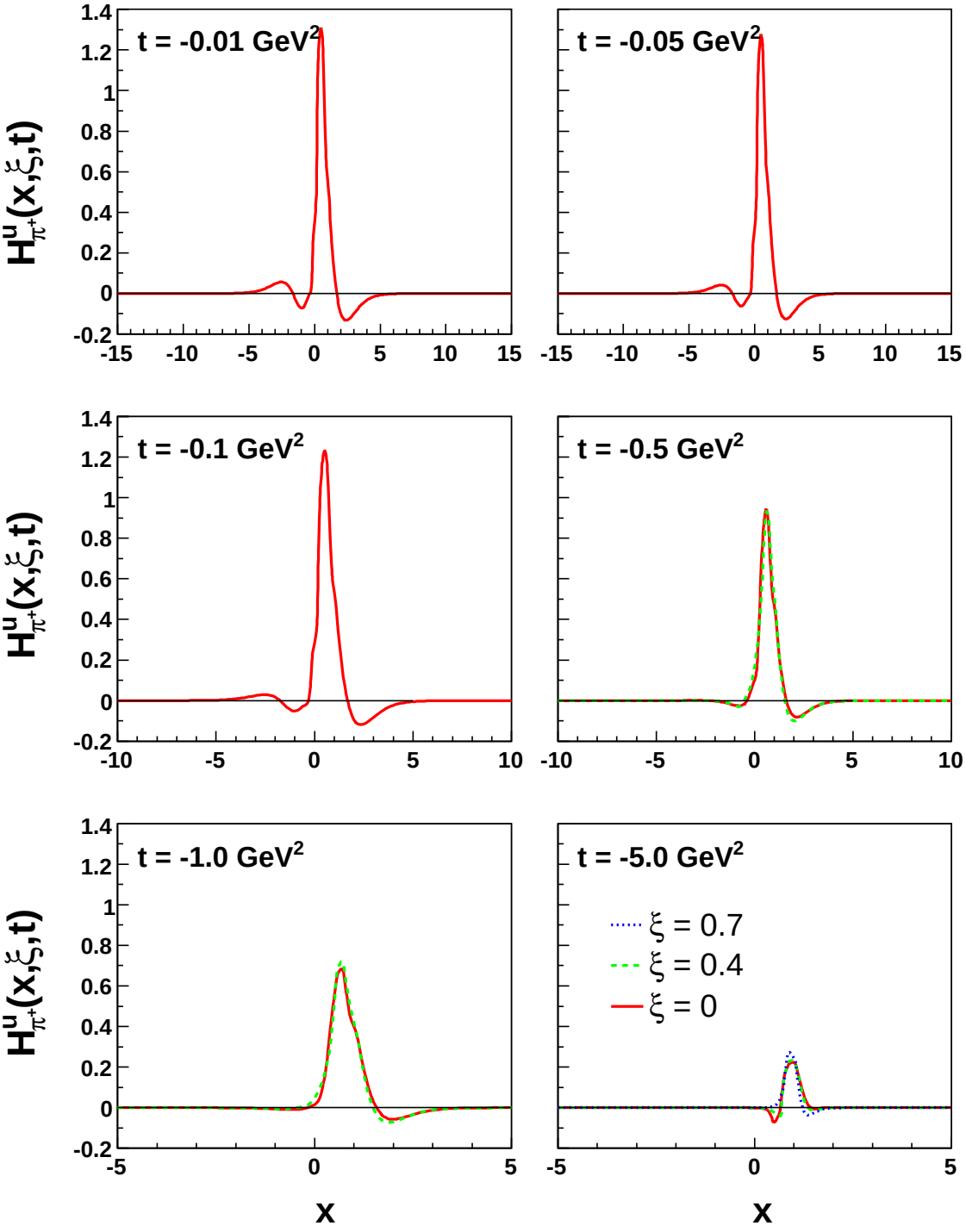

Figure 5.6 Same plots as in Fig. 5.5, but for a broader region in x.

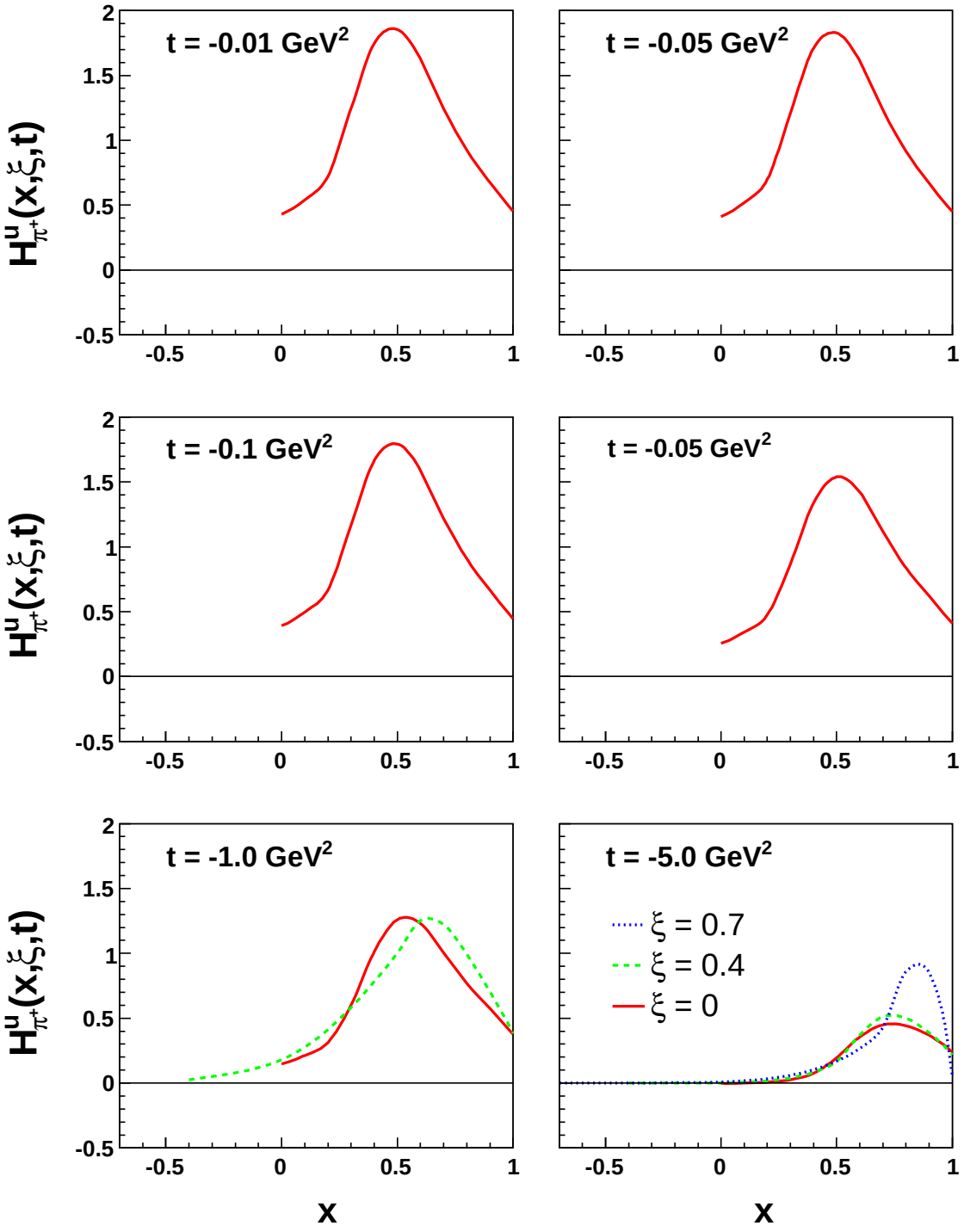

Figure 5.7 The pion GPD $H^u_{\pi^+}$ in the IQM model. Results are shown for the supported ERBL and DGLAP regions at different values of t. Values for ξ shown are $\xi = 0$ (red, solid line), $\xi = 0.4$ (green, dashed line) and $\xi = 0.7$ (blue, dotted line).

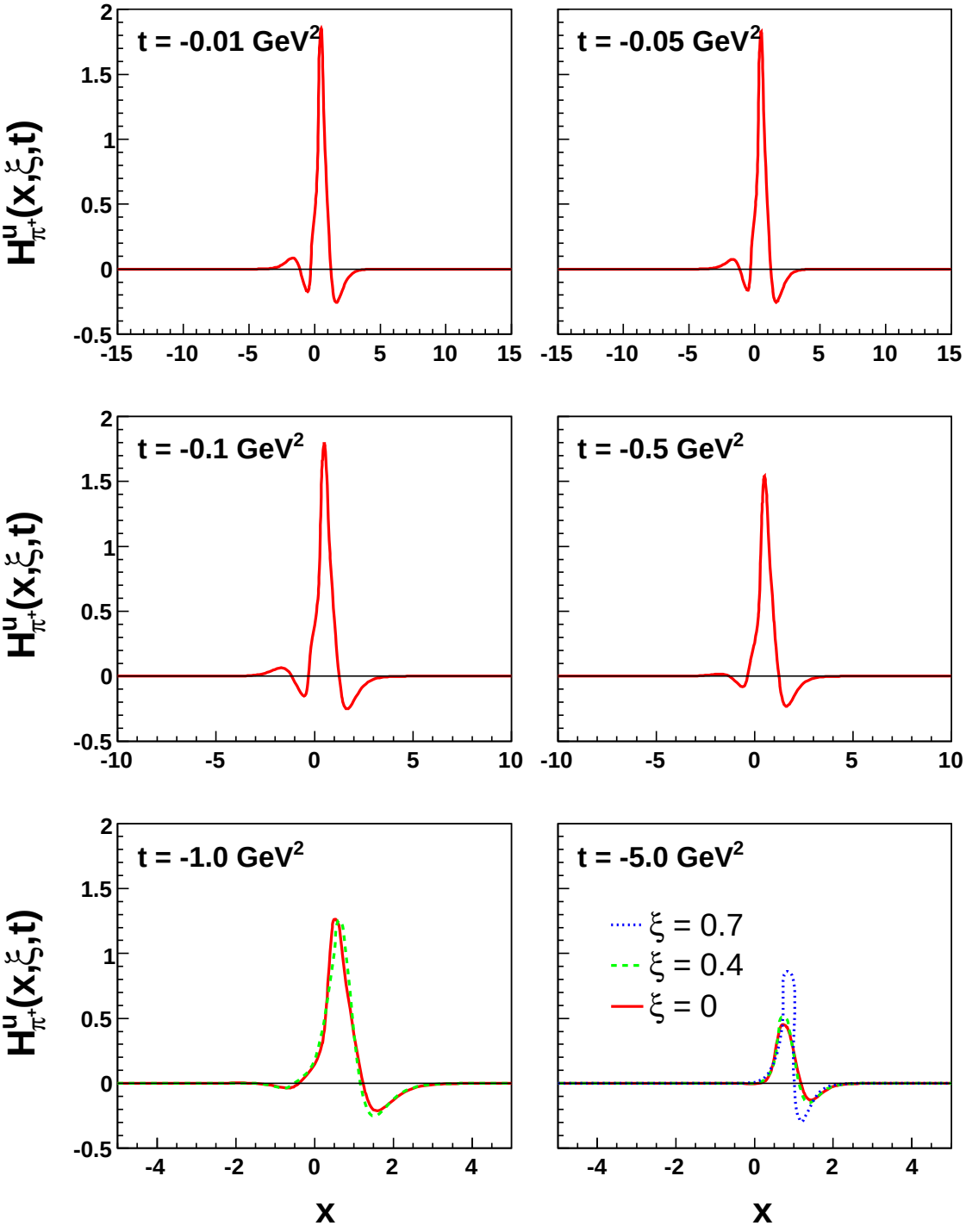

Figure 5.8 Same plots as in Fig. 5.7, but for a broader region in x.

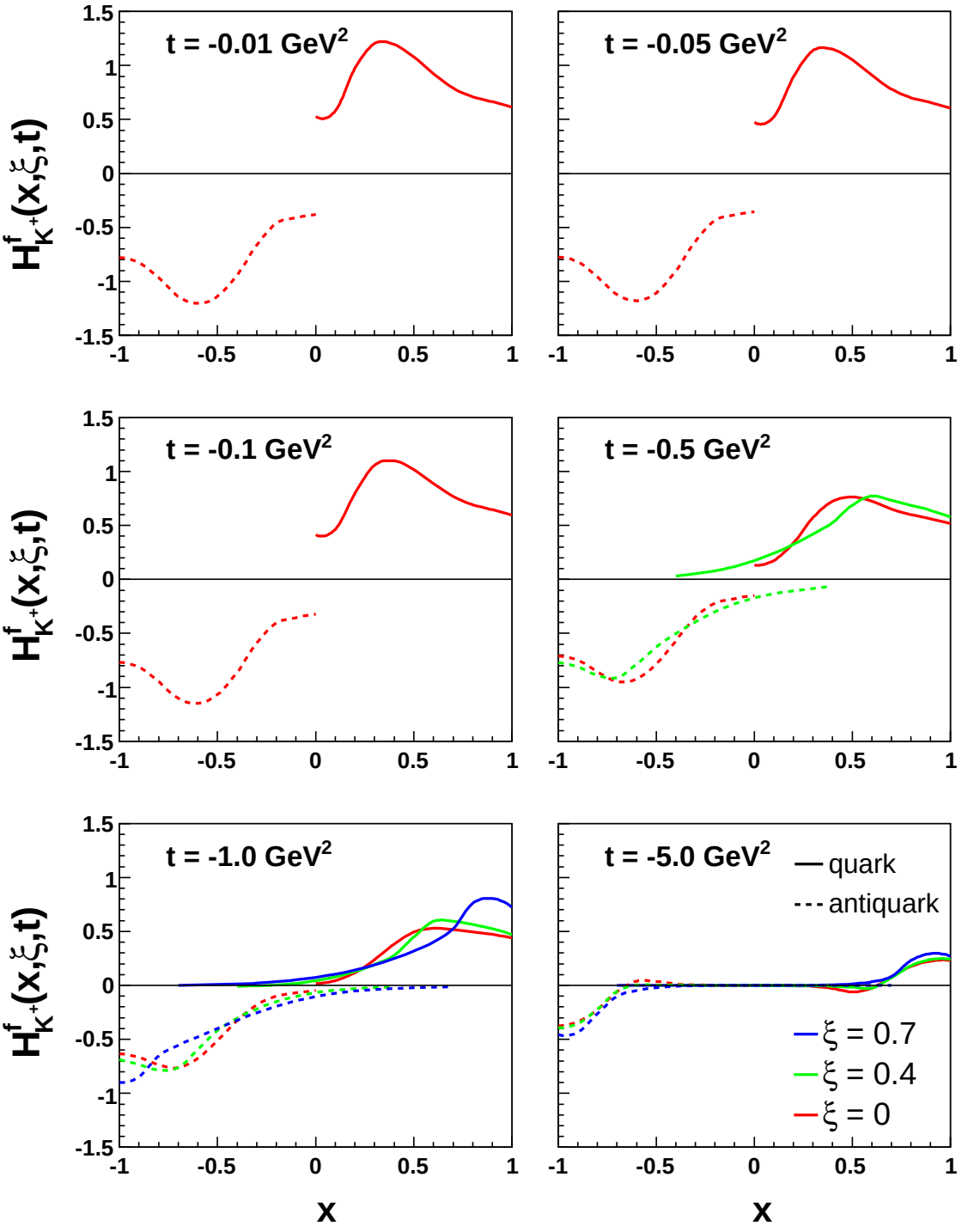

Figure 5.9 The kaon GPDs $H^u_{K^+}$ and $H^s_{K^+}$ in the full model. Results are shown for the supported ERBL and DGLAP regions at different values of t. Values for ξ shown are $\xi = 0$ (red line), $\xi = 0.4$ (green line) and $\xi = 0.7$ (blue line). The solid line refers to the up-quark GPD, the dashed line to the strange-antiquark GPD.

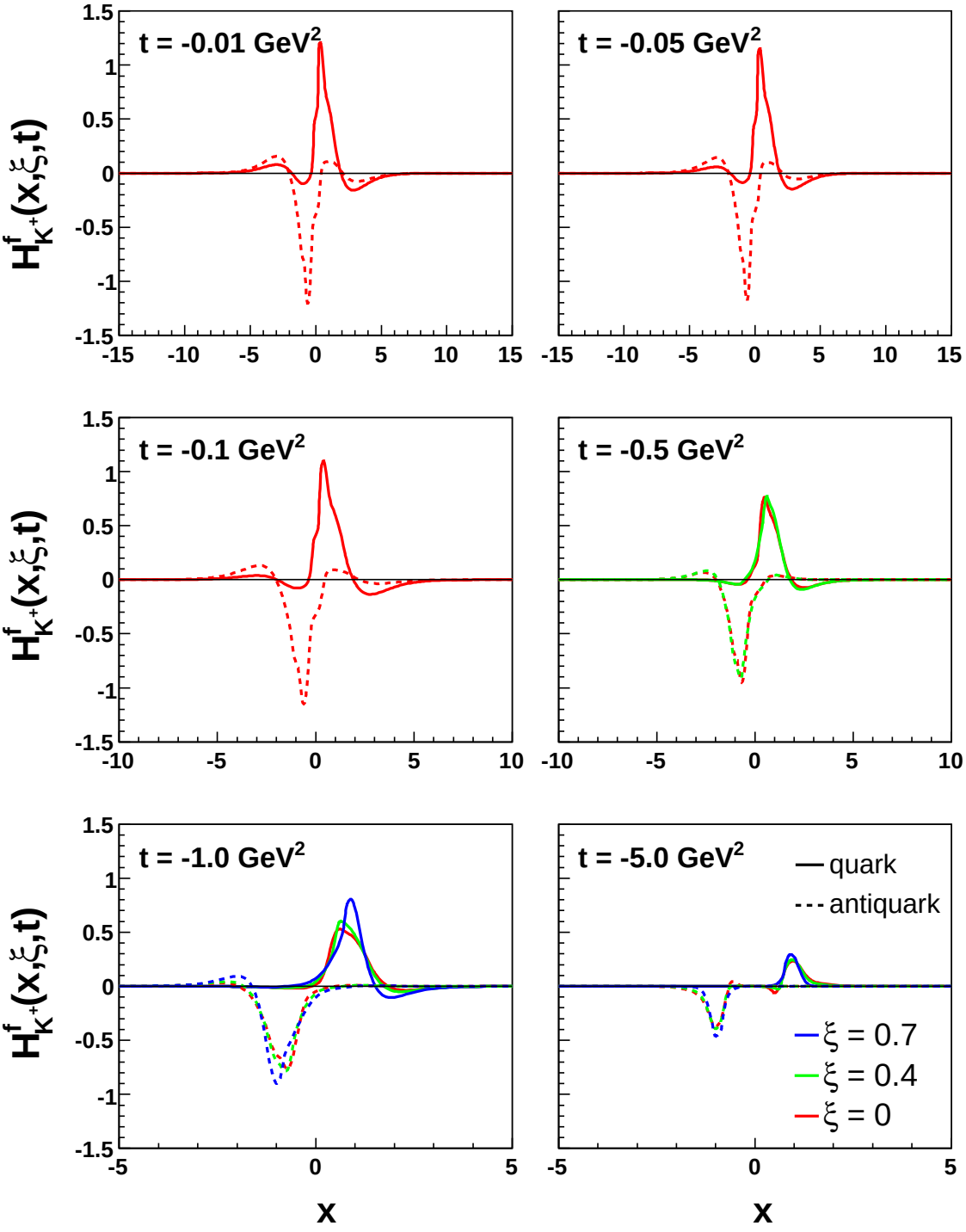

Figure 5.10 Same plots as in Fig. 5.9, but for a broader region in x.

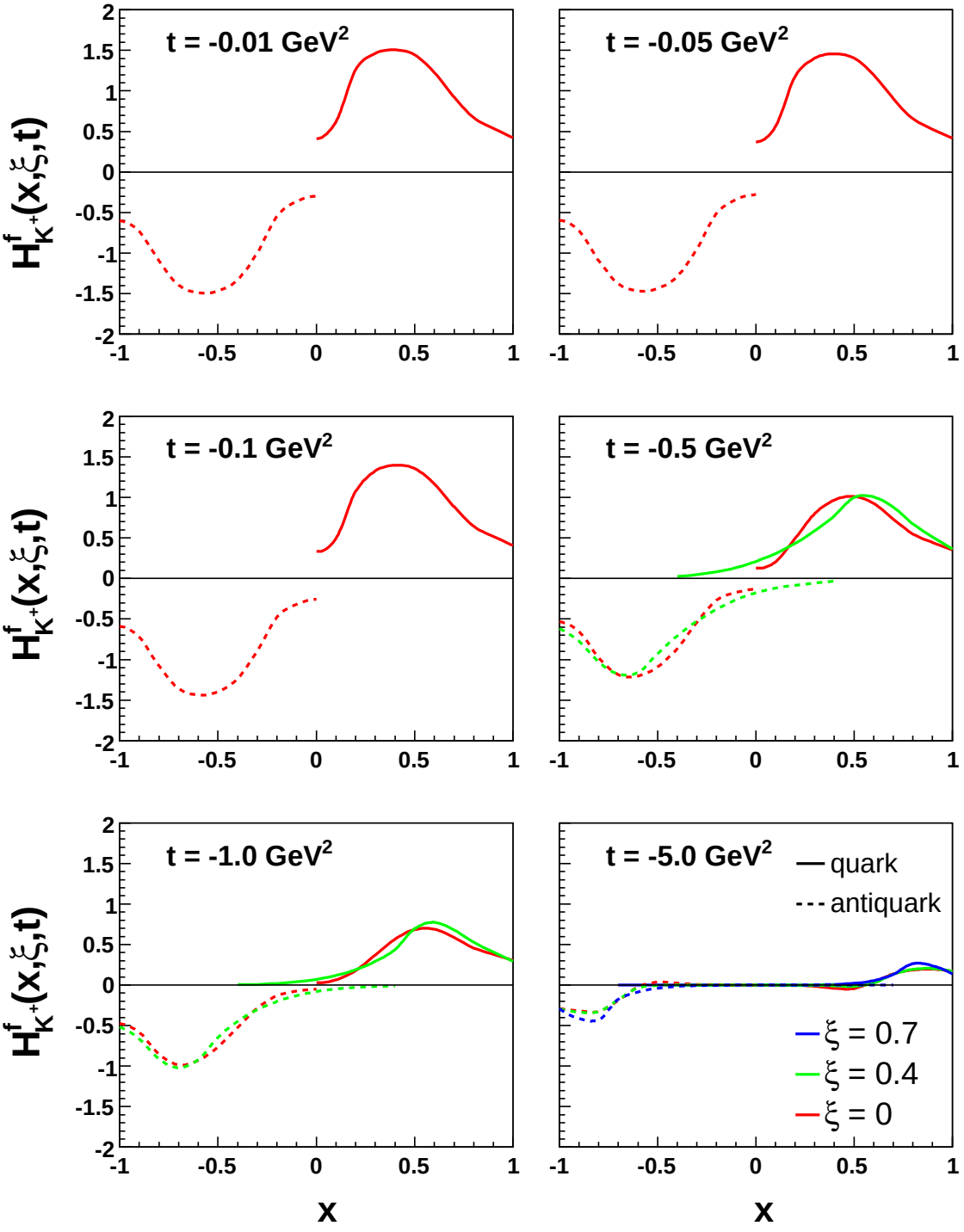

Figure 5.11 The kaon GPDs $H^u_{K^+}$ and $H^s_{K^+}$ in the reduced model. Results are shown for the supported ERBL and DGLAP regions at different values of t. Values for ξ shown are $\xi = 0$ (red line), $\xi = 0.4$ (green line) and $\xi = 0.7$ (blue line). The solid line refers to the up-quark GPD, the dashed line to the strange-antiquark GPD.

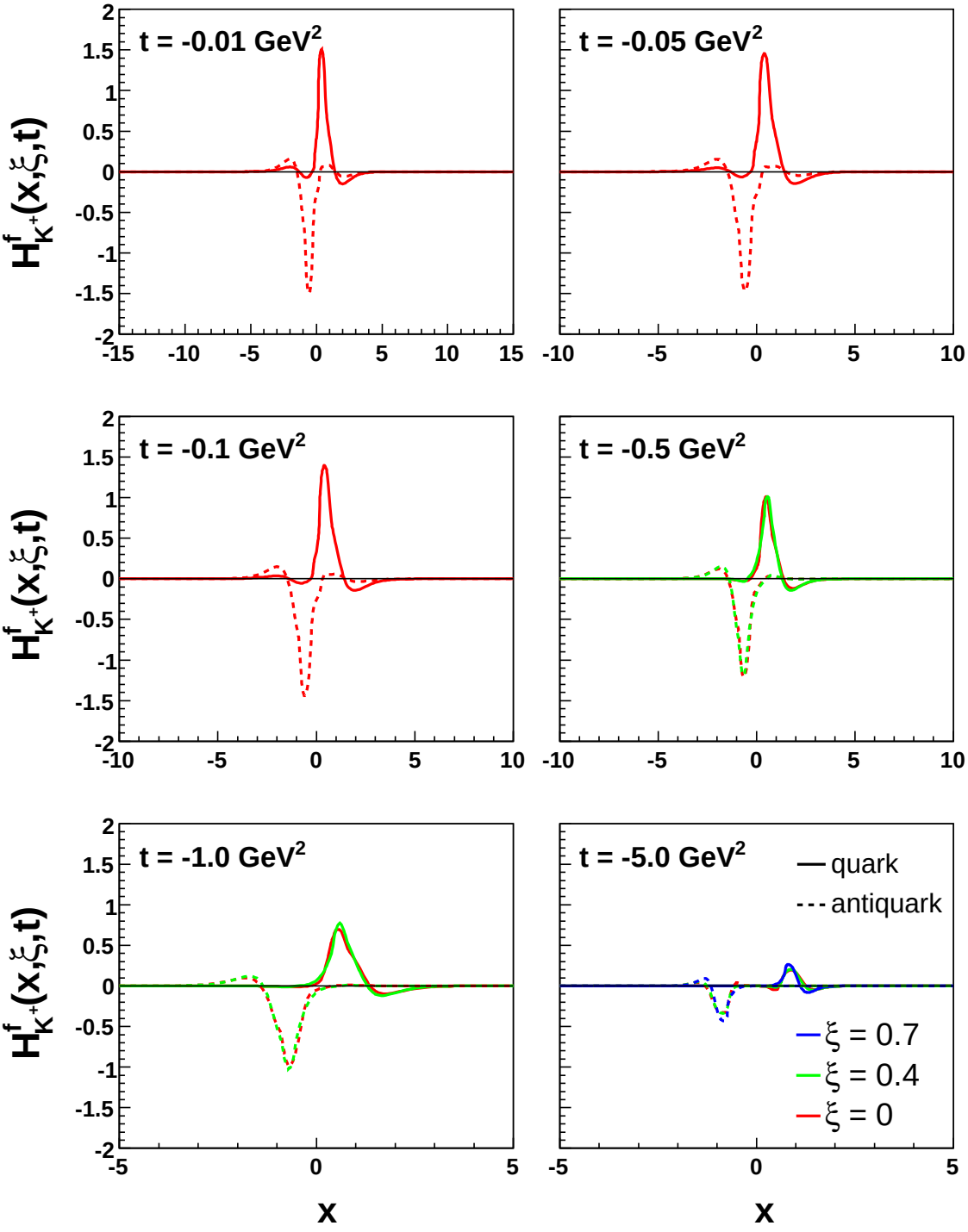

Figure 5.12 Same plots as in Fig. 5.11, but for a broader region in x.

Model	$\|t\|$ (GeV^2)	ξ	FF via GPD	FF	δ
Full model	0.01	0	0.936	0.927	0.010
	0.05	0	1.028	1.020	0.008
		0.4	1.032		0.012
	0.1	0	1.103	1.105	0.002
		0.4	1.105		0
		0.7	1.108		0.003
	0.5	0	0.662	0.666	0.006
		0.4	0.662		0.006
		0.7	0.662		0.006
	1.0	0	0.393	0.398	0.013
		0.4	0.394		0.010
		0.7	0.393		0.013
	5.0	0	0.0893	0.0924	0.034
		0.4	0.0854		0.076
		0.7	0.0897		0.029
Reduced model	0.01	0	0.984	0.976	0.008
	0.05	0	0.935	0.926	0.010
	0.1	0	0.884	0.875	0.010
	0.5	0	0.619	0.611	0.013
		0.4	0.619		0.013
	1.0	0	0.423	0.419	0.010
		0.4	0.424		0.012
	5.0	0	0.0857	0.0853	0.005
		0.4	0.0862		0.011
		0.7	0.0847		0.007
IQM model	0.01	0	0.994	0.983	0.011
	0.05	0	0.968	0.957	0.011
	0.1	0	0.937	0.926	0.012
	0.5	0	0.751	0.741	0.013
	1.0	0	0.599	0.590	0.015
		0.4	0.598		0.014
	5.0	0	0.153	0.150	0.020
		0.4	0.153		0.020
		0.7	0.155		0.033

Table 5.3 The electromagnetic form factor of the pion in the three different models, calculated through relation (5.6) (column 'FF via GPD') and with a direct calculation in the Bonn model [19] (column 'FF'). The last column shows the relative difference between both and is calculated with Eq. (5.8).

Form factor

In Chapter 2, it was pointed out that the GPD is related to the electromagnetic form factor through relation (2.22),

$$F^f(t) = \int dx H^f(x,\xi,t)\,, \tag{5.5}$$

where f stands for the quark flavor and the ξ-dependence disappears. Combining the quark and antiquark GPDs weighted with the up and down electromagnetic charges, we can write

$$e_u \int_{-\infty}^{+\infty} \mathrm{d}x H^u_{\pi^+}(x,\xi,t) + e_d \int_{-\infty}^{+\infty} \mathrm{d}x H^d_{\pi^+}(x,\xi,t) = F_{\pi^+}(t)\,.$$

Taking into account the isospin symmetry relation Eq. (5.4) and inserting the electromagnetic charges of the up and down quark, $e_u = 2/3$ and $e_d = -1/3$, this equation can be rewritten as

$$\int_{-\infty}^{+\infty} \mathrm{d}x H^u_{\pi^+}(x,\xi,t) = F_{\pi^+}(t)\,. \tag{5.6}$$

Notice that, due to the support properties of the GPDs here presented, the integration domain is $x \in (-\infty, +\infty)$. For the kaon, the relation becomes

$$e_u \int_{-\infty}^{+\infty} \mathrm{d}x H^u_{K^+}(x,\xi,t) + e_s \int_{-\infty}^{+\infty} \mathrm{d}x H^s_{K^+}(x,\xi,t) = F_{K^+}(t)\,, \tag{5.7}$$

where $e_s = -1/3$ is the electromagnetic strange quark charge. Since the GPD curves are relatively smooth, Eqs. (5.6) and (5.7) are calculated numerically with Simpson's quadrature algorithm.

The form factor data collected through Eqs. (5.6) and (5.7) are tabulated in Tables 5.3 and 5.4, respectively (column 'FF via GPD'), and compared to the result of the direct calculation of the electromagnetic form factor in the Bonn model [19] (column 'FF'). Both calculations are performed independently from each other. The last column of both tables shows their relative difference:

$$\delta = \frac{|(\text{FF via GPD}) - \text{FF}|}{\text{FF}}\,. \tag{5.8}$$

The tables make clear that for the majority of the kinematic conditions, the form factors as computed from the x-dependence of the GPDs match the numbers from a direct calculation at the 1%-level. The tiny differences can be understood as numerical inaccuracies. Notice that the form factors are ξ-independent, as required by Eq. (2.22).

With respect to the binding energy dependence of the support problem, the following conclusions can be drawn. Whereas the electromagnetic form factor is only slightly

Model	$\|t\|$ (GeV^2)	ξ	FF via GPD	FF	δ
Full model	0.01	0	0.982	0.973	0.009
	0.05	0	0.925	0.915	0.011
	0.1	0	0.870	0.861	0.010
	0.5	0	0.664	0.659	0.008
		0.4	0.665		0.009
	1.0	0	0.514	0.512	0.004
		0.4	0.514		0.004
		0.7	0.514		0.004
	5.0	0	0.150	0.150	0
		0.4	0.150		0
		0.7	0.149		0.007
Reduced model	0.01	0	0.985	0.978	0.007
	0.05	0	0.941	0.934	0.007
	0.1	0	0.892	0.885	0.008
	0.5	0	0.621	0.613	0.013
		0.4	0.623		0.016
	1.0	0	0.425	0.420	0.012
		0.4	0.426		0.014
	5.0	0	0.0761	0.0754	0.009
		0.4	0.0765		0.015
		0.7	0.0738		0.021

Table 5.4 The electromagnetic form factor of the kaon in the full and the reduced model, calculated through relation (5.7) (column 'FF via GPD') and with a direct calculation in the Bonn model [19] (column 'FF'). The last column shows the relative difference between both and is calculated with Eq. (5.8).

influenced[2] by the relative binding energy (see left figure in Fig. 5.13), the pion GPD peaks at $t = -0.01$ GeV^2 increase from approximately 0.6 in the full model (Fig. 5.4) to around 1.3 in the reduced model (Fig. 5.6) and even approximately 1.9 in the IQM model (Fig. 5.8). Moreover, the x-value belonging to the maximum of the GPD curves is clearly affected by the binding energy. It is therefore to be expected that the (relative) binding energy will indeed affect the support properties of the GPD curves. We will zoom in on these effects, after the discussion of the polynomiality condition in the Bonn model.

[2]The artifact at small $|t|$ which is observed in the full model curve of Fig. 5.13, is described in detail in Refs. [98, 121].

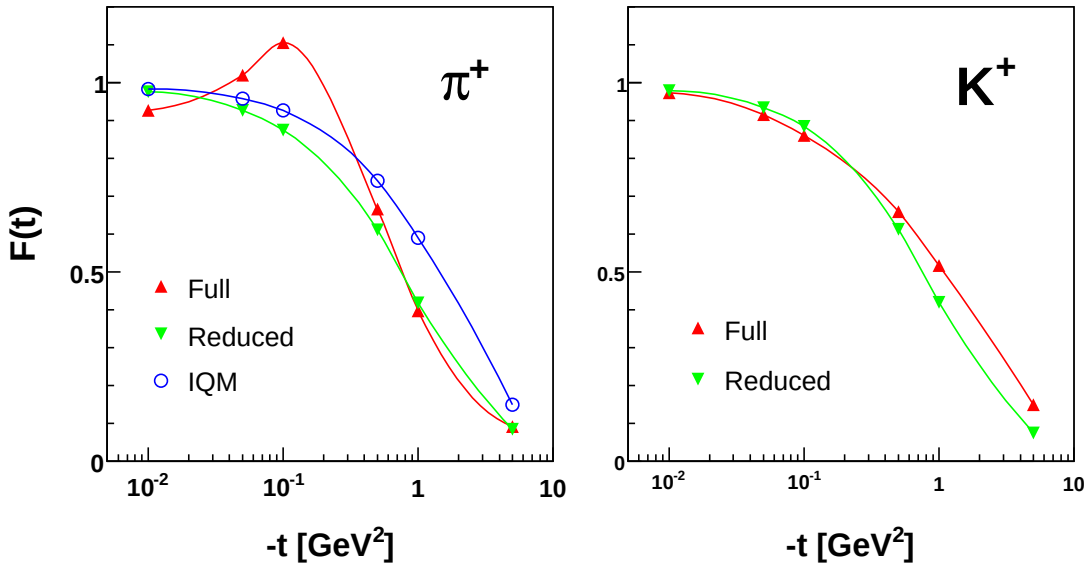

Figure 5.13 The π^+ (left) and K^+ (right) form factors F_{π^+} and F_{K^+} as a function of t. The form factors were calculated directly in the Bonn model [19].

Polynomiality

A more stringent test than the form factor condition of Eq. (2.22), is the polynomiality condition of Eq. (2.23), which states that the nth Mellin moments of the generalized parton distributions,

$$\int \mathrm{d}x\, x^{n-1} H^f(x,\xi,t) = P_n^f(\xi,t), \tag{5.9}$$

yield polynomials in ξ of order $\leq n$. It is clear that the form factor relations of Eqs. (5.6) and (5.7) represent the $n = 1$ case, where the order of the polynomial is 0.

In Fig. 5.14, the moments of order $n = 1$ to 5 of the GPD $H^u_{\pi^+}(x,\xi,t)$ in the full model are shown for $t = -0.5$ GeV^2 and $t = -1.0$ GeV^2. A polynomial of order $\leq n$ is fitted to the corresponding moments. The point $\xi = 0.1$ was omitted in the fit. Its form factor prediction (0.64 at $t = -0.5$ GeV^2, 0.34 at $t = -1.0$ GeV^2) deviates from the values for the other ξ's (0.66 and 0.39, respectively). This is due to an instability in the numerical code which is observed *only* for the pion GPD at low $\xi \neq 0$ and for $x \in [0.9, 1.2]$ in the full model. It is obvious that the underestimate is larger for higher-order Mellin moments, due to the occurrence of x^n in the integrand. We have tracked down the origin of the instability and hope to solve it in the near future.

For other ξ, it is clear that these polynomials give a satisfactory result and that a higher order is not needed in the fit. We conclude that the polynomiality condition is

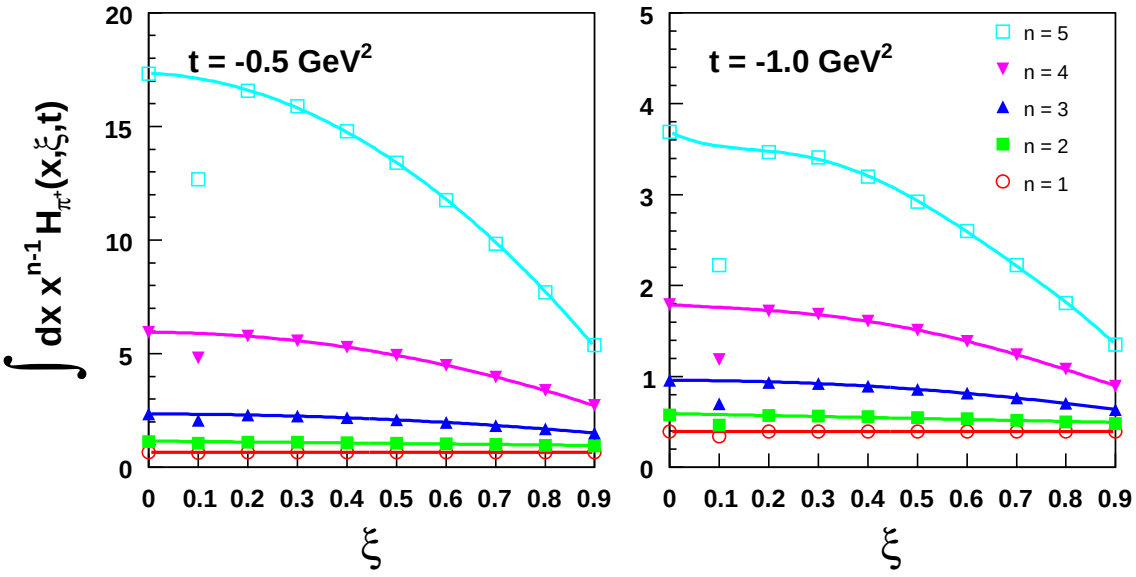

Figure 5.14 Mellin moments of order $n = 1$ to 5 of the full model GPD $H^u_{\pi^+}(x, \xi, t)$ for $t = -0.5$ GeV^2 (left) and $t = -1.0$ GeV^2 (right). A polynomial of order not higher than n is fitted to the calculated moments, showing that the polynomiality condition is fulfilled.

fulfilled in our model.

After checking that the three model constraints from Chapter 2 are met, we are ready to explore the structure of the GPD curves and the origin of the support problem in greater detail.

Shape of the GPD curves

The GPDs of Figs. 5.1 and 5.3 - 5.12 clearly exhibit a support problem. In general, the curves tend to have longer tails as $|t|$ decreases. Especially for the deeply bound pion in the full model, this effect is obvious (see Fig. 5.15). As the relative binding energy decreases, the effect becomes smaller. The forward limit of the generalized parton distributions ($t \to 0, \xi \to 0$) is given by the PDFs, which have a probabilistic interpretation. Therefore, we can conclude that the probed constituents (constituent quark and antiquark) are highly off-shell within the strongly bound pion. Remark, however, that the GPD at $t = -0.01$ GeV^2 becomes negative for certain x-values outside the support regions, which could point at an inconcistency with the probabilistic interpretation.

At low $|t|$, a local maximum is observed for the full model pion calculation at $x \approx 0$. Also for the other pion and kaon results, some structure is observed at this x-value at low t. From the $t = -0.1$ GeV^2 plot in Fig. 5.4, it is seen that the node is most

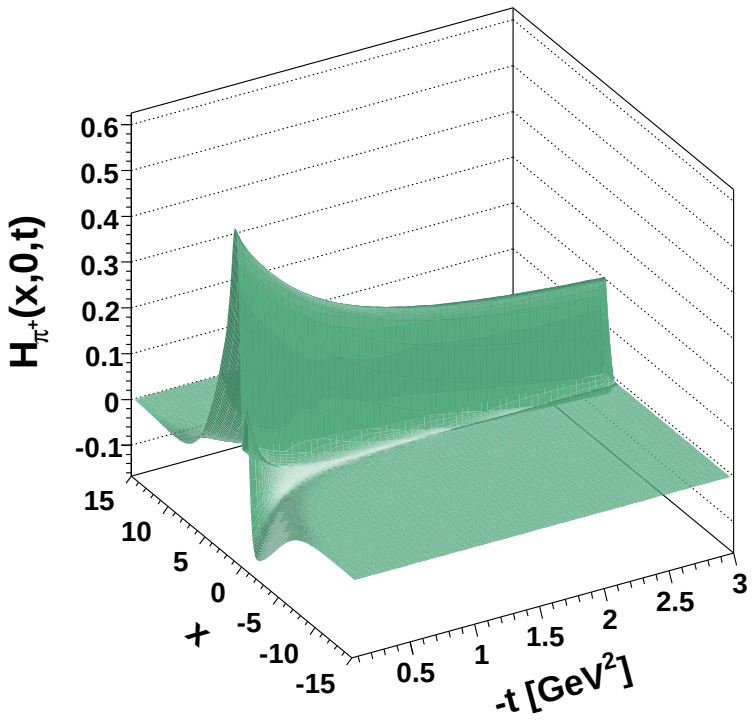

Figure 5.15 Three-dimensional picture of the GPD $H^u_{\pi^+}(x, 0, t)$ in the full model. It is observed that with decreasing $|t|$, the curve broadens and its peak value increases.

prominent for low ξ. The observed t- and ξ-dependence again suggests a link with the forward limit and hence with the probabilistic interpretation of the parton distribution functions.

Another observation which can be made, is the fact that whereas the maximum of the GPD curve lies outside the support region for the deeply bound pion in the full model (peak value at $|x| > 1$), it lies within the support interval for the other pion and kaon calculations.

The model dependence of the observed GPD properties points at a significant relative binding energy dependence of the support of the generalized parton distributions in the Bonn model. In the next paragraph, we will elaborate on this and quantify the support problem.

In the margin of the above discussion on the shape of the GPD curves, it is interesting to remark that the well-known fact that the electromagnetic form factor decreases with increasing $|t|$ (except for the full model pion form factor at low $|t|$) is reflected in the GPD curves by a lower peak value at higher $|t|$.

Model	ξ	t (GeV^2) -0.01	-0.05	-0.1	-0.5	-1.0	-5.0
Full model	0	0.08	0.11	0.13	0.21	0.20	0.17
	0.4	-	0.12	0.14	0.21	0.22	0.17
	0.7	-	-	0.12	0.17	0.20	0.12
Reduced model	0	0.60	0.62	0.64	0.69	0.69	0.63
	0.4	-	-	-	0.70	0.71	0.61
	0.7	-	-	-	-	-	0.56
IQM model	0	0.66	0.67	0.67	0.71	0.73	0.68
	0.4	-	-	-	-	0.75	0.70
	0.7	-	-	-	-	-	0.64

Table 5.5 Values of the pion support parameter ϕ of Eq. (5.2) corresponding to Figs. 5.3 - 5.8.

Support parameter

Table 5.5 lists the values of the support parameter ϕ, defined in Eq. (5.2), belonging to the different pion GPD curves. Table 5.6 shows the values of the parameters ϕ^q and $\phi^{\bar{q}}$ (Eq. (5.3)) which belong to the kaon curves.

For the pion GPD, it is obvious from Table 5.5 that the support is much better in the reduced and the IQM models than in the full model. In going from the full model to either of the two other models in which the pion is less deeply bound, the support parameter increases significantly (*e.g.* from 0.08 in the full model to 0.60 in the reduced and 0.66 in the IQM model for $t = -0.01$ GeV^2 and $\xi = 0$). We observed in the previous paragraph that, especially for the pion in the full model, the GPD curves tend to broaden with decreasing $|t|$. Table 5.5 shows that this behaviour can in general be linked with the support properties of the curves. Indeed, the support parameter decreases with $|t|$ in the full model. This relation does not hold for very high $|t|$, however, as can be seen from the $t = -5.0$ GeV^2 columns. For the other models, the relation is less obvious. From Table 5.5, no clear dependence on the skewedness ξ can be discovered.

Also for the kaon GPD, the support improves when the instanton induced interaction is switched off. Notice that the values of the two support parameters ϕ^q and $\phi^{\bar{q}}$ are similar. This result is compatible with the finding that the quark and antiquark GPD have similar shapes and shows that the small differences between both GPDs do not alter the support significantly. Combining these observations with the fact that the support does improve significantly in the IQM model with respect to the full model, we conclude that the binding energy is more important for the support than the particular

Parameter	Model	ξ	t (GeV^2) -0.01	-0.05	-0.1	-0.5	-1.0	-5.0
ϕ^q	Full model	0	0.46	0.48	0.50	0.58	0.61	0.47
		0.4	-	-	-	0.60	0.62	0.48
		0.7	-	-	-	-	0.56	0.56
	Reduced model	0	0.68	0.69	0.70	0.73	0.73	0.64
		0.4	-	-	-	0.76	0.75	0.62
		0.7	-	-	-	-	-	0.63
$\phi^{\bar{q}}$	Full model	0	0.43	0.45	0.47	0.56	0.61	0.42
		0.4	-	-	-	0.58	0.61	0.43
		0.7	-	-	-	-	0.55	0.57
	Reduced model	0	0.65	0.66	0.67	0.72	0.73	0.65
		0.4	-	-	-	0.73	0.74	0.64
		0.7	-	-	-	-	-	0.69

Table 5.6 Values of the kaon quark and antiquark support parameters of Eq. (5.3) corresponding to Figs. 5.9 - 5.12.

constituent quark mass or flavor.

It is clear that the conclusions drawn from the support parameter values are compatible with the observations regarding the shape of the GPD curves which we made in the previous paragraph. We are now able to address the issues raised in the outset of this section:

- There exists a strong correlation between the support and the (relative) binding energy of the meson. The deep binding of the pion worsens the support problem significantly.

- The kinematical variable ξ does not influence the support. The variable t has a small impact.

- The constituent quark masses have an impact on the support, but only through the (relative) binding energy. A mass difference between constituent quarks hardly affects the GPD curves.

An important remark, though, is that although in general the support improves when the (relative) binding energy decreases, a support of *e.g.* 71% still poses a serious problem. None of the models used in this chapter give rise to GPDs that can be evolved with the DGLAP and ERBL equations. Therefore, the interpretation of the GPDs remains unclear for all models tested in this chapter.

However, as we pointed out in Sect. 2.3, it is possible to evolve the Mellin moments for $\xi = 0$ according to Eq. (2.34), so that these could be checked with lattice QCD results. Performing this evolution will be the next step in our research project.

6 Conclusions

People do not like to think.
If one thinks, one must reach conclusions.
Conclusions are not always pleasant.

H. Keller

In this work, we have presented results for the calculation of the twist-two generalized parton distributions of pseudoscalar mesons. We use the framework of the Poincaré covariant Bethe-Salpeter constituent quark model developed by the Bonn group. The various aspects of the model were outlined and their impact on the GPD results was discussed.

We have introduced generalized parton distributions as non-forward matrix elements of a bilocal current on the light-cone. As such, they represent a correlation between partons in a hadron, where a parton is taken out of the hadron with a certain longitudinal momentum fraction and put back with another. Being non-perturbative objects, GPDs enable us to further unravel the complex internal structure of hadrons. For nucleons, they are particularly helpful in the much debated spin puzzle. The relation between GPDs, parton distribution functions and form factors was discussed. The calculation of GPDs from first QCD principles is not feasible, and constituent quark models can help to predict the GPD values at low energy scales. With the DGLAP and ERBL evolution equations, the GPDs can be determined at any scale. In CQMs, the degrees of freedom are the valence quarks, effectively dressed with the sea quarks and gluons. It was mentioned that some CQMs have trouble predicting the correct support regions. It is not always clear from the start, however, whether a particular CQM will run into a support problem.

The Bonn CQM used in this work is based on the relativistically covariant Bethe-Salpeter equation. It adopts two major assumptions: first, the interaction kernel is assumed instantaneous (*i.e.*, independent of the relative energy in the meson rest frame).

This established a close connection with the non-relativistic CQM which proved surprisingly successful for the calculation of hadron masses and magnetic moments. Second, the quark self-energy which occurs in the dressed quark propagators is assumed momentum-independent. This gives rise to the introduction of an effective constituent quark mass. With these approximations, the (unsolvable) Bethe-Salpeter equation can be reduced to the solvable Salpeter equation without giving up formal covariance. The meson spectrum is calculated from this equation and its normalization condition. The interactions used in the Bonn model are the confinement interaction, which acts on all meson states in the spectrum, and the residual 't Hooft instanton induced interaction, which acts only on the (pseudo-)scalar states.

Since the Bonn model provides satisfactory results for the meson spectrum, the baryon spectrum and several dynamic observables like the electromagnetic form factors, the calculation of GPDs is a logical next step. In this work, we have shown how a prescription for the calculation of GPDs in the Bonn model can be derived from the six-point Green's function (4.3). In lowest order, the GPD was found as the sum of two terms, which reflect the coupling to the two constituents (quark and antiquark).

With respect to the support of GPDs, it was proven that the assumption of instant-frame instantaneous interaction kernels could result in a support problem, whereas constant or p^--independent kernels have the correct support properties by construction. The presented results show the presence of a support problem. To interpret our results for the pion and the kaon GPDs, we introduced the support parameters as a measure of the severeness of the support problem. For the pion, one support parameter ϕ was sufficient due to the isospin symmetry. For the kaon, we distinguished between the support parameter for the quark GPD (ϕ^q) and that for the antiquark GPD ($\phi^{\bar{q}}$). Our computer code was tested successfully for stability against the various choices for the radial basis and the proper convergence of the amount of basis states.

To investigate which physical properties influence the GPD support, we introduced three different models. The first was the full model, which provides an accurate description of the meson spectrum and dynamic properties such as form factors and decay widths. In the second model, which we have coined the reduced model, the 't Hooft instanton induced interaction was omitted. The pion mass increases significantly in this model. The third and final model was the increased quark mass (IQM) model, where we increased the mass of the non-strange constituent quarks. By looking at the relative binding energy of the pion (defined as the pion binding energy divided by its mass) in these models, it was observed that in the reduced and the IQM model, the pion was significantly weaker bound than in the full model. For the kaon, only the

full and the reduced model were considered. This pseudoscalar meson turned out to be weaker bound in the reduced model as well, although its binding in the full model is by far not as deep as that of the pion.

It was discussed that the three models meet the isospin symmetry constraint for the pion GPD. The first Mellin moment of the computed GPD was checked to yield the pion form factor, as required. Also for the kaon in the full and the reduced model, the validity of the form factor sum rule was proven. The polynomiality condition is fulfilled, and was illustrated for the pion in the full model.

To test whether the support problem could be solved by altering the model parameters, we have finally compared the GPD results in the different models. It was shown that in particular for the pion in the full model, the GPD curves tend to broaden as $|t|$ decreases. This resulted in a lower support parameter for low $|t|$. For the reduced and IQM models, where this broadening of the curves was not observed, the relation between $|t|$ and the support parameter was not as obvious. The various data presented in this work showed that a dependence of the support on ξ could not be proven.

The observation that the relative binding energy has an impact on the support of the generalized parton distributions in the Bonn model, was confirmed by the calculation of the support parameter. The pion support parameter in the full model was shown to be significantly smaller than the parameter in either of the two other models (where the pion is much weaker bound). For $t = -0.01$ GeV^2, the violation was shown to be reduced from more than 90% in the full model to around 60% in the other models. For $t = -1.0$, the violation decreases from 80% to 25%. Also for the kaon, the support improves enormously when switching off the 't Hooft interaction.

The support parameters of the kaon, ϕ^q and $\phi^{\bar{q}}$, did not differ significantly. This finding was reflected in the similarity between the GPD curves of the quark and the antiquark GPD. Combining this observation with the fact that the support properties of the pion GPD improved significantly in the IQM model, we concluded that in our model, the quark flavor and mass have a smaller impact on the support than the relative binding energy of the meson.

Although the support of the GPDs is heavily affected by the relative meson binding energy, none of the models produces results that could be evolved with the available evolution equations. Since we know from Sections 3.3 and 5.2 that in particular the three-dimensional reduction of the Bethe-Salpeter equation to the Salpeter equation in the instant frame influences the support properties of the equations, we conclude that to achieve the correct support, an alternative reduction is required.

The observed support properties of our model can be interpreted as follows. As the

Bonn model is a *soft scale* model, and therefore does not contain either on-shell particles or asymptotic freedom (which the *hard scale* parton model does contain), the support violation can be considered as a manifestation of soft scale physics. This prohibits the extrapolation of the evolution equations to the scale of the model. In constrast, a low-scale model with the correct support properties can be evolved. It should be clear, however, that also in this case, the use of the evolution equations relies on an extrapolation of perturbative QCD to soft scales.

Additionally, it should be noted that the Mellin moments of the GPDs at $\xi = 0$ can be evolved, even in the case of a support violation. As indicated by Eq. (2.33), the relevant quantities in the much debated proton spin sum rule are the second-order Mellin moments. In view of these observations, we present four future projects.

Outlook

The evolution of the $\xi = 0$ Mellin moments to lattice QCD scales would present a way to test our model performance against calculations from first principles. It should be noted that lattice QCD calculations are usually performed for unphysically high pion masses. Therefore, the evolution should preferably be carried out with the Mellin moments from the reduced model, the IQM model, or a combination of both.

A second possible extension of the work presented in this thesis is the study of the pion GPDs in the impact parameter space, which give access to the transverse spin structure of the pion. Again, it would be interesting to compare the resulting Mellin moments with those obtained in lattice QCD [68].

Because of the importance of proton GPD calculations in the question of the origin of proton spin, we believe that a numerical calculation in the Bonn model (using the equations derived in this work) would be interesting. Regarding the support of the proton GPDs, we expect better results than for the pion GPD. This is due to the binding energy-dependence of the support properties. However, the support properties might be completely different in the proton case (see Sect. 5.2), and it is even not excluded that the proton GPD could manifest the correct support. A numerical calculation is necessary to give a decisive answer. However, as remarked above, the spin sum rule contains *only* Mellin moments of the GPDs, which can be always evolved at $\xi = 0$.

Another route which could be followed, is the development of a Bethe-Salpeter quark model that combines properties of the Bonn model (*e.g.* the use of the confinement and the 't Hooft interaction) with a support guaranteeing three-dimensional reduction. A challenging problem to solve in this context, is how to treat confinement on the light cone.

A Notations and conventions

A.1 Units

In this thesis, the *natural units* $\hbar = c = 1$ are adopted. In this system, the mass of a particle is equal to its rest energy.

A.2 Four-vectors

For a four-vector $a^\mu = (a^0, a^1, a^2, a^3) = (a^0, \boldsymbol{a})$, the metric tensor

$$g^{\mu\nu} = \begin{pmatrix} 1 & 0 & 0 & 0 \\ 0 & -1 & 0 & 0 \\ 0 & 0 & -1 & 0 \\ 0 & 0 & 0 & -1 \end{pmatrix}$$

is used. The light-cone variables $a^\pm$ are defined as follows:

$$a^\pm = \frac{1}{\sqrt{2}}(a^0 \pm a^3)\,.$$

The corresponding Minkowski scalar product is then

$$\begin{aligned} a \cdot b = a^\mu b_\mu &= a^0 b_0 - \boldsymbol{a} \cdot \boldsymbol{b} \\ &= a^+ b^- + a^- b^+ - \boldsymbol{a}_\perp \cdot \boldsymbol{b}_\perp\,, \end{aligned}$$

with the two-dimensional transverse vector $\boldsymbol{a}_\perp = (a^1, a^2)$.

A.3 Dirac matrices

The Dirac matrices γ^μ satisfy the anticommutation relation $\{\gamma^\mu, \gamma^\nu\} = 2g^{\mu\nu}$. Whenever a specific choice appears necessary, we use the Dirac representation:

$$\gamma^0 = \begin{pmatrix} \mathbb{1}_2 & 0 \\ 0 & -\mathbb{1}_2 \end{pmatrix} \quad \text{and} \quad \gamma^k = \begin{pmatrix} 0 & \sigma^k \\ -\sigma^k & 0 \end{pmatrix} \ (k = 1, 2, 3)\ ,$$

with σ^k the 2x2 Pauli matrices. Furthermore, $\gamma^5 = i\gamma^0\gamma^1\gamma^2\gamma^3$ and $\sigma^{\mu\nu} = \frac{i}{2}[\gamma^\mu, \gamma^\nu]$.

A.4 Products of four-point functions

In this thesis, the indices in Dirac (α), flavor (f) and color (c) space are combined in the multi-indices $\alpha \equiv (\alpha, f, c)$. The Einstein convention is adopted, *i.e.* the summation over repeated indices is implicitly understood. Moreover, we define the product of two four-point functions A and B as

$$[AB]_{\alpha\alpha'\beta\beta'} = A_{\alpha\gamma\beta\delta} B_{\gamma\alpha'\delta\beta'} \,. \tag{A.1}$$

To keep the notation concise, these indices are often omitted. Integrations over internal variables are usually written implicitly:

$$[AB](x_1, x_2; x_1', x_2') = \int \mathrm{d}^4 y_1 \int \mathrm{d}^4 y_2 A(x_1, x_2; y_1, y_2) B(y_1, y_2; x_1', x_2') \,. \tag{A.2}$$

The generalization to n-point functions is straightforward.

A.5 Bound states

In this work we come across bound states in both the off-shell and on-shell situation. The notation regarding their momenta is the following:

- Three-momenta are written as bold symbols, *e.g.* $\boldsymbol{P}$.
- On-shell four-momenta are written with a bar. Accordingly, a bound state $|\bar{P}\rangle$ has a four-momentum $\bar{P} = (\omega_P, \boldsymbol{P})$, with energy $\omega_P = \sqrt{|\boldsymbol{P}|^2 + M^2}$. M denotes the mass of the bound state.
- The energy of an off-shell four-momentum P is not subject to any constraints. We write $P = (P^0, \boldsymbol{P})$.

B Fourier transformed expressions for the six-point Green's function

In Chapter 4, an expression was derived for the generalized parton distribution of pseudoscalar mesons in a lowest-order Bethe-Salpeter formalism. This appendix provides a concise overview of the steps needed to derive Eqs. (4.9) and (4.13).

B.1 The matrix element expression in momentum space

In this section, we will prove Eq. (4.9) which states that the bilocal current matrix element is found as the residue of the six-point Green's function G^μ at the bound state poles. We will start by writing the Fourier transform of the Green's function (4.7), which is defined as

$$\begin{aligned} G^\mu_{\alpha\alpha'\beta\beta'}(p_1', p_2'; k', k; p_1, p_2) = \int \mathrm{d}^4x_1 \mathrm{d}^4x_2 \mathrm{d}^4x_1' \mathrm{d}^4x_2' \mathrm{d}^4y \mathrm{d}^4y' \; e^{i(p_1'\cdot x_1' + p_2'\cdot x_2' - p_1\cdot x_1 - p_2\cdot x_2 + k\cdot y + k'\cdot y')} \\ \times \; G^\mu_{\alpha\alpha'\beta\beta'}(x_1', x_2'; y', y; x_1, x_2)\,. \end{aligned} \tag{B.1}$$

Inserting Eq. (4.7) in this definition and slightly altering the notation with respect to the momenta yields

$$\begin{aligned} G^\mu_{\alpha\alpha'\beta\beta'}(p_1', p_2'; k', k; p_1, p_2) = \int \mathrm{d}^4x_1 \mathrm{d}^4x_2 \mathrm{d}^4x_1' \mathrm{d}^4x_2' \mathrm{d}^4Z \mathrm{d}^4z \int \frac{\mathrm{d}^3P_1}{(2\pi)^3\, 2\omega_{P_1}} \frac{\mathrm{d}^3P_2}{(2\pi)^3\, 2\omega_{P_2}} \\ \times \; e^{-i(\bar{P}_1 - \bar{P}_2)\cdot Z}\; e^{i(p_1'\cdot x_1' + p_2'\cdot x_2' - p_1\cdot x_1 - p_2\cdot x_2 + (k+k')\cdot Z + \frac{k-k'}{2}\cdot z)} \\ \times \; \chi_{\bar{P}_2\alpha\beta}(x_1', x_2') \langle \bar{P}_2 | O^\mu(-\frac{z}{2}, \frac{z}{2}) | \bar{P}_1 \rangle \bar{\chi}_{\bar{P}_1\beta'\alpha'}(x_1, x_2) \\ \times \; \theta\left(\min(x_1'^0, x_2'^0) - Z^0 - \frac{1}{2}|z^0|\right) \\ \times \; \theta\left(-\frac{1}{2}|z^0| - \max(x_1^0, x_2^0) + Z^0\right) \\ + \; O.T. \end{aligned} \tag{B.2}$$

Adopting Jacobi coordinates $P^{(\prime)} = p_1^{(\prime)} + p_2^{(\prime)}$ and $p^{(\prime)} = (p_1^{(\prime)} - p_2^{(\prime)})/2$ for the incoming and outgoing particles and omitting the multi-indices α yields

$$\begin{aligned} G^{\mu}_{P;P'}(p';k',k;p) = &\int \mathrm{d}^4X\mathrm{d}^4\zeta\mathrm{d}^4X'\mathrm{d}^4\zeta'\mathrm{d}^4Z\mathrm{d}^4z \int \frac{\mathrm{d}^3P_1}{(2\pi)^3\ 2\omega_{P_1}}\frac{\mathrm{d}^3P_2}{(2\pi)^3\ 2\omega_{P_2}} \\ &\times\ e^{i(P'-\bar{P}_2)\cdot X' - i(P-\bar{P}_1)\cdot X + ip'\cdot\zeta' - ip\cdot\zeta + i\frac{k-k'}{2}\cdot z + i(\bar{P}_2-\bar{P}_1+k+k')\cdot Z} \\ &\times\ \chi_{\bar{P}_2}(\zeta')\langle\bar{P}_2|O^{\mu}(-\frac{z}{2},\frac{z}{2})|\bar{P}_1\rangle\bar{\chi}_{\bar{P}_1}(\zeta) \\ &\times\ \theta\left(X'^0 - Z^0 + \min(\frac{1}{2}\zeta'^0, -\frac{1}{2}\zeta'^0) - \frac{1}{2}|z^0|\right) \\ &\times\ \theta\left(Z^0 - X^0 - \frac{1}{2}|z^0| - \max(\frac{1}{2}\zeta^0, -\frac{1}{2}\zeta^0)\right) \\ &+\ O.T., \end{aligned} \tag{B.3}$$

where we have made use of the relations

$$\begin{aligned} &\chi_{\bar{P}_2}(x_1',x_2') = e^{-i\bar{P}_2\cdot X'}\chi_{\bar{P}_2}(\zeta') \text{ and} \\ &\bar{\chi}_{\bar{P}_1}(x_1,x_2) = e^{i\bar{P}_1\cdot X}\bar{\chi}_{\bar{P}_1}(\zeta)\,. \end{aligned} \tag{B.4}$$

The Fourier transform of the Heaviside step function $\theta(x)$ is defined as

$$\theta(x) = i\int_{-\infty}^{\infty}\frac{\mathrm{d}\omega}{2\pi}\frac{e^{-i\omega x}}{\omega + i\epsilon}\,, \tag{B.5}$$

ϵ being infinitely small and positive. We insert this definition in the above equation (B.3) to obtain

$$\begin{aligned} G^{\mu}_{P;P'}(p';k',k;p) = -&\int \mathrm{d}^4X\mathrm{d}^4\zeta\mathrm{d}^4X'\mathrm{d}^4\zeta'\mathrm{d}^4Z\mathrm{d}^4z \int \frac{\mathrm{d}^3P_1}{(2\pi)^3\ 2\omega_{P_1}}\frac{\mathrm{d}^3P_2}{(2\pi)^3\ 2\omega_{P_2}} \\ &\times\ e^{i(P'-\bar{P}_2)\cdot X' - i(P-\bar{P}_1)\cdot X + ip'\cdot\zeta' - ip\cdot\zeta + i(\bar{P}_2-\bar{P}_1+k+k')\cdot Z + i\frac{k-k'}{2}\cdot z}\chi_{\bar{P}_2}(\zeta') \\ &\times\ \langle\bar{P}_2|O^{\mu}(-\frac{z}{2},\frac{z}{2})|\bar{P}_1\rangle\bar{\chi}_{\bar{P}_1}(\zeta)\int_{-\infty}^{\infty}\frac{\mathrm{d}\omega}{2\pi}\frac{e^{-i\omega(Z^0 - X^0 - \frac{1}{2}|z^0| - \frac{1}{2}|\zeta^0|)}}{\omega + i\epsilon} \\ &\times\ \int_{-\infty}^{\infty}\frac{\mathrm{d}\omega'}{2\pi}\frac{e^{-i\omega'(X'^0 - Z^0 - \frac{1}{2}|\zeta'^0| - \frac{1}{2}|z^0|)}}{\omega' + i\epsilon} \\ &+\ O.T. \end{aligned} \tag{B.6}$$

Making use of the definition of the δ-function, it is clear that

$$\int \mathrm{d}^4X e^{-i(P-\bar{P}_1)\cdot X + i\omega X^0} = (2\pi)^4\delta^{(3)}(\boldsymbol{P} - \boldsymbol{P}_1)\delta(\omega_{P_1} + \omega - P^0)\,, \tag{B.7}$$

so that

$$
\begin{aligned}
G^{\mu}_{P;P'}(p';k',k;p) = -\int \mathrm{d}^4\zeta \mathrm{d}^4\zeta' \mathrm{d}^4 Z \mathrm{d}^4 z \int \frac{\mathrm{d}^3 P_1}{2\omega_{P_1}} \frac{\mathrm{d}^3 P_2}{2\omega_{P_2}} \int \mathrm{d}\omega \mathrm{d}\omega' \\
\times\ e^{ip'\cdot\zeta' - ip\cdot\zeta + i(\bar{P}_2 - \bar{P}_1 + k + k')\cdot Z + i\frac{k-k'}{2}\cdot z} e^{-i\omega(Z^0 - \frac{1}{2}|z^0| - \frac{1}{2}|\zeta^0|)} \\
\times\ e^{-i\omega'(-Z^0 - \frac{1}{2}|\zeta'^0| - \frac{1}{2}|z^0|)} \frac{\chi_{\bar{P}_2}(\zeta')\langle \bar{P}_2 | O^{\mu}(-\frac{z}{2},\frac{z}{2}) | \bar{P}_1\rangle \bar{\chi}_{\bar{P}_1}(\zeta)}{(\omega + i\epsilon)(\omega' + i\epsilon)} \\
\times\ \delta^{(3)}(\boldsymbol{P}_2 - \boldsymbol{P}')\delta(P'^0 - \omega_{P_2} - \omega') \\
\times\ \delta^{(3)}(\boldsymbol{P} - \boldsymbol{P}_1)\delta(\omega_{P_1} + \omega - P^0) + O.T.
\end{aligned}
\tag{B.8}
$$

With the δ-functions one can perform the integrations over $\boldsymbol{P_1}$, $\boldsymbol{P_2}$, ω and ω':

$$
\begin{aligned}
G^{\mu}_{P;P'}(p';k',k;p) = -(2\pi)^4 \int \mathrm{d}^4\zeta \mathrm{d}^4\zeta' \mathrm{d}^4 z \frac{1}{2\omega_P} \frac{1}{2\omega_{P'}}\ e^{ip'\cdot\zeta' - ip\cdot\zeta + i\frac{k-k'}{2}\cdot z} \\
\times\ e^{i(P'^0 - \omega_{P'})(\frac{1}{2}|z^0| + \frac{1}{2}|\zeta'^0|)}\ e^{i(P^0 - \omega_P)(\frac{1}{2}|\zeta^0| + \frac{1}{2}|z^0|)} \\
\times\ \frac{\chi_{\bar{P}'}(\zeta')\langle \bar{P}' | O^{\mu}(-\frac{z}{2},\frac{z}{2}) | \bar{P}\rangle \bar{\chi}_{\bar{P}}(\zeta)}{((P^0 - \omega_P) + i\epsilon)((P'^0 - \omega_{P'}) + i\epsilon)} \delta^{(4)}(P' - P + k + k') \\
+\ O.T.
\end{aligned}
\tag{B.9}
$$

The six-point Green's function of Eq. (B.9) has poles when the four-momenta P and P' are on-shell, which is exactly the situation we want to describe. The "other terms" are regular for $\omega_P \to P^0$ and/or $\omega_{P'} \to P'^0$ and will thus be negligible in this limit. In the vicinity of the "double" pole, we can write the Green's function (B.9) in momentum space as

$$
\begin{aligned}
G^{\mu}_{P;P'}(p';k',k;p) \xrightarrow{P^{(\prime)0} \to \omega^{(\prime)}_P} -\frac{(2\pi)^4}{4\omega_P\omega_{P'}} \frac{\chi_{\bar{P}'}(p')\langle \bar{P}' | O^{\mu}(\frac{k-k'}{2}) | \bar{P}\rangle \bar{\chi}_{\bar{P}}(p)}{((P'^0 - \omega_{P'}) + i\epsilon)((P^0 - \omega_P) + i\epsilon)} \\
\times\ \delta^{(4)}(P' - P + k + k') \\
+\ \text{regular terms}\,.
\end{aligned}
\tag{B.10}
$$

This is the equation we wanted to prove. The Fourier transformed Bethe-Salpeter amplitudes which are used in the above equation, are defined as

$$
\begin{aligned}
\chi_{\bar{P}'}(p') &= \int \mathrm{d}^4\zeta' e^{ip'\cdot\zeta'} \chi_{\bar{P}'}(\zeta')\,, \\
\bar{\chi}_{\bar{P}}(p) &= \int \mathrm{d}^4\zeta e^{-ip\cdot\zeta} \bar{\chi}_{\bar{P}}(\zeta)\,,
\end{aligned}
\tag{B.11}
$$

while the definition of the Fourier transform of the bilocal current operator is

$$
O^{\mu}(\frac{k-k'}{2}) = \int \mathrm{d}^4 z e^{i\frac{k-k'}{2}\cdot z} O^{\mu}(-\frac{z}{2},\frac{z}{2})\,. \tag{B.12}
$$

B.2 The kernel in momentum space

Also the Fourier transform of Eq. (4.12), which gives an expression for the six-point Green's function G^μ via the Mandelstam formalism, needs to be calculated. Making use of the definition of the Fourier transform of the six-point Green's function of Eq. (B.1), omitting the indices α and inserting Eq. (4.12), we find

$$\begin{aligned} G^\mu(p_1', p_2'; k', k; p_1, p_2) = &\int \mathrm{d}^4x_1 \mathrm{d}^4x_2 \mathrm{d}^4x_1' \mathrm{d}^4x_2' \mathrm{d}^4Z \mathrm{d}^4z \int \mathrm{d}^4x_1'' \mathrm{d}^4x_2'' \mathrm{d}^4x_1''' \mathrm{d}^4x_2''' \\ &\times \int \frac{\mathrm{d}^3P_1}{(2\pi)^3\, 2\omega_{P_1}} \frac{\mathrm{d}^3P_2}{(2\pi)^3\, 2\omega_{P_2}} e^{i(p_1'\cdot x_1' + p_2'\cdot x_2' - p_1\cdot x_1 - p_2\cdot x_2 + (k+k')\cdot Z + \frac{k-k'}{2}\cdot z)} \\ &\times e^{-i(\bar{P}_1 - \bar{P}_2)\cdot Z} \chi_{\bar{P}_2}(x_1', x_2') \bar{\chi}_{\bar{P}_2}(x_1'', x_2'') K^\mu(x_1'', x_2''; -\frac{z}{2}, \frac{z}{2}; x_1''', x_2''') \\ &\times \chi_{\bar{P}_1}(x_1''', x_2''') \bar{\chi}_{\bar{P}_1}(x_1, x_2)\, \theta\left(\min(x_1'^0, x_2'^0) - Z^0 - \max(x_1''^0, x_1''^0)\right) \\ &\times \theta\left(\min(x_1'''^0, x_2'''^0) + Z^0 - \max(x_1^0, x_2^0)\right) + \ O.T. \end{aligned} \tag{B.13}$$

By moving to Jacobi coordinates for the incoming and outgoing particles, we obtain

$$\begin{aligned} G^\mu_{P;P'}(p'; k', k; p) = &\int \mathrm{d}^4X \mathrm{d}^4\zeta \mathrm{d}^4X' \mathrm{d}^4\zeta' \mathrm{d}^4Z \mathrm{d}^4z \int \mathrm{d}^4X'' \mathrm{d}^4\zeta'' \mathrm{d}^4X''' \mathrm{d}^4\zeta''' \\ &\times \int \frac{\mathrm{d}^3P_1}{(2\pi)^3\, 2\omega_{P_1}} \frac{\mathrm{d}^3P_2}{(2\pi)^3\, 2\omega_{P_2}} e^{i(P'\cdot X' + p'\cdot\zeta' - P\cdot X - p\cdot\zeta + (k+k')\cdot Z + \frac{k-k'}{2}\cdot z)} \\ &\times e^{-i(\bar{P}_1 - \bar{P}_2)\cdot Z} e^{-i\bar{P}_2\cdot X'} \chi_{\bar{P}_2}(\zeta') e^{i\bar{P}_2\cdot X''} \bar{\chi}_{\bar{P}_2}(\zeta'') \\ &\times K^\mu(X'', \zeta''; -\frac{z}{2}, \frac{z}{2}; X''', \zeta''') e^{-i\bar{P}_1\cdot X'''} \chi_{\bar{P}_1}(\zeta''') e^{i\bar{P}_1\cdot X} \bar{\chi}_{\bar{P}_1}(\zeta) \\ &\times \theta\left(X'^0 - Z^0 - X''^0 + \min(\frac{1}{2}\zeta'^0, -\frac{1}{2}\zeta'^0) - \max(\frac{1}{2}\zeta''^0, -\frac{1}{2}\zeta''^0)\right) \\ &\times \theta\left(X'''^0 + Z^0 - X^0 + \min(\frac{1}{2}\zeta'''^0, -\frac{1}{2}\zeta'''^0) - \max(\frac{1}{2}\zeta^0, -\frac{1}{2}\zeta^0)\right) \\ &+ \ O.T. \end{aligned} \tag{B.14}$$

Inserting the Fourier transforms of the Heaviside step functions, defined by Eq. (B.5), gives

$$
\begin{aligned}
G^{\mu}_{P;P'}(p';k',k;p) = -\int \mathrm{d}^4X\mathrm{d}^4\zeta\mathrm{d}^4X'\mathrm{d}^4\zeta'\mathrm{d}^4Z\mathrm{d}^4z \int \mathrm{d}^4X''\mathrm{d}^4\zeta''\mathrm{d}^4X'''\mathrm{d}^4\zeta''' \\
\times \int \frac{\mathrm{d}^3P_1}{(2\pi)^3\,2\omega_{P_1}}\frac{\mathrm{d}^3P_2}{(2\pi)^3\,2\omega_{P_2}}\, e^{i(P'\cdot X'+p'\cdot\zeta'-P\cdot X-p\cdot\zeta+(k+k')Z+\frac{k-k'}{2}\cdot z)} \\
\times\; e^{-i(\bar{P}_1-\bar{P}_2)Z}e^{-i\bar{P}_2X'}\chi_{\bar{P}_2}(\zeta')e^{i\bar{P}_2X''}\bar{\chi}_{\bar{P}_2}(\zeta'')K^{\mu}(X'',\zeta'';-\frac{z}{2},\frac{z}{2};X''',\zeta''') \\
\times\; e^{-i\bar{P}_1X'''}\chi_{\bar{P}_1}(\zeta''')e^{i\bar{P}_1X}\bar{\chi}_{\bar{P}_1}(\zeta)\int_{-\infty}^{+\infty}\frac{\mathrm{d}\omega}{2\pi}\frac{e^{-i\omega(X'''^0+Z^0-X^0-\frac{1}{2}|\zeta^0|-\frac{1}{2}|\zeta'''^0|)}}{\omega+i\epsilon} \\
\times \int_{-\infty}^{+\infty}\frac{\mathrm{d}\omega'}{2\pi}\frac{e^{-i\omega'(X'^0-Z^0-X''^0-\frac{1}{2}|\zeta'^0|-\frac{1}{2}|\zeta''^0|)}}{\omega'+i\epsilon} \\
+\; O.T.,
\end{aligned}
\tag{B.15}
$$

so that using the definition of the δ-function, we find

$$
\begin{aligned}
G^{\mu}_{P;P'}(p';k',k;p) = -\int \mathrm{d}^4\zeta\mathrm{d}^4\zeta'\mathrm{d}^4Z\mathrm{d}^4z \int \mathrm{d}^4X''\mathrm{d}^4\zeta''\mathrm{d}^4X'''\mathrm{d}^4\zeta''' \int \frac{\mathrm{d}^3P_1}{2\omega_{P_1}}\frac{\mathrm{d}^3P_2}{2\omega_{P_2}} \\
\times \int \mathrm{d}\omega\mathrm{d}\omega'\; e^{i(p'\cdot\zeta'-p\cdot\zeta+(k+k')Z+\frac{k-k'}{2}\cdot z)}e^{-i(\bar{P}_1-\bar{P}_2)Z}\chi_{\bar{P}_2}(\zeta') \\
\times\; e^{i\bar{P}_2X''}\bar{\chi}_{\bar{P}_2}(\zeta'')K^{\mu}(X'',\zeta'';-\frac{z}{2},\frac{z}{2};X''',\zeta''')e^{-i\bar{P}_1X'''}\chi_{\bar{P}_1}(\zeta''')\bar{\chi}_{\bar{P}_1}(\zeta) \\
\times\; \frac{e^{-i\omega(X'''^0+Z^0-\frac{1}{2}|\zeta^0|-\frac{1}{2}|\zeta'''^0|)}}{\omega+i\epsilon}\frac{e^{-i\omega'(-Z^0-X''^0-\frac{1}{2}|\zeta'^0|-\frac{1}{2}|\zeta''^0|)}}{\omega'+i\epsilon} \\
\times\; \delta^{(3)}(\boldsymbol{P'}-\boldsymbol{P_2})\delta(P'^0-\omega_{P_2}-\omega')\delta^{(3)}(\boldsymbol{P_1}-\boldsymbol{P})\delta(\omega_{P_1}+\omega-P^0) \\
+\; O.T.\,,
\end{aligned}
\tag{B.16}
$$

and eventually

$$
\begin{aligned}
G^{\mu}_{P;P'}(p';k',k;p) = -(2\pi)^4\int \mathrm{d}^4\zeta\mathrm{d}^4\zeta'\mathrm{d}^4z \int \mathrm{d}^4X''\mathrm{d}^4\zeta''\mathrm{d}^4X'''\mathrm{d}^4\zeta'''\frac{1}{2\omega_P}\frac{1}{2\omega_{P'}} \\
\times\; e^{i(p'\cdot\zeta'-p\cdot\zeta+\frac{k-k'}{2}\cdot z)}\chi_{\bar{P}'}(\zeta')e^{i\bar{P}'\cdot X''}\bar{\chi}_{\bar{P}'}(\zeta'')K^{\mu}(X'',\zeta'';-\frac{z}{2},\frac{z}{2};X''',\zeta''') \\
\times\; e^{-i\bar{P}\cdot X'''}\chi_{\bar{P}}(\zeta''')\bar{\chi}_{\bar{P}}(\zeta)\frac{e^{-i(P^0-\omega_P)(X'''^0-\frac{1}{2}|\zeta^0|-\frac{1}{2}|\zeta'''^0|)}}{(P^0-\omega_P)+i\epsilon} \\
\times\; \frac{e^{-i(P'^0-\omega_{P'})(-X''^0-\frac{1}{2}|\zeta'^0|-\frac{1}{2}|\zeta''^0|)}}{(P'^0-\omega_{P'})+i\epsilon}\delta^{(4)}(P'-P+k+k')+\; O.T.
\end{aligned}
\tag{B.17}
$$

The above equation has poles when the four-momenta P and P' are on-shell. Also in this equation, the "other terms" are regular in the vicinity of the "double" pole.

Introducing the Fourier transform of the bilocal current kernel K^{μ} as

$$K^{\mu}_{\bar{P};\bar{P}'}(p'';\frac{k-k'}{2};p''') = \int \mathrm{d}^4X''\mathrm{d}^4X'''\mathrm{d}^4\zeta''\mathrm{d}^4\zeta'''\mathrm{d}^4z\; e^{i(\bar{P}'\cdot X''+p''\cdot\zeta''-\bar{P}\cdot X'''-p'''\cdot\zeta'''+\frac{k-k'}{2}\cdot z)} \times\; K^{\mu}(X'',\zeta'';-\frac{z}{2},\frac{z}{2};X''',\zeta'''), \tag{B.18}$$

and making use of the definitions of the Fourier transforms of the Bethe-Salpeter amplitudes (Eq. (B.11)), the above equation (B.17) can be rewritten near the "double" pole as

$$\begin{aligned} G'^{\mu}_{P;P'}(p';k',k;p) \xrightarrow{P^{(\prime)0}\to\omega^{(\prime)}} -(2\pi)^4 \int \frac{\mathrm{d}^4p''}{(2\pi)^4}\frac{\mathrm{d}^4p'''}{(2\pi)^4}\frac{1}{2\omega_P}\frac{1}{2\omega_{P'}}\chi_{\bar{P}'}(p')\bar{\chi}_{\bar{P}'}(p'') \\ \times\; K^{\mu}_{\bar{P};\bar{P}'}(p'';\frac{k-k'}{2};p''')\chi_{\bar{P}}(p''')\bar{\chi}_{\bar{P}}(p) \\ \times\; \frac{1}{((P^0-\omega_P)+i\epsilon)((P'^0-\omega_{P'})+i\epsilon)} \\ \times\; \delta^{(4)}(P'-P+k+k') + \text{ regular terms.} \end{aligned} \tag{B.19}$$

C The Bonn model for baryons

Chapter 3 introduced the Bonn model for mesons, which are bound $q\bar{q}$ pairs. Baryons, which have a qqq valence quark structure, can also be described in a Bethe-Salpeter framework. In this appendix, we highlight the differences between the meson and the baryon model.

C.1 The Bethe-Salpeter equation for baryons

The Bethe-Salpeter equation for baryons is derived starting from the following six-point Green's function, which describes the propagation of three fermions with a similar notation as in Chapter 3:

$$\begin{aligned} &G_{\alpha\alpha'\alpha''\beta\beta'\beta''}(x_1', x_2', x_3'; x_1, x_2, x_3) \\ &\qquad = -\langle\Theta|T\{\psi_\alpha(x_1')\psi_{\alpha'}(x_2')\psi_{\alpha'''}(x_3')\bar{\psi}_\beta(x_1)\bar{\psi}_{\beta'}(x_2)\bar{\psi}_{\beta''}(x_3)\}|\Theta\rangle\,, \end{aligned} \tag{C.1}$$

Remark that this six-point Green's function is not the same as the function G^μ in Eq. (4.3), which contains the vector operator O^μ. The Bethe-Salpeter amplitude describing a qqq bound state is defined as

$$\chi_{\bar{P}\alpha\alpha'\alpha''}(x_1, x_2, x_3) = \langle\Theta|T\{\psi_\alpha(x_1)\psi_{\alpha'}(x_2)\psi_{\alpha''}(x_3)\}|\bar{P}\rangle\,, \tag{C.2}$$

while the Bethe-Salpeter equation now reads

$$\chi_{\bar{P}} = -iG_{0\bar{P}}(K^{(3)}_{\bar{P}} + \bar{K}^{(2)}_{\bar{P}})\chi_{\bar{P}}\,. \tag{C.3}$$

The two-particle interaction kernel K from the meson model is replaced by the sum of a two- and a three-particle irreducible interaction kernel, $K^{(2)}$ and $K^{(3)}$. The irreducibility is now defined according to the number of quark lines: an n-particle interaction diagram is called irreducible when it cannot be split into two simpler graphs by cutting only n internal fermion lines. The kernel $\bar{K}^{(2)}$ in the above Bethe-Salpeter equation is a three-body kernel, defined as the sum of the possible two-quark interaction

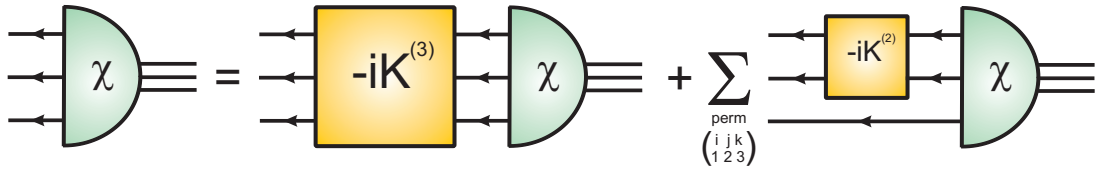

Figure C.1 Diagrammatic representation of the Bethe-Salpeter equation for baryons (C.3).

kernels, each multiplied with the corresponding inverse spectator quark propagator:

$$\bar{K}^{(2)}(x_1', x_2', x_3'; x_1, x_2, x_3) = \sum_{\substack{perm. \\ \binom{ijk}{123}}} K^{(2)}(x_i', x_j'; x_i, x_j) \left[S_F^k\right]^{-1}(x_k', x_k)\,. \tag{C.4}$$

The diagrammatic analogue of Eq. (C.3) is drawn in Fig. C.1. The normalization equation is analogous to that in the meson model:

$$\bar{\chi}_{\bar{P}} \left[P^\mu \frac{\partial}{\partial P^\mu} \left(G_{0P}^{-1} + i(K^{(3)} + \bar{K}_P^{(2)}) \right) \right]_{P=\bar{P}} \chi_{\bar{P}} = 2iM^2\,. \tag{C.5}$$

C.2 Reduction to the Salpeter equation

Just as in the meson case, the Bethe-Salpeter equation (C.3) turns out to be unsolvable. The reduction to the Salpeter equation is performed by assuming instantaneous interactions and free fermion propagators with an effective constituent quark mass m_j (see Sect. 3.3.1). However, whereas these approximations allow for a straightforward reduction in the meson model, the situation is more complicated for baryons due to the occurrence of three- *and two*-particle irreducible interaction kernels. As shown in Eq. (C.4), the latter class of interaction kernels contains an inverse quark propagator for the spectator quark. This quark is off-shell in general. As a result, a relative energy dependence will remain even if the two-particle interaction kernel $K^{(2)}$ is chosen instantaneous.

This complex problem was tackled in Ref. [93], and it was proven that in order to reconstruct the Bethe-Salpter amplitude χ, one does not need the full Salpeter equation. In fact, it suffices to only use its projected part on the states with a purely positive and negative energy. The full derivation of the Salpeter equation would take us too far, and we refer to Refs. [93, 114] for more details. We only mention the result, which is written in terms of the Jacobi coordinates

$$\begin{cases} X &= \frac{1}{3}(x_1 + x_2 + x_3) \\ \zeta &= x_1 - x_2 \\ \eta &= \frac{1}{2}(x_1 + x_2 - 2x_3) \end{cases} \quad \text{and} \quad \begin{cases} P &= p_1 + p_2 + p_3 \\ p_\zeta &= \frac{1}{2}(p_1 - p_2) \\ p_\eta &= \frac{1}{3}(p_1 + p_2 - 2p_3) \end{cases}, \tag{C.6}$$

and reads for the projected Salpeter amplitudes

$$\Phi_M^\Lambda(\boldsymbol{p_\zeta}, \boldsymbol{p_\eta}) = \left[\Lambda_1^+(\boldsymbol{p_1}) \otimes \Lambda_2^+(\boldsymbol{p_2}) \otimes \Lambda_3^+(\boldsymbol{p_3}) + \Lambda_1^-(\boldsymbol{p_1}) \otimes \Lambda_2^-(\boldsymbol{p_2}) \otimes \Lambda_3^-(\boldsymbol{p_3})\right] \times \int \frac{\mathrm{d}p_\zeta^0}{(2\pi)} \frac{\mathrm{d}p_\eta^0}{(2\pi)} \chi_M(p_\zeta, p_\eta)\,, \tag{C.7}$$

in the baryon rest frame:

$$\begin{aligned}\Phi_M^\Lambda(\boldsymbol{p_\zeta}, \boldsymbol{p_\eta}) = &\left[\frac{\Lambda_1^+(\boldsymbol{p_1}) \otimes \Lambda_2^+(\boldsymbol{p_2}) \otimes \Lambda_3^+(\boldsymbol{p_3})}{M - \Omega(\boldsymbol{p_\zeta}, \boldsymbol{p_\eta}) + i\epsilon} + \frac{\Lambda_1^-(\boldsymbol{p_1}) \otimes \Lambda_2^-(\boldsymbol{p_2}) \otimes \Lambda_3^-(\boldsymbol{p_3})}{M + \Omega(\boldsymbol{p_\zeta}, \boldsymbol{p_\eta}) - i\epsilon}\right] \gamma^0 \otimes \gamma^0 \otimes \gamma^0 \\ &\times \int \frac{\mathrm{d}^3 p'_\zeta}{(2\pi)^3} \frac{\mathrm{d}^3 \boldsymbol{p'_\eta}}{(2\pi)^3} V^{(3)}(\boldsymbol{p_\zeta}, \boldsymbol{p_\eta}; \boldsymbol{p'_\zeta}, \boldsymbol{p'_\eta}) \Phi_M^\Lambda(\boldsymbol{p'_\zeta}, \boldsymbol{p'_\eta}) \\ &+ \left[\frac{\Lambda_1^+(\boldsymbol{p_1}) \otimes \Lambda_2^+(\boldsymbol{p_2}) \otimes \Lambda_3^+(\boldsymbol{p_3})}{M - \Omega(\boldsymbol{p_\zeta}, \boldsymbol{p_\eta}) + i\epsilon} + \frac{\Lambda_1^-(\boldsymbol{p_1}) \otimes \Lambda_2^-(\boldsymbol{p_2}) \otimes \Lambda_3^-(\boldsymbol{p_3})}{M + \Omega(\boldsymbol{p_\zeta}, \boldsymbol{p_\eta}) - i\epsilon}\right] \\ &\times \int \frac{\mathrm{d}^3 p'_\zeta}{(2\pi)^3} \left[\left[\gamma^0 \otimes \gamma^0 V^{(2)}(\boldsymbol{p_\zeta}, \boldsymbol{p'_\zeta})\right] \otimes \mathbb{1}\right] \Phi_M^\Lambda(\boldsymbol{p'_\zeta}, \boldsymbol{p_\eta}) \\ &+\text{cyclic permutation in quarks (123)}\,.\end{aligned} \tag{C.8}$$

Here, the energy projection operators $\Lambda_j^\pm$ have the same definition as in the meson model: $\Lambda_j^\pm = (\omega_j \pm H_j)/(2\omega_j)$, with the Dirac Hamiltonian $H_j(\boldsymbol{p_j}) = \gamma^0(\boldsymbol{\gamma}\cdot\boldsymbol{p_j} + m_j)$ and the energy $\omega_j = \sqrt{m_j^2 + |\boldsymbol{p_j}|^2}$ for the jth constituent quark. Ω is the sum of the energies of the individual constituent quarks: $\Omega = \sum_{j=1}^3 \omega_j$. $V^{(2)}$ and $V^{(3)}$ are the instantaneous two- and three-particle interaction kernels.

C.3 Interactions

The interactions adopted in the Bonn model for baryons are the confinement interaction and the 't Hooft instanton induced interaction. The first is used to model the three-quark interaction kernel. In the implementation of a linearly rising confinement interaction, some freedom exists in the radial dependence. Contrary to the $q\bar{q}$ case where the interquark distance r is readily defined as $|\boldsymbol{x_1} - \boldsymbol{x_2}|$, the distance between the three constituent quarks in a baryon can be defined in various ways. Three conventions are commonly used in literature: the Δ-, Y- and H-configurations (see Fig. C.2). The particular choice turns out to influence the results in the Bonn model only slightly. Results from lattice QCD seem to favor a combination of the Δ- and Y-configurations. In Bonn model calculations, the Δ-configuration is usually chosen, for which the interquark distance is defined as

$$r_{3q} = \sum_{i<j} |x_i - x_j|\,. \tag{C.9}$$

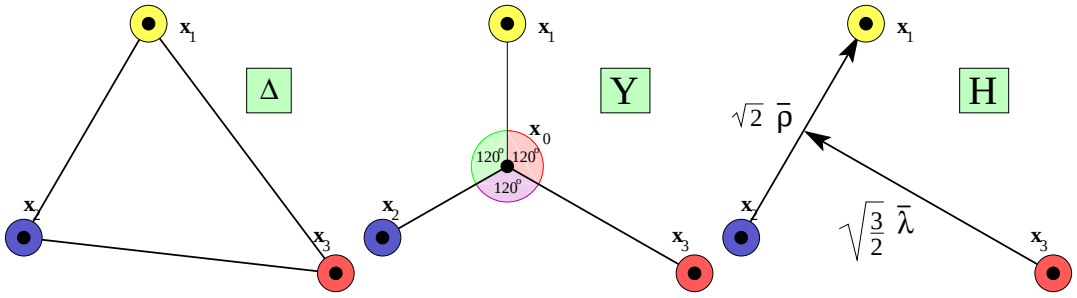

Figure C.2 The Δ-, Y- and H-configurations for the interquark distance in a baryon. Picture taken from Ref. [29].

The confinement interaction potential can then be written as

$$V_C(r_{3q}) = a_c \mathcal{W}_{off} + b_c \mathcal{W}_{str} r_{3q}\,, \tag{C.10}$$

where a_c and b_c are model parameters, while $\mathcal{W}_{off}$ and $\mathcal{W}_{str}$ denote the specific Dirac structure of the interaction.

As in the meson case, the confinement interaction acts on all states in the spectrum. To describe the mass splittings between the spin-$3/2$ decuplet and the spin-$1/2$ octet ground state baryons, however, a residual interaction is needed. Again, this role is played by the 't Hooft instanton induced interaction, which is implemented as a two-body potential in the Bonn model:

$$\begin{aligned} V^{(2)}_{III}(x_1, x_2; x_1', x_2') = &-4\mathcal{R}_\Lambda(\boldsymbol{x_1} - \boldsymbol{x_2}) \left(\mathbb{1}\otimes\mathbb{1} + \gamma^5\otimes\gamma^5\right) \\ &\times \mathcal{P}^{\mathcal{D}}_{S_{12}=0} \otimes \left(g_{nn}\mathcal{P}^{\mathcal{F}}_A(nn) + g_{ns}\mathcal{P}^{\mathcal{F}}_A(ns)\right) \otimes \mathcal{P}^{\mathcal{C}}_{\bar{3}} \\ &\times \delta(x_1^0 - x_2^0)\delta^{(4)}(x_1 - x_1')\delta^{(4)}(x_2 - x_2')\,, \end{aligned} \tag{C.11}$$

with $\mathcal{R}_\Lambda$ as defined in Eq. (3.30). The projectors $\mathcal{P}$ in Eq. (C.11) make sure the 't Hooft interaction acts only on states which are antisymmetric in Dirac ($\mathcal{D}$), flavor ($\mathcal{F}$) and color ($\mathcal{C}$) spaces separately. For instance, this interaction will not act on the $\Delta(1232)$ resonance, which has a symmetric spin wave function (see Chapter 1). The nucleon however, fulfills the conditions for the 't Hooft interaction, so that this interaction will lower the nucleon mass with respect to the Δ.

Bibliography

[1] K. G. Wilson, Scientific American **241**, 140 (1979).

[2] W. Greiner and B. Müller, *Gauge theory of weak interactions* (Springer-Verlag, Berlin, 2000).

[3] G. Ross, *Grand unified theories* (Addison-Wesley Publishing Company, Inc., Redwood City, California, 2003).

[4] M. Gell-Mann, Phys. Rev. **125**, 1067 (1962).

[5] M. Gell-Mann, Phys. Lett. **8**, 214 (1964).

[6] Y. Ne'eman, Nucl. Phys. **26**, 222 (1961).

[7] G. Zweig, CERN Reports **8182/TH**, 401 (1964).

[8] G. Zweig, CERN Reports **8419/TH**, 412 (1964).

[9] Y. Nambu, in *Preludes in Theoretical Physics in Honor of V. F. Weisskopf*, edited by A. De Shalit, H. Feshbach, and L. Van Hove (North-Holland, Amsterdam, 1966), Chap. A Systematics of Hadrons in Subnuclear Physics, p. 133.

[10] M. Han and Y. Nambu, Phys. Rev. **139**, B1006 (1965).

[11] M. E. Peskin and D. V. Schroeder, *An Introduction to Quantum Field Theory* (Perseus Books Publishing, Reading, Massachusetts, 1995).

[12] G. 't Hooft, talk at the "Conference on Lagrangian Field Theory", Marseille, 1972 (unpublished).

[13] D. J. Gross and F. Wilczek, Phys. Rev. Lett. **30**, 1343 (1973).

[14] D. J. Gross and F. Wilczek, Phys. Rev. **D8**, 3633 (1973).

[15] H. D. Politzer, Phys. Rev. Lett. **30**, 1346 (1973).

[16] H. D. Politzer, Phys. Rep. **14**, 129 (1974).

[17] G. Münster and M. Walzl, hep-lat/0012005 (2000).

[18] H. Leutwyler, hep-ph/0008124 (2000).

[19] M. Koll *et al.*, Eur. Phys. J. **A9**, 73 (2000).

[20] J. C. Collins, L. Frankfurt, and M. Strikman, Phys. Rev. **D56**, 2982 (1997).

[21] J. C. Collins and A. Freund, Phys. Rev. **D59**, 074009 (1999).

[22] D. Mueller *et al.*, Fortschr. Phys. **42**, 101 (1994).

[23] X. Ji, Phys. Rev. Lett. **78**, 610 (1997).

[24] A. Radyushkin, Phys. Rev. **D56**, 5524 (1997).

[25] M. Diehl, Phys. Rept. **388**, 41 (2003).

[26] K. Goeke, M. Polyakov, and M. Vanderhaeghen, Prog. Part. Nucl. Phys. **47**, 401 (2001).

[27] A. V. Belitsky and A. V. Radyushkin, Phys. Rept. **418**, 1 (2005).

[28] S. Boffi and B. Pasquini, arXiv:0711.2625 [hep-ph] (2007).

[29] T. Van Cauteren, Ph.D. thesis, Universiteit Gent, 2005.

[30] C. F. Perdrisat, V. Punjabi, and M. Vanderhaeghen, Prog. Part. Nucl. Phys. **59**, 694 (2007).

[31] J. Kelly, Phys. Rev. **C66**, 065203 (2002).

[32] W. Panofsky, in *Proceedings International Symposium on High Energy Physics*, Vienna, 1968.

[33] B. Povh, K. Rith, C. Scholz, and F. Zetsche, *Particles and Nulei*, 2nd ed. (Springer-Verlag, Berlin, 1999).

[34] A. W. Thomas and W. Weise, *The structure of the nucleon* (Wiley-VCH, Berlin, 2001).

[35] R. G. Roberts, *The structure of the proton* (Cambridge University Press, Cambridge, 1990).

[36] P. J. Mulders, Prog. Part. Nucl. Phys. **55**, 243 (2005).

[37] S. Chekanov and the ZEUS collaboration, Phys. Lett. **B573**, 46 (2003).

[38] A. Aktas and the H1 collaboration, Eur. Phys. J. **C44**, 1 (2005).

[39] C. Muñoz Camacho and the Jefferson Lab Hall A collaboration, Phys. Rev. Lett. **97**, 262002 (2006).

[40] A. Airapetian and the HERMES collaboration, Phys. Rev. **D75**, 011103 (2007).

[41] R. De Masi and the CLAS collaboration, Nucl. Phys. Proc. Suppl. **174**, 15 (2007).

[42] M. Mazouz and the Jefferson Lab Hall A collaboration, arXiv:0709.0450 [nucl-ex] (2007).

[43] C. Hadjidakis and the CLAS collaboration, Phys. Lett. **B605**, 256 (2005).

[44] S. Chekanov and the ZEUS collaboration, Nucl. Phys. **B718**, 3 (2005).

[45] A. Vandenbroucke, Ph.D. thesis, Universiteit Gent, 2007.

[46] A. Airapetian and the HERMES collaboration, Phys. Lett. **B659**, 486 (2008).

[47] X. Ji, J. Phys. **G24**, 11811 (1998).

[48] M. Burkardt, Phys. Rev. **D62**, 071503 (2000).

[49] A. Belitsky and D. Müller, Nucl. Phys. **A711**, 118 (2002).

[50] X. Ji, Phys. Rev. **D58**, 056003 (1998).

[51] S. Bass, Rev.Mod.Phys. **77**, 1257 (2005).

[52] P. Hägler, private communication.

[53] V. N. Gribov and L. N. Lipatov, Sov. J. Nucl. Phys. **15**, 675 (1972).

[54] G. Altarelli and G. Parisi, Nucl. Phys. **B126**, 298 (1977).

[55] Y. L. Dokshitzer, Sov. Phys. JETP **46**, 641 (1977).

[56] A. V. Efremov and A. V. Radyushkin, Theor. Math. Phys. **42**, 97 (1980).

[57] G. P. Lepage and S. J. Brodsky, Phys. Lett. **B87**, 359 (1979).

[58] R. Jaffe, Phys. Lett. B **93**, 313 (1980).

[59] W. Broniowski, E. R. Arriola, and K. Golec-Biernat, arXiv:0712.1012 [hep-ph] (2007).

[60] S. Scopetta and V. Vento, Eur. Phys. J. **A16**, 527 (2003).

[61] S. Scopetta, Phys. Rev. D **69**, 094004 (2004).

[62] S. Noguera, S. Scopetta, and V. Vento, Phys. Rev. 094018 (2004).

[63] A. Van Dyck, T. Van Cauteren, and J. Ryckebusch, Phys. Lett. B, in press (2008), arXiv:0710.2271.

[64] P. Hägler *et al.*, Eur. Phys. J. **70**, 094018 (2004).

[65] P. Hägler and the LHPC collaboration, Phys. Rev. **D68**, 034505 (2003).

[66] M. Gockeler *et al.*, Nucl. Phys. Proc. Suppl. **153**, 146 (2006).

[67] J.-W. Chen, W. Detmold, and B. Smigielski, Phys. Rev. **D75**, 074003 (2007).

[68] D. Brömmel and the QCDSF/UKQCD collaboration, arXiv:0708.2249 [hep-lat] (2007).

[69] A. V. Radyushkin, in *Boris Ioffe Festschrift 'At the Frontier of Particle Physics / Handbook of QCD'* (World Scientific, Singapore, 2001), Chap. Generalized parton distributions, hep-ph/0101225.

[70] I. V. Musaov and A. V. Radyushkin, Phys. Rev. **D61**, 074027 (2000).

[71] M. Guidal, M. V. Polyakov, A. V. Radyushkin, and M. Vanderhaeghen, Phys. Rev. **D72**, 054013 (2005).

[72] S. Ahmad, H. Honkanen, S. Liuti, and S. K. Taneja, Phys. Rev. **D75**, 094003 (2007).

[73] X. Ji, W. Melnitchouk, and X. Song, Phys. Rev. **D56**, 5511 (1997).

[74] M. Wakamatsu and Y. Nakakoji, Phys. Rev. **D74**, 054006 (2006).

[75] B. Pasquini and S. Boffi, Phys. Rev. **D73**, 094001 (2006).

[76] B. Pasquini and S. Boffi, Nucl. Phys. **A782**, 86 (2007).

[77] S. Boffi, B. Pasquini, and M. Traini, Nucl. Phys. **B649**, 243 (2003).

[78] S. Boffi, B. Pasquini, and M. Traini, Nucl. Phys. **B680**, 147 (2004).

[79] S. Noguera, L. Theußl, and V. Vento, Eur. Phys. J. **A20**, 483 (2004).

[80] F. Bissey *et al.*, Phys.Lett. **B587**, 189 (2004).

[81] B. Tiburzi and G. Miller, Phys. Rev. **D65**, 074009 (2002).

[82] B. Tiburzi and G. Miller, Phys. Rev. **D67**, 054014 (2003).

[83] B. Tiburzi and G. Miller, Phys. Rev. **D67**, 054015 (2003).

[84] L. Kisslinger, H.-M. Choi, and C.-R. Ji, Phys. Rev. **D63**, 113005 (2001).

[85] H.-M. Choi, C.-R. Ji, and L. Kisslinger, Phys. Rev. **D64**, 093006 (2001).

[86] H.-M. Choi, C.-R. Ji, and L. Kisslinger, Phys. Rev. **D66**, 053011 (2002).

[87] A. Van Dyck *et al.*, Prog. Part. Nucl. Phys., in press (2008).

[88] N. Isgur and G. Karl, Phys. Rev. **D18**, 4187 (1978).

[89] N. Isgur and G. Karl, Phys. Rev. **D19**, 2653 (1979).

[90] C. R. Münz, J. Resag, B. C. Metsch, and H. R. Petry, Nucl. Phys. **A578**, 418 (1994).

[91] J. Resag, C. R. Münz, B. C. Metsch, and H. R. Petry, Nucl. Phys. **A578**, 397 (1994).

[92] C. R. Münz, Ph.D. thesis, Rheinische Friedrich-Wilhelms-Universität Bonn, Germany, 1994.

[93] U. Löring, K. Kretzschmar, B. Metsch, and H.-R. Petry, Eur. Phys. J. **A10**, 309 (2001).

[94] U. Löring, B. Metsch, and H.-R. Petry, Eur. Phys. J. **A10**, 395 (2001).

[95] U. Löring, B. Metsch, and H.-R. Petry, Eur. Phys. J. **A10**, 447 (2001).

[96] K. Kretzschmar, Ph.D. thesis, Rheinische Friedrich-Wilhelms-Universität Bonn, Germany, 2001.

[97] M. Gell-Mann and F. Low, Phys. Rev. **84**, 350 (1951).

[98] M. Koll, Ph.D. thesis, Rheinische Friedrich-Wilhelms-Universität Bonn, Germany, 2001.

[99] E. E. Salpeter and H. A. Bethe, Physical Review **84**, 1232 (1951).

[100] Y. Nambu and G. Jona-Lasinio, Phys. Rev. **122**, 345 (1961).

[101] Y. Nambu and G. Jona-Lasinio, Phys. Rev. **124**, 246 (1961).

[102] S. Biswas, S. Choudhury, K. Datta, and A. Goyal, Phys. Rev. **D26**, 1983 (1982).

[103] D. Merten *et al.*, Eur. Phys. J. **A14**, 477 (2002).

[104] T. V. Cauteren *et al.*, Eur. Phys. J. **A20**, 283 (2004).

[105] S. Wallace and V. Mandelzweig, Nucl.Phys. **A503**, 673 (1989).

[106] E. E. Salpeter, Phys. Rev. **87**, 328 (1952).

[107] D. H. Perkins, *Introduction to high energy physics* (Addison-Wesley Publishing Company, Inc., Menlo Park, California, 1987).

[108] G. S. Bali, Phys. Rept. **343**, 1 (2000).

[109] P. de Forcrand and O. Jahn, Nucl. Phys. **A755**, 475c (2005).

[110] R. Ricken, Ph.D. thesis, Rheinische Friedrich-Wilhelms-Universität Bonn, Germany, 2001.

[111] W.-M. Yao *et al.*, Journal of Physics G **33**, 1+ (2006).

[112] B. C. Metsch and H. R. Petry, Acta Phys. Polon. **B27**, 3307 (1996).

[113] G. 't Hooft, Phys.Rev. **D14**, 3432 (1976).

[114] U. Löring, Ph.D. thesis, Rheinische Friedrich-Wilhelms-Universität Bonn, Germany, 2001.

[115] S. Mandelstam, Proc. Roy. Soc. **233**, 248 (1955).

[116] A. L. Fetter and J. D. Walecka, *Quantum Theory of Many-Particle Systems* (Dover Publications, Inc., Mineola, New York, 2003).

[117] M. Abramowitz and I. Stegun, *Handbook of mathematical functions* (Dover Publications Inc., New York, 1972).

[118] W. I. Giersche, Master's thesis, Rheinische Friedrich-Wilhelms-Universität Bonn, Germany, 1996.

[119] H. Giersche, Master's thesis, Rheinische Friedrich-Wilhelms-Universität Bonn, Germany, 1996.

[120] A. Van Dyck *et al.*, manuscript in preparation.

[121] C. R. Münz, J. Resag, B. C. Metsch, and H.-R. Petry, Phys. Rev. **C52**, 2110 (1995).

Samenvatting

Inleiding

Het idee dat materie is opgebouwd uit discrete bouwstenen bestaat al duizenden jaren. Verschillende eeuwen voor de Griekse filosoof Demokritos de term ἄτομος (ondeelbaar) reserveerde voor de veronderstelde materiedeeltjes, bestudeerde men al het bestaan van kleine materie-eenheden aan Indische filosofiescholen. Toen Dalton aan het begin van de negentiende eeuw zijn atomaire theorie formuleerde, verloor het concept zijn louter filosofische betekenis en werd het het onderwerp van vele wetenschappelijke studies.

Het is mogelijk om macroscopische objecten te beschrijven zónder in te gaan op hun microscopische structuur. Wanneer men bijvoorbeeld de aantrekkingskracht tussen een tafel en de aarde wil berekenen, zou een atomaire benadering de wiskundige beschrijving aanzienlijk moeilijker maken. Aan de andere kant is het natuurlijk ook mogelijk dat men van diezelfde tafel wil weten van welke houtsoort hij gemaakt is. In dat geval moet men microscopische eigenschappen onderzoeken, namelijk de DNA-keten. Deze twee voorbeelden tonen aan dat bij het beschrijven van een object, de *schaal* waarop men kijkt van fundamenteel belang is. De schaal bepaalt de vrijheidsgraden van het systeem: hoe kleiner de schaal, des te kleiner de bouwstenen die nodig zijn om een fysisch object te modelleren.

De inhoud van dit proefschrift situeert zich in de "hadronenfysica". Hadronen, bvb. kerndeeltjes als protonen, neutronen en pionen, bestaan uit quarks en gluonen. Men kan twee deelgroepen onderscheiden binnen de hadronen: *baryonen*, die fermionische deeltjes zijn en een halftallige spin hebben, en *mesonen*, die bosonisch zijn en een heeltallige spin bezitten. De wetten waaraan deze deeltjes moeten voldoen, staan beschreven in het *standaardmodel van de deeltjesfysica*, dat in de jaren zeventig van de vorige eeuw werd ontwikkeld. In dit standaardmodel worden de elementaire deeltjes en hun interacties beschreven. De elementaire deeltjes worden onderverdeeld in twee families: de *leptonen* (electron, muon en tau, en drie corresponderende neutrino's) en

de *quarks* (up, down, strange, charm, bottom en top). Deze deeltjes communiceren met elkaar via de elektromagnetische, de zwakke en de sterke interactie, meer bepaald door het uitwisselen van *ijkbosonen* (fotonen voor de elektromagnetische interactie, de $W^{\pm}$ en Z^0 voor de zwakke wisselwerking en gluonen voor de sterke interactie). Een elementair deeltje kan aan een ijkboson koppelen indien het de lading bezit die bij de wisselwerking hoort (resp. elektromagnetische lading, zwakke lading en kleurlading).

De relatieve eenvoud van het standaardmodel betekent echter niet dat de interacties tussen de verschillende bouwstenen van de materie volledig begrepen zijn. Ook nu nog blijven een heleboel vragen onbeantwoord. Vele daarvan hebben te maken met de sterke interactie die beschreven wordt in de kwantumchromodynamica of QCD.

In de jaren zestig van de vorige eeuw postuleerden Gell-Mann, Ne'eman en Zweig het bestaan van quarks in een poging om de vele sterk interagerende deeltjes te ordenen die in de jaren voordien waren ontdekt in reacties met kosmische straling en experimenten met deeltjesversnellers. Eén deeltje bleef hen echter parten spelen: het Δ^{++} bleek symmetrisch in smaak-, configuratie- én spinruimte apart, een situatie die in de kwantummechanica verboden is door het Pauliprincipe. Het antwoord op dit probleem kwam van Nambu en Han, die een nieuw kwantumgetal, *kleur*, in het leven riepen. Deze kleur was een exclusieve eigenschap van quarks, en bestond in drie varianten: rood, groen en blauw (met de corresponderende antikleuren voor de antiquarks). Volgens de theorie van Nambu en Han vormden deze kleuren en antikleuren de fundamentele tripletten van een nieuwe ijkgroep, $SU(3)_c$ of kleur-$SU(3)$. Als het Δ^{++} een antisymmetrische golffunctie moest hebben, kon dat met een antisymmetrische kleurgolffunctie, zodat het Δ^{++} zelf *kleurloos* of *wit* zou zijn. Het probleem van het Δ^{++} werd op deze manier opgelost, en de kwantumchromodynamica was geboren.

Hoewel er vele gelijkenissen bestaan tussen de sterke en de elektromagnetische wisselwerking (die beschreven wordt in de goed begrepen kwantumelektrodynamica of QED), is er één significant verschil tussen beide: fotonen zijn elektrisch neutraal, terwijl gluonen een kleurlading dragen. Deze kleurlading stelt de gluonen in staat om zelf te gaan interageren met andere gluonen. Het blijkt dat de zelfinteractie van de gluonen een belangrijk effect heeft op de eigenschappen van de sterke interactie. Zo zorgt ze ervoor dat de koppelingsconstante van de sterke interactie, α_s, groter wordt naarmate quarks verder van elkaar verwijderd zijn, zodat men geen vrije quarks en gluonen kan waarnemen bij eindige energieën. Dit effect noemt men *confinement*, en het rigoureuze bewijs ervan is één van de belangrijkste onopgeloste vragen binnen de theoretische fysica.

Wanneer de afstand tussen de quarks daarentegen zeer klein wordt (en de energie-

schaal dus vergroot), verkleint ook α_s. Dit fenomeen, dat *asymptotische vrijheid* wordt genoemd, is in tegenstelling tot confinement wel goed begrepen: de ontdekking van asymptotische vrijheid leverde Gross, Wilczek en Politzer in 2004 de Nobelprijs voor de natuurkunde op.

Door het aparte gedrag van de sterke koppelingsconstante komt men verschillende schalen tegen wanneer men de sterke interactie bestudeert, en dus ook verschillende vrijheidsgraden. Bij hoge energie kan men een niet-exotisch baryon zoals het proton beschrijven als een amalgama van drie valentiequarks, een zee van quark-antiquarkparen en gluonen. Een niet-exotisch meson, *bvb.* het pion, bestaat dan uit een valentiequark-antiquarkpaar, omgeven door gluonen en zeequarks. Wanneer men echter gaat kijken naar de eigenschappen van deze hadronen bij lage energieschalen (*i.e.* van de orde van een typische hadronmassa, $\mu \sim 1$ GeV), wordt het moeilijk om de relevante vrijheidsgraden te definiëren. Het gevolg daarvan is dat er een waaier aan methodes en modellen bestaat waarmee hadronen beschreven kunnen worden, elk met hun eigen vrijheidsgraden. In dit werk werd gekozen voor een constituentenquarkmodel. De vrijheidsgraden in zo'n model worden constituentenquarks genoemd en kunnen geïnterpreteerd worden als "aangeklede" valentiequarks, waarbij de effecten van de gluonen en de zee opgenomen zijn in een effectieve constituentenquarkmassa.

Veralgemeende partondistributies

Wanneer men een elementair deeltje (bijvoorbeeld een geladen lepton) laat verstrooien aan een hadron, bevat de werkzame doorsnede van de reactie typisch niet-perturbatieve grootheden die de interne structuur van het hadron weergeven. Dit komt doordat hadronen bij een lage energieschaal niet beschreven kunnen worden met de technieken van perturbatierekening. Voorbeelden van deze grootheden zijn vormfactoren, partondistributiefuncties (PDF's) en veralgemeende partondistributies (GPD's).

Vormfactoren worden bestudeerd in elastische verstrooiingsprocessen. In één bepaald soort referentiestelsel, met name een Breit-stelsel, kunnen ze geïnterpreteerd worden als de Fouriergetransformeerde ladings- en magnetisatiedichtheid. Vormfactoren hangen af van de energie en impuls die van het ene naar het andere hadron zijn overgedragen: $F(t)$. Partondistributiefuncties worden daarentegen onderzocht via diep-inelastische verstrooiingsprocessen. In het *infinite momentum frame*, waarin het hadron een oneindig grote impuls heeft in de 3-richting, is de PDF $f(x_B)$ de waarschijnlijkheidsdichtheid om in het hadron een consituent ("parton") aan te treffen van

smaak f dat een fractie x_B van de totale hadronimpuls draagt.

Veralgemeende partondistributiefuncties $H^f(x,\xi,t)$ ten slotte kwamen in 1997 in de aandacht toen Ji ontdekte dat ze de zogenaamde "spincrisis" van het proton zouden kunnen helpen oplossen. De processen waarmee men GPD's bestudeert zijn diepvirtuele Comptonverstrooiing (DVCS, zie Fig. C.3) en harde exclusieve mesonproductie (HEMP). Net als in diep-inelastische verstrooiing, is er in dit soort processen typisch sprake van een "harde" en een "zachte" schaal. Het harde proces, de verstrooiing van een parton, kan berekend worden in perturbatieve QCD. Het zachte proces daarentegen vereist een niet-perturbatieve behandeling en wordt vaak berekend met de hierboven beschreven modellen. Het blijkt dat GPD's een brug vormen tussen vormfactoren en PDF's en dus gezien kunnen worden als unificerende grootheden. De PDF's worden gevonden als voorwaartse limiet van de GPD's ($t = 0$, $\xi = 0$); de vormfactoren vindt men terug na integratie over x (waarbij de ξ-afhankelijkheid wegvalt). In tegenstelling tot de partondistributiefuncties, kunnen veralgemeende partondistributies niet gezien worden als een waarschijnlijkheidsdichtheid, maar eerder als een *interferentie* tussen verschillende hadrontoestanden. Dit is een rechtstreeks gevolg van het niet-voorwaartse karakter van de GPD's.

Behalve hun relatie met vormfactoren en partondistributiefuncties, blijken GPD's nog andere bijzondere eigenschappen te hebben. Zo blijkt bijvoorbeeld dat de integraal $\int \mathrm{d}x\; x^{n-1} H^f(x,\xi,t)$, die men het n-de orde Mellinmoment noemt, een veelterm in ξ oplevert, waarvan de orde niet hoger is dan n (zowel voor oneven n en spin-$1/2$ baryonen als als voor pseudoscalaire mesonen) of $n-1$ (voor even n en spin-$1/2$ baryonen). Dit noemt men de polynomialiteitseigenschap van GPD's. Wanneer het onderzochte hadron een pion is, geldt bovendien de isospinsymmetrie-eigenschap $H^u_{\pi^+}(x,\xi,t) = -H^d_{\pi^+}(-x,\xi,t)$. De polynomialiteitsconditie en de isospinsymmetrie vormen twee belangrijke modeltesten in het resultatenhoofdstuk van dit werk.

Tot hiertoe hebben we nog niet gezegd waarvoor de variabelen x, ξ en t precies staan. Nochtans is hun betekenis van cruciaal belang voor het verhaal van deze thesis. De variabele t staat, net als voor vormfactoren, voor de energie en impuls die van het inkomende naar het uitgaande hadron zijn overgedragen. Schrijven we de energie-impulsviervector van het inkomende hadron als $\bar{P}$ en die van het uitgaande hadron als $\bar{P}'$, dan is $t = (\bar{P}' - \bar{P})^2$. De betekenis van de andere twee variabelen, x en ξ, is het duidelijkst in het *infinite momentum frame*. Daar staat ξ voor de fractie aan plus-impuls die verloren gaat in het proces, terwijl x de gemiddelde fractie aan plus-impuls is van het parton dat de interactie aangaat (zie Fig. C.3). Aangezien partonen in een hadron on-shell zijn (asymptotische vrijheid), kan de plus-impulsfractie nooit groter worden

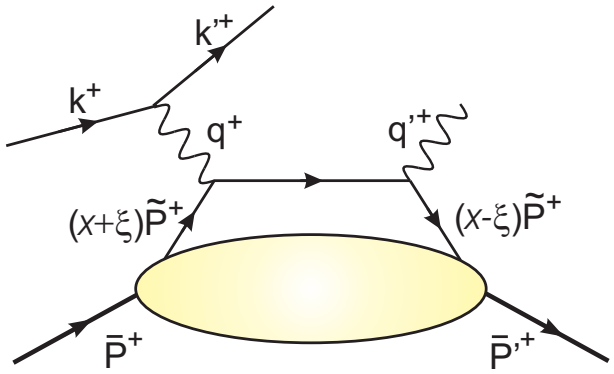

Figuur C.3 Het diagram van diep-virtuele Comptonverstrooiing, een van de reacties waarmee men veralgemeende partondistributies bestudeert.

dan 1. Men kan bewijzen dat ξ beperkt is tot het interval $[0, \xi_{max}]$ met

$$\xi_{max} = \sqrt{\frac{-t}{4M^2 - t}},$$

met M de hadronmassa, terwijl x beperkt is tot het interval $[-1, 1]$. Dit betekent dat de GPD buiten dit interval moet verdwijnen (nul worden). Het gebied $[-1, 1]$ wordt daarom het *supportgebied* genoemd.

Het belang van het supportgebied wordt duidelijk wanneer we de evolutie van GPD's bestuderen. Veralgemeende partondistributies zijn in feite schaalafhankelijke grootheden: bij lage energieën ziet men immers minder partonstructuur in het hadron dan bij hoge energieën. Het verband tussen de GPD bij een lage energieschaal en die bij hoge schaal wordt gegeven door de evolutievergelijkingen, een set van vergelijkingen die gebaseerd is op perturbatieve QCD. In het supportgebied kan men drie deelgebieden onderscheiden, volgens de evolutievergelijkingen die men er moet gebruiken (DGLAP- of ERBL-vergelijkingen). Buiten het supportgebied *moet* de GPD wegvallen en zijn er dus geen evolutievergelijkingen.

Nu zijn dynamische modellen, waarmee GPD's vaak berekend worden, niet noodzakelijk compatibel met het partonmodel (waarin de partonen on-shell zijn). Als gevolg daarvan kan het voorkomen dat de GPD's niet verdwijnen voor $|x| > 1$. Men spreekt dan van een *supportprobleem*. Het is niet duidelijk hoe GPD's in dit geval geevolueerd dienen te worden, zodat vergelijking met experimentele data en andere modellen (die doorgaans een andere schaal bezitten) sterk bemoeilijkt wordt.

Het Bonnmodel

Het constituentenquarkmodel dat in dit werk gebruikt werd, is het covariante Bethe-Salpetermodel dat ontwikkeld werd aan de universiteit van Bonn. Eigenlijk bestaan er twee varianten van het Bonnmodel: een model voor mesonen en een voor baryonen. In deze thesis worden er resultaten van het Bonnmodel voor mesonen getoond.

In het Bonnmodel wordt een gebonden (relativistische) $q\bar{q}$-toestand beschreven door de Bethe-Salpeteramplitude, welke op haar beurt de oplossing is van de Bethe-Salpetervergelijking. In principe zouden deze vergelijking en de bijbehorende normalisatievoorwaarde voldoende zijn om het mesonspectrum te berekenen, ware het niet dat zowel de quarkpropagatoren als de interactiekernen ongekende QCD-grootheden zijn. Met gepaste benaderingen (instantane benadering van de interactiekernen, effectieve quarkmassa's in de propagatoren) worden de Bethe-Salpetervergelijking en haar normalisatievoorwaarde in het Bonnmodel gereduceerd tot de oplosbare Salpetervergelijking en de bijbehorende normalisatievoorwaarde, die samen leiden tot het discrete massaspectrum van de mesonen.

In het Bonnmodel worden twee interacties gebruikt: de confinementinteractie, die op alle toestanden tegelijk inwerkt en lineair afhankelijk is van de afstand tussen quark en antiquark, en de residuele instantoninteractie. Deze laatste werkt enkel in op de scalaire en pseudoscalaire mesonen, en zorgt zo voor de reproductie van enkele bijzondere eigenschappen van het mesonspectrum, zoals de (extreem) lage pionmassa.

Veralgemeende partondistributies in het Bonnmodel

Het intrinsiek covariante karakter van het Bethe-Salpeterformalisme laat toe om zowel statische als dynamische eigenschappen van mesonen te berekenen. Het formalisme werd in het verleden al succesvol toegepast voor de berekening van elektromagnetische vormfactoren. Het is dan ook een logische stap om het te testen voor veralgemeende partondistributies.

Deze functies kunnen in het Bonnmodel berekend worden via het Mandelstamformalisme en het theorema van Wick. In dit werk wordt een laagste-ordebenadering van de GPD van pseudoscalaire mesonen rigoureus afgeleid. De implementatie van de op deze manier bekomen vergelijking vereist enige zorg, vooral wat betreft de integratie over de interne momenta.

GPD's van pseudoscalaire mesonen

In hoofdstukken 3 en 4 werd een Lorentz-covariant formalisme uitgewerkt waarmee GPD's berekend kunnen worden. In hoofdstuk 5 tonen we de resultaten van de berekeningen voor pseudoscalaire mesonen. We focussen daarbij op twee mesonen: het π^+ en het K^+.

Het is eerst van belang om stil te staan bij de analytische eigenschappen van de GPD-vergelijking. Het blijkt dat de juiste support niet kan gegarandeerd worden omwille van de specifieke vorm van de reductie naar de Salpetervergelijking, meer bepaald de instantane benadering. Aan de andere kant kan ook niet aangetoond worden dat er met zekerheid een supportprobleem zal zijn. Daarom beslissen we dat een nauwgezette berekening nodig is. Om een eventueel supportprobleem te kunnen kwantificeren, wordt de supportparameter $\phi \in [0, 1]$ ingevoerd. De waarde $\phi = 1$ betekent dat er geen supportprobleem is. Hoe dichter de waarde bij nul ligt, des te groter is het probleem.

Eerst wordt getest of ons model voldoet aan twee belangrijke voorwaarden, namelijk de onafhankelijkheid van de gekozen radiale basisfuncties en de gepaste convergentie-eigenschappen van de basis. Eerdere berekeningen met het Bonnmodel werden gedaan met 10 radiale basisfuncties, en dat blijkt ook voor de GPD-berekeningen een prima benadering te zijn. Ook de onafhankelijkheid van de basisfuncties wordt aangetoond: het verschil tussen de resultaten met de Jacobi- en de Laguerrebasisfuncties aan de ene kant, en de harmonische-oscillatorfuncties aan de andere kant is maximaal 3% van de piekhoogte (Fig. 5.1). In deze figuur wordt echter ook duidelijk dat het constituentenquarkmodel van Bonn met een supportprobleem te kampen heeft. We gingen dan ook na welke fysische eigenschappen het supportprobleem beïnvloeden. Omdat het pion een diepgebonden toestand is, zoeken we onder andere uit of de bindingsenergie een effect heeft.

We introduceren drie varianten op het Bonnmodel voor mesonen. Deze modellen noemen we het *volledige model*, het *gereduceerde model* en het *verhoogde-quarkmassa-model* of IQM-model. In het volledige model zijn alle parameters zodanig gekozen dat het een realistische beschrijving geeft van het mesonspectrum. In dit model is het pion een diepgebonden toestand, met een relatieve bindingsenergie (gedefinieerd als de bindingsenergie gedeeld door de massa) van 4.39. De relatieve bindingsenergie van het kaon is in dit model 0.84.

In het gereduceerde model wordt de instantoninteractie afgezet. Aangezien deze interactie verantwoordelijk is voor de diepe binding van het pion, verwachten we

dat dit model een antwoord kan geven op de bindingsenergie-afhankelijkheid van het supportprobleem. Het pion heeft in dit model een relatieve bindingsenergie van 0.33, die van het kaon is 0.28.

Naast de instantoninteractie heeft ook de massa van de niet-vreemde quarks een invloed op de bindingsenergie van het pion. Daarom introduceren we het IQM-model, waarin de massa van deze quarks gevoelig wordt verhoogd. In dit model werd enkel het pion berekend. De relatieve bindingsenergie van het pion bedraagt ditmaal 0.46.

Eerst werd nagegaan of de GPD's die met het Bonnmodel berekend werden, voldoen aan de basiseigenschappen van GPD's. De pion-GPD's voldoen exact aan de vereiste isospinsymmetrie-eigenschap. Voor het kaon gaat deze eigenschap niet op, wat klopt met het feit dat in het kaon een vreemd quark aanwezig is. Wanneer de GPD's geïntegreerd worden over x, wordt de vormfactor gevonden (hiertoe dient wel de integraal over het volledige x-gebied berekend te worden). De grote meerderheid van de op die manier berekende vormfactoren verschillen slechts ongeveer 1% van de vormfactoren uit een rechtstreekse berekening in het Bonnmodel. Tot slot werd ook de polynomialiteitsconditie geverifieerd.

De vorm van de berekende curves suggereert dat de relatieve bindingsenergie van het meson inderdaad een invloed heeft op de supporteigenschappen van de GPD's. Wanneer we de supportparameter berekenen, wordt deze indruk kwantitatief bevestigd. Het blijkt dat deze parameter significant hoger is in het gereduceerde en het IQM-model dan in het volledige model. Ook voor het kaon blijken de supporteigenschappen beter te zijn dan voor het pion. Bovendien is ook de support van de kaon-GPD beter in het gereduceerde dan in het volledige model. We besluiten daarom dat de bindingsenergie inderdaad een grote rol speelt, en dat de supporteigenschappen beter zijn bij minder diepgebonden mesonen.

Een afhankelijkheid van de variabele ξ kan niet worden aangetoond. De GPD's blijken wel lichtjes afhankelijk te zijn van t, hoewel deze afhankelijkheid vooral duidelijk is in het volledige model.

De berekeningen van de kaon-GPD tonen aan dat hoewel de constituentenquarkmassa een rol speelt, dit enkel gebeurt via de relatieve bindingsenergie. De specifieke smaak van de constituentenquarks beïnvloedt de supporteigenschappen van de GPD's amper.

We besluiten het resultatenhoofdstuk met een belangrijke opmerking: hoewel de supporteigenschappen gevoelig verbeteren wanneer de (relatieve) bindingsenergie verkleint, hebben alle modellen last van een supportprobleem. Geen enkele van de GPD's kan geëvolueerd worden met de bestaande evolutievergelijkingen. De interpretatie

van de GPD's is dan ook onduidelijk. Hierbij moet opgemerkt worden dat de Mellinmomenta van de GPD's bij $\xi = 0$ wel kunnen geëvolueerd worden, ondanks het supportprobleem.

Vooruitzichten

Rekening houdend met de resultaten uit deze thesis, stellen we enkele mogelijke vervolgprojecten voor. Om te beginnen zou de evolutie van de Mellinmomenta van de berekende GPD's bij $\xi = 0$ naar de gebruikelijke energieschaal van rooster-QCD een manier vormen om de performantie van het Bonnmodel te testen.

Aangezien GPD's een belangrijk nieuw licht kunnen werpen op de oorsprong van de kwantummechanische spin van het proton, achten wij een numerieke berekening van de GPD's van het proton in het Bonnmodel noodzakelijk. In de spinsomregel treden de GPD's op via de Mellinmomenta van tweede orde, dewelke voor $\xi = 0$ kunnen geëvolueerd worden. Het is niet uitgesloten dat de GPD's de goede supporteigenschappen vertonen. Om te beginnen blijkt uit de resultaten bij pseudoscalaire mesonen dat de supporteigenschappen afhankelijk zijn van de bindingsenergie, die lager is in het proton dan in het pion. De tweede en belangrijkste reden is echter dat de analyse van de supporteigenschappen uit Sectie 5.2 niet opgaat voor baryonen met spin-$1/2$.

Een derde weg die kan gevolgd worden, is de ontwikkeling van een nieuw quarkmodel dat gebaseerd is op het Bethe-Salpeterformalisme, waarin eigenschappen van het Bonnmodel (*bv.* de gebruikte interacties) gecombineerd worden met een instantane benadering die de goede support kan garanderen. In dit verband zal eerst moeten nagedacht worden over een manier om de confinementinteractie compatibel te maken met een "lichtkegelversie" van de instantane benadering.